

5-1-2021

## Dynamic Analysis of a Microgrid Powered With an Inverter and Machine-Based Distributed Resources

Brandon William Blackstone

Follow this and additional works at: <https://digitalscholarship.unlv.edu/thesesdissertations>



Part of the [Electrical and Computer Engineering Commons](#), [Oil, Gas, and Energy Commons](#), and the [Sustainability Commons](#)

---

### Repository Citation

Blackstone, Brandon William, "Dynamic Analysis of a Microgrid Powered With an Inverter and Machine-Based Distributed Resources" (2021). *UNLV Theses, Dissertations, Professional Papers, and Capstones*. 4122.

<http://dx.doi.org/10.34917/25374006>

This Dissertation is protected by copyright and/or related rights. It has been brought to you by Digital Scholarship@UNLV with permission from the rights-holder(s). You are free to use this Dissertation in any way that is permitted by the copyright and related rights legislation that applies to your use. For other uses you need to obtain permission from the rights-holder(s) directly, unless additional rights are indicated by a Creative Commons license in the record and/or on the work itself.

This Dissertation has been accepted for inclusion in UNLV Theses, Dissertations, Professional Papers, and Capstones by an authorized administrator of Digital Scholarship@UNLV. For more information, please contact [digitalscholarship@unlv.edu](mailto:digitalscholarship@unlv.edu).

DYNAMIC ANALYSIS OF A MICROGRID POWERED WITH AN INVERTER AND  
MACHINE-BASED DISTRIBUTED RESOURCES

By

Brandon William Blackstone

Bachelor of Science in Engineering – Electrical Engineering  
University of Nevada, Las Vegas  
2003

Master of Science in Engineering – Electrical Engineering  
University of Nevada, Las Vegas  
2006

A dissertation submitted in partial fulfillment  
of the requirements for the

Doctor of Philosophy – Electrical Engineering

Department of Electrical and Computer Engineering  
Howard R. Hughes College of Engineering  
The Graduate College

University of Nevada, Las Vegas  
May 2021



## **Dissertation Approval**

The Graduate College  
The University of Nevada, Las Vegas

December 18, 2018

This dissertation prepared by

Brandon William Blackstone

entitled

Dynamic Analysis of a Microgrid Powered With an Inverter and Machine-Based  
Distributed Resources

is approved in partial fulfillment of the requirements for the degree of

Doctor of Philosophy – Electrical Engineering  
Department of Electrical and Computer Engineering

Yahia Baghzouz, Ph.D.  
*Examination Committee Chair*

Kathryn Hausbeck Korgan, Ph.D.  
*Graduate College Dean*

Emma Regentova, Ph.D.  
*Examination Committee Member*

Sahjendra Singh, Ph.D.  
*Examination Committee Member*

Evangelos Yfantis, Ph.D.  
*Graduate College Faculty Representative*

## **Abstract**

The proliferation of renewable distributed energy resources, particularly photovoltaic (PV) power systems, and the increasing need for a reliable power supply has led to the concept of microgrids, a mini-grid that consists of locally connected power generation units and needs, able to operate connected or disconnected from the utility grid, using controlled and coordinated methods to provide for the users of the microgrid the best possible conditions for their needs. The main technical issues facing microgrids include some of the following, seamless transition from stand-alone to utility grid connected operation, how to preserve frequency and voltage stability, and provide the lowest cost power among numerous power resources. Technologies that will be used in the future smart grid will be built, tested, and fielded in modern microgrids with many national laboratories, utility companies, and universities using microgrids of all different types for research and development.

This dissertation describes the design, fabrication, and testing of a microgrid facility which comprises adjustable resistive and inductive loads, a diesel-powered generator (DG), an advanced inverter PV system, a battery energy storage system (BESS), monitoring, protection, and control devices. The microgrid facility was built with the foresight that it would be used for conducting tests and experiments related to microgrid technical challenges, thus ease of access and expandability were built in which allows it to be used for both research and education purposes. Numerous experimental tests conducted include the following: (a) the dynamic response of a DG to load changes, (b) an advanced PV inverters autonomous functions, (c) advanced inverter islanding test, (d) load sharing among the DG and PV system, (e) PV and battery storage systems load sharing, (d) dynamic performance of an advanced PV inverter and a DG during unintentional islanding under different power export/import conditions, and (e) BESS

response to utility outage under different PV operating conditions. Attempts to improve reliability and power quality are made by expanding the PV inverter ride-through times during frequency and voltage abnormalities. An economic analysis in terms of Net Present Value (NPV) is conducted on a residential application where a BESS is paired with a PV system to shift solar energy in favor Time-of-Use (ToU) pricing and to provide ancillary grid services.

## **Acknowledgements**

I would like to express my very great appreciation to Dr. Baghzouz for his valuable and constructive suggestions during the planning and development of this research work. His willingness to give his time so generously has been very much appreciated. I would also like to thank my committee member, Dr. Emma Rengentova, Dr. Sahjendra Singh, Dr. Evangelos Yfantis for providing a steady guiding hand and helping me during this process.

I wish to thank Chris Hicks and Wenxin Peng for their assistance with the experiments and data collection used in this dissertation. I would further like to thank Octavio Gonzalez and Travis Taylor for all their assistance and knowledge in the building, commissioning, and instruction on the use of the UNLV microgrid.

Finally, I wish to thank my family, my wife Karina, my son Nicholas, my father John, and all the rest, without their patience and support none of this would be possible.

Parts of this work were supported by the National Science Foundation EPSCoR Program under Grant No. IIA-1301726, and San Diego Gas & Electric (SDGE).

## Table of Contents

|  |     |
|--|-----|
| Abstract .....   | iii |
| Acknowledgements.....  | v   |
| List of Tables .....   | x   |
| List of Figures .....  | xi  |
| Chapter 1: Introduction .....  | 1   |
| Chapter 2: Microgrid Design and Implementation .....                             | 7   |
| 2.1: Photovoltaic System .....   | 7   |
| 2.2: Battery Energy Storage System (BESS).....                                   | 8   |
| 2.3: Diesel Generator .....  | 9   |
| 2.4: Load Banks .....  | 10  |
| 2.5: Generator and Inverter Controls .....                                       | 11  |
| Chapter 3: Diesel Generator Modeling and Testing .....                           | 16  |
| 3.1: Generator Dynamic Model .....   | 16  |
| 3.2: Automatic Voltage Regulator Model.....                                      | 18  |
| 3.3: Governor Control Model .....  | 19  |
| 3.4: Generator Response to Load Acceptance and Rejection .....                   | 22  |
| Chapter 4: PV System Modeling and Testing of Inverter Autonomous Functions ..... | 30  |
| 4.1: Photovoltaic System and Inverter Model.....                                 | 30  |

|   |    |
|---|----|
| 4.2: Review of Interconnection Standards .....  | 35 |
| 4.3: Test Plan and Experimental Setup .....   | 39 |
| 4.4: Test Procedure and Results .....   | 43 |
| 4.4.1: Soft Reconnect .....   | 43 |
| 4.4.2: Non-unity PF .....   | 46 |
| 4.4.3: Over- and Under-Voltage Ride Through .....   | 48 |
| 4.4.4: Over/Under Frequency Ride Through .....  | 52 |
| 4.4.5: Dynamic Volt/VAR Control .....   | 53 |
| Chapter 5: Islanding Test of Advanced Inverter .....                                      | 59 |
| 5.1: Potential Interference of Autonomous Functions with Islanding Detection Schemes .... | 59 |
| 5.2: Experimental Setup .....   | 65 |
| 5.3: Test Findings .....  | 66 |
| 5.3.1: Operation at Unity PF .....  | 66 |
| 5.3.2: Over- and Under-Voltage and Frequency Ride Through .....                           | 69 |
| 5.3.3: Inverter Operation with a Setting of Non-unity PF .....                            | 71 |
| 5.3.4: Operation under Dynamic Volt/VAR Control .....                                     | 73 |
| Chapter 6: Unintentional Islanding of Diesel Generator – PV Microgrid .....               | 76 |
| 6.1: Unintentional Islanding of Operational Microgrid .....                               | 77 |
| 6.1.1: Inverter Operation under Default Settings .....                                    | 77 |



|  |     |
|--|-----|
| 6.1.2: Inverter Operation under Advanced Settings.....                 | 80  |
| 6.2: Microgrid Operation in Islanded Mode .....                        | 85  |
| Chapter 7: Pairing a Battery Energy Storage System (BESS) with PV..... | 91  |
| 7.1: Experimental Setup for BESS Testing.....                          | 92  |
| 7.2: Test Results.....   | 93  |
| 7.2.1: Power Quality Test .....  | 94  |
| 7.2.2: Dynamic Response Test.....                                      | 96  |
| 7.3: Residential Application.....                                      | 99  |
| 7.3.1: Solar Energy Shifting during Summer-on-Peak Period.....         | 100 |
| 7.3.2: Additional BESS Services .....                                  | 103 |
| 7.4: Case Study .....  | 105 |
| 7.4.1: Local Energy Cost and Incentive Programs .....                  | 106 |
| 7.4.2: Residential Load .....  | 107 |
| 7.4.3: PV System Addition .....  | 109 |
| 7.4.4: BESS Addition.....  | 111 |
| Chapter 8: Conclusions .....   | 115 |
| Appendix.....  | 118 |
| 1. PV Module Technical Specs.....                                      | 118 |
| 2. Inverter Technical Specs.....                                       | 120 |

|  |     |
|--|-----|
| 3. Diesel Generator Reactances and Time Constants .....  | 122 |
| 3.1 Additional Diesel Generator Data.....                | 122 |
| 4. Diesel Generator Synchronizing Module Spec Sheet..... | 124 |
| 5. Automatic Voltage Regulator (AVR) Spec Sheet .....    | 125 |
| 6. Diesel Generator Governor Spec Sheet .....            | 127 |
| 7. Inductor Technical Specs.....                         | 128 |
| References.....  | 129 |
| Curriculum Vitae .....                                   | 135 |

**List of Tables**

Table 4.1 Original and Revised Interconnection Standard Dealing with Ride Through Times to Irregular Voltages [20]..... 36

Table 4.2 Original and Revised Interconnection Standard Dealing with Ride Through Times to Irregular Frequencies [20]..... 36

Table 4.3 CA Rule 21 Inverter Response to Abnormal Voltages [22]. ..... 37

Table 4.4 CA Rule 21 Inverter Response to Abnormal Frequencies [22]. ..... 38

Table 4.5 CA Rule 21 Default Volt/VAR Control Settings [22] ..... 39

Table 4.6 Inverter Software Settings (Parameter, Range, Clearing Times) [29] ..... 44

Table 5.1 Parameter Values Used in Islanding Tests [32]..... 68

Table 7.1 Local Electricity Rates for Single-Family Homes..... 107

Table 7.2 Customer Energy Cost Breakdown with PV and BESS. .... 111

## List of Figures

|   |    |
|---|----|
| Figure 2.1 Microgrid Physical Location on UNLV Campus ( $36^{\circ}06'50''$ N $115^{\circ}18'40''$ W) ..... | 7  |
| Figure 2.2 PV Array Layout. ....  | 8  |
| Figure 2.3 Diagram of Generator Excitation System [36]. ....  | 10 |
| Figure 2.4 Image of Inverter Controller with Router. ....   | 12 |
| Figure 2.5 Communication with Smart PV Inverter. ....   | 12 |
| Figure 2.6 Frequency and Voltage Disturbances Controller. ....  | 15 |
| Figure 3.1 Diesel Generator Block Diagram with Mechanical and Electric Subsystem [37]. ....                 | 17 |
| Figure 3.2 Automatic Voltage Control Model. ....  | 19 |
| Figure 3.3 Governor Control Model. ....   | 21 |
| Figure 3.4 Complete Generator Model with Controls. ....   | 22 |
| Figure 3.5 Frequency and Voltage Deviations Due to 12 kW Resistive Load Elimination [33].                   | 24 |
| Figure 3.6 Frequency and Voltage Changes Due to 9 kVAR Inductive Load Addition [33]. ....                   | 24 |
| Figure 3.7 Measure and Simulated Voltage for 9 kVAR Load Acceptance. ....                                   | 28 |
| Figure 4.1 A Solar Cells Equivalent Circuit. ....   | 31 |
| Figure 4.2 Typical Circuit Diagram of Single-Phase Grid-Tied Inverter. ....                                 | 34 |
| Figure 4.3 Common of Volt/VAR Using Piece-Wise Linear Curve [22]. ....                                      | 39 |
| Figure 4.4 Experimental Setup Block Diagram. ....   | 41 |
| Figure 4.5 An Image of the Advanced Inverters Experimental Test Setup. ....                                 | 42 |

|   |    |
|---|----|
| Figure 4.6 Ramp-Up Adjustment (10%, 100%, 1,000%) of Soft-Start Function [29].  | 46 |
| Figure 4.7 PF Adjustment (100%, 90% and 80% Under-Excited and Over-Excited).  | 48 |
| Figure 4.8 Temporary 82% Under-Voltage.   | 50 |
| Figure 4.9 Voltage Variation between 90% and 108%.  | 51 |
| Figure 4.10 Temporary 112% Over-Voltage.  | 51 |
| Figure 4.11 Temporary 117% Over-Voltage.  | 52 |
| Figure 4.12 Temporary 58 Hz Under-Frequency.  | 54 |
| Figure 4.13 Frequency Deviation between 59.5 Hz and 60.5 Hz.  | 55 |
| Figure 4.14 Temporary 61.5 Hz Over-Frequency  | 55 |
| Figure 4.15 Temporary 62.5 Hz Over-Frequency  | 56 |
| Figure 4.16 Dynamic Volt/VAR Baseline Test with Gradual Voltage Changes [29].   | 58 |
| Figure 4.17 Dynamic Volt/VAR Baseline Test with Fast and Temporary Voltage Changes [29].                              | 58 |
| .....   | 58 |
| Figure 5.1 Circuit Block Diagram of the Utility Grid, PV System, and Local Load [33].                                 | 60 |
| Figure 5.2 Characteristic Volt/VAR and Watt/Hz Inverter Contour [32].   | 65 |
| Figure 5.3 Case 1 ( $P_G=0$ , $Q_G=0$ ) Unity PF Operation of Inverter [32].  | 69 |
| Figure 5.4 Case 2 ( $P_G=0$ , $Q_G=130$ ) Unity PF Operation of Inverter [32].  | 69 |
| Figure 5.5 Case 3 (Ride Through Activated of OUV and OUF Conditions) with the Inverter<br>Operating at Unity PF [32]. | 71 |
| Figure 5.6 Case 4 Non-unity PF (85.6%) Operation of Inverter [32].  | 72 |

|  |    |
|--|----|
| Figure 5.7 Case 4 Non-unity PF (97%) Operation of Inverter [32].....   | 73 |
| Figure 5.8 Islanding During Dynamic Volt/VAR Control [32].....   | 75 |
| Figure 6.1 The Microgrid and its Components under Study. ....  | 77 |
| Figure 6.2 Advanced Inverters Voltage and Power Response to Utility Disconnect, Utility<br>Supplying 1 kW and 0 kW (250ms Sample Period) [29]. ....                      | 79 |
| Figure 6.3 Advanced Inverters Voltage and Power Response to Utility Disconnect, Utility<br>Supplying 1 kW and 0 kW (250ms Sample Period) [30]. ....                      | 80 |
| Figure 6.4 Advanced Inverters Current and Voltage Waveforms Response to Utility Disconnect<br>[29].....  | 81 |
| Figure 6.5 Advanced Inverters Current (Red) and Voltage (Green) Response to Utility<br>Disconnect, Utility Absorbing 2 kW. ....  | 82 |
| Figure 6.6 Advanced Inverters Voltage and Power Response to Utility Disconnect, Utility<br>Absorbing 1 kW and 0 kW (250ms Sample Period).....                            | 83 |
| Figure 6.7 Advanced Inverters Frequency and Power Response to Utility Disconnect, Utility<br>Absorbing 1 kW, 0 kW, and Utility Supplying 1 kW (250ms Sample Period)..... | 84 |
| Figure 6.8 Advanced Inverters Voltage and Power Response to Utility Disconnect, Importing 2<br>kW (250ms Sampling Period).....   | 84 |
| Figure 6.9 Advanced Inverters Current (Red) and Voltage (Green) Response to Utility<br>Disconnect, Utility Supplying 2 kW.....   | 85 |
| Figure 6.10 DG and PV System (Low Solar Irradiance) Load Sharing. ....   | 86 |

|   |    |
|---|----|
| Figure 6.11 Advanced Inverters Power Production Response to Rapid Changes in Load (Inverter Software - Default Values). ..... | 88 |
| Figure 6.12 Disturbances in Voltage Due to Rapid Changes in Load Shown in Fig. 6.11. ....                                     | 89 |
| Figure 6.13 Disturbances in Frequency Due to Rapid Changes in Load Shown in Fig. 6.11 .....                                   | 89 |
| Figure 6.14 Advanced Inverters Power Production Response to Rapid Load Changes (Inverter Software - Modified Values). .....   | 90 |
| Figure 7.1 Experimental Test Setup for PV + BESS. ....  | 94 |
| Figure 7.2 BESS Current and Voltage Waveforms When Load Sharing with the PV Inverter. ..                                      | 96 |
| Figure 7.3 BESS Current and Voltage Waveforms to Resistive Load, No PV Generation. ....                                       | 97 |
| Figure 7.4 Battery Current and Voltage Response to Utility Disconnect, RMS Values, (No PV Generation). .....                  | 98 |
| Figure 7.5 Battery Current and Voltage Response to Utility Disconnect, Instantaneous Values, (No PV Generation). .....        | 99 |
| Figure 7.6 Battery Current and Voltage Response to Utility Disconnect, Instantaneous Values, (with PV Generation). .....      | 99 |

## **Chapter 1: Introduction**

A microgrid is a local energy grid that can function in a regulated and coordinated way, consisting of local loads and generation units that can operate either connected or disconnected from the utility grid. Little local networks, or microgrids, were the earliest electricity grids before they were connected to make the utility grid we know today. In remote areas, microgrids are the only way to have electrical power and therefore have existed for quite some time. In regions where grid connections are possible, microgrids are used to back up or serve critical loads, loads that even momentary power outages can be catastrophic. Proliferation of renewable distributed energy generation sources, chiefly solar photovoltaic systems, will make microgrids spread quickly into the residential and commercial areas in urban and rural areas with electricity. The future “smart” electric power infrastructure will be based on microgrids and will be among the major technical cornerstones [1]. Modern microgrid development, over the past two decades, is being driven by multiple items which include but are not limited to the spread of renewable distributed resources, rising electricity demands, and increasing necessity for reliable power electric supply. [2]–[4]

Microgrids offer considerable potential in many aspects of how electric energy is generated and delivered, from operating connected to the local grid or in stand-alone mode, thus they have different ways to meet utilities and electric customers’ demands, they can provide electric energy as either physical and/or economic conditions dictate [5]. They can provide electricity through local generation to meet attached demand which can, in turn, lower the cost of electricity, make access to power secure and reliable, improve the quality of the power used, and through renewable power generation support sustainability, and enhance the resiliency of the power grid [6]. Many universities have developed or/are developing the teaching tools and for a power



systems curriculum to teach modern microgrids because they will play a significant part in the smart grid development. The curriculum will not only be hardware-based laboratory microgrids, but software development, hardware-in-the-loop, and even PV and/or wind power simulators. [7]–[13]. Depending on each university’s unique objectives which will in turn create different laboratory settings for microgrid education and research, most will share similarities such as being a reconfigurable experimental platform. While in theory, a common approach to microgrid design sounds great, it will inescapably drive up costs and not be appropriate [14].

In a microgrid configuration, control and protection represent challenges that can be difficult to deal with, which include the following. Stability of the voltage and frequency, able to transition from a grid connected system to freestanding (islanded) system, protect the system from electrical faults, hardened to cyber-attacks but able to communicate to the rest of the grid, and continue to operate using the lowest cost source of electric power among the various generation resources at the microgrids disposal. Meaningful research continues to build upon the successes of the past at research institutions worldwide with the most prominent in North America being the CERTS microgrid Facility [6]. In recent years the research on microgrids has focused on microgrid control [5], [15]–[17]. DG’s are the backbone of most microgrids because they have been proven very reliable and the most part practical, they can be turned on, and convert chemical energy to electrical energy when sustainable energy sources cannot provide enough energy to meet the local demand. In an effort to rely less on generators, but still have the same reliability, other forms of energy sources such as batteries which can ensure power quality are gaining wider use in the distributed resources market [18]. Battery storage schemes are not economically worthwhile and are expensive to procure except in areas that offer significant incentives for PV self-consumption or energy management [19].

The microgrid was built as an outdoor facility at the University of Nevada, Las Vegas campus and is described in this dissertation. It is comprised of a reliable standalone energy source in the form of a DG, a grid-interactive advanced inverter supplied by a 12 kW PV array, and a load with selectable discrete steps. In grid disconnected (islanded) operation, the DG is the grid-forming voltage/power source for the microgrid and the PV system is the grid-following source. The DG is controlled by an automatic voltage regulator (AVR), used to control the voltage output, and a speed control governor for regulation of the frequency. A microcontroller based circuit was developed in house to produce repeatable and controllable voltage and frequency instabilities, which makes this microgrid different from others found in the literature. The IEEE Standard for Interconnecting Distributed Resources with Electric Power Systems IEEE Std. 1547-2018 [20] is newly apprised and is focused on advanced inverter functionalities which will unleash their application to common voltage regulation issues found in areas where there is PV penetration is at high levels [21]. Numerous investigational tests will be covered in this dissertation.

Software applications control advanced inverters making many of their electrical characteristics adjustable by commands and settings found in the software and with manufacture configured settings even allow the inverters “autonomous” control of their power output to assist power quality and system reliability to the local circumstances. For advanced inverters and their common functions, references [22], [23] were reviewed to learn how these functions could be applied to operational challenges found in area power systems. While numerous computer simulations on how to apply these inverter functions to mitigate specific problems that have been reported, published experimental and field tests are not readily available as power utility companies are slow to use the updated interconnection standard due to many governing controls

and regulations. Reference [23] provided the general guidelines on test equipment necessities and setup, including PV and grid simulators, allowing for verification of advanced inverter functional interoperability. The PV inverter's ability to function in constant reactive power or constant Power Factor (PF) control was tested in Reference [24]. Sania reported on tests using communications-based controls of some of the inverter functionalities [25]. Finally, Southern California Edison's Advanced Technology Group recently published results from successful tests on numerous advanced inverter functionalities [26]–[28]. The first test reported in this dissertation involves using a physical PV array connected to an advanced inverter where select critical autonomous functionalities would be of interest, an adjustable load bank, a local utility source, and a DG [29]. The functionalities to be tested comprise “soft restart”, “dynamic Volt/Var control”, “over/under voltage (OUV) ride through”, “non-unity PF operation”, and “over/under frequency (OUF) ride through”.

Interference of some of the above functionalities is a concern with the inverter islanding detection methods. Grid support functions envisioned to help alleviate frequency and voltage deviations, are diametrically opposed to features found in active islanding detection methods, destabilizing voltage, and destabilizing frequency. This becomes a greater issue when the load matches inverter supply or when multiple dissimilar companies' inverters are connected to the same local grid. [30], [31]. Hence, the second test reported involves efforts in which an islanded condition of an advanced inverter was imposed while generation and load were closely matched and with the inverter having certain functions activated [32]. Tested were the following capabilities of the inverter, a broader tolerance of frequency and voltage instabilities, dynamic Volt/VAR control, and the operation of the inverter with a PF less than one.

The third test explains the dynamic performance of a PV inverter, a passive resistive-inductive load, and a DG based microgrid during an imposed islanding (utility disconnect) [33]. The experiments performed were to see if the microgrid would stay connected during grid disconnect and if the reliability and power quality could be enhanced by different inverter settings, settings that control the time of ride through in frequency, and voltage disturbances while adjusting the import/export power conditions.

For electric utility customers that have behind-the-meter battery energy storage systems that have ToU rates available to them can arbitrage their energy production from low-price to high price periods. A Net Present Value (NPV) of a battery system must be a positive value to gain wide acceptance and to facilitate this outcome, an increased battery systems revenue stream is required. It is proposed in this dissertation that this marketplace can be used for energy arbitrage which is possible by the use of a utility or regional Energy Imbalance Market (EIM) controlled second Battery Energy Storage (BES) service. The method proposed does not require complicated co-optimization algorithms and is accomplished by executing in series the two services with no time overlap. A case study illustrates the method by utilizing actual household power demands, power provided by PV sources, energy rates, and incentives in Southwest US [34].

This dissertation is organized as follows: Chapter 2 describes the design and fabrication of the microgrid under test including a description of the various components. Chapter 3 describes the characteristics of the DG containing the governor and voltage regulation controllers. Dynamic response to unexpected load deviations is performed through simulations and experimental tests. Chapter 4 addresses the performance of a finite number of the autonomous functions of the advanced inverter. Chapter 5 summarizes islanding tests on the advanced

inverter under various power mismatch conditions. Chapter 6 describes the DG - PV microgrid dynamic response during unintentional islanding from the local grid, and during stand-alone operation. Chapter 7 summarizes an experimental investigation into transient and steady-state conditions of a BESS system integrated into a PV system. This is followed by a residential application where the BESS is used to shift solar energy in regions that provide ToU electricity pricing, and other additional grid services. Finally, Chapter 8 ends the dissertation with a conclusion.

## Chapter 2: Microgrid Design and Implementation

The studied microgrid is comprised of a PV system, a DG, a BESS, a local discrete step adjustable load, instrumentation, and controls. Its physical location is shown in Figure 2.1 below. A description of the various components and their associated controls follows.



Figure 2.1 Microgrid Physical Location on UNLV Campus (36°06'50" N 115°18'40" W)

### 2.1: Photovoltaic System

The PV system contains 4 parallel strings of PV panels, with the panels rated for 270 W under Standard Test Condition (STC) with each string containing 11 panels connected in series. It is ground mounted with a tilt angle of 25° facing south. This configuration makes it a 12-kW array that is connected to a 3-phase 12 kVA advanced PV inverter which has an output voltage

of 480/277 which is converted to 208/120 V via 30 kVA transformer. The common microgrid bus voltage local grid voltage is 208/120 V.

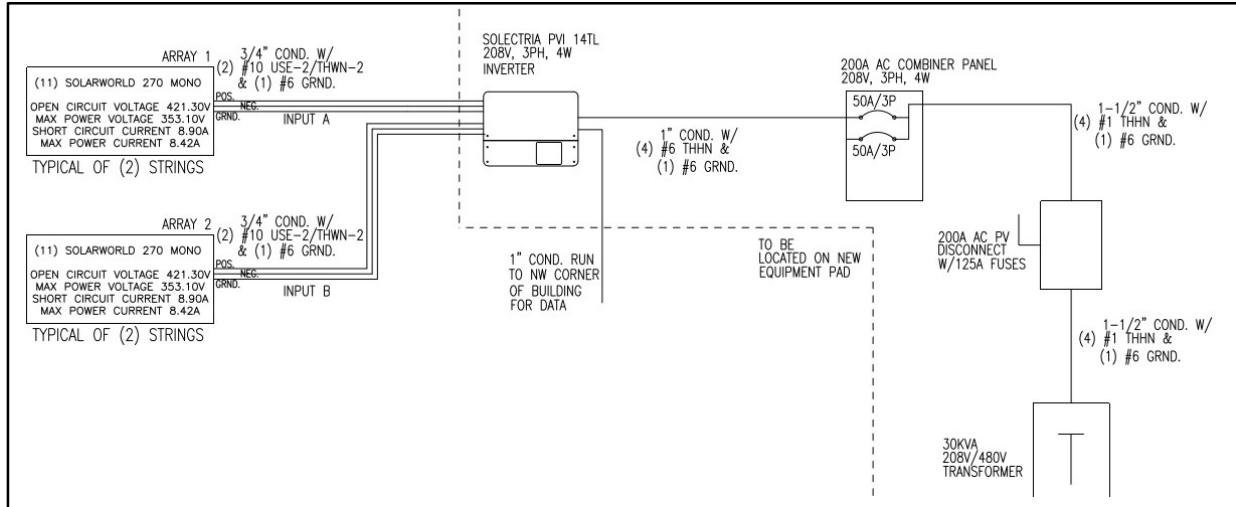


Figure 2.2 PV Array Layout.

## 2.2: Battery Energy Storage System (BESS)

A Tesla Powerwall 2<sup>TM</sup>, the installed BESS, is an integrated AC energy storage system that contains an integrated bidirectional inverter and liquid cooling system and has a useable capacity of 13.5 kWh. The BESS has a maximum continuous power charge/discharge rate of 5 kW with an efficiency of 90%, round-trip, when in an environmental temperature of 77° F the continuous power charge/discharge rate is 3.3 kW [35]. The Tesla Powerwall 2<sup>TM</sup> is a complete package that can detect a utility disconnect by the voltage and current of the device, activate its

communication and control protocols to disconnect from the grid by use of a switch, and restore power to the local grid. All this can be accomplished in a fraction of a second but the Tesla Powerwall 2™ also assists utilities in stopping utility customers that own the system from recycling grid electricity by prohibiting its use as a revenue generator which would be possible by storing and selling grid electricity via Net Energy Metering (NEM) and TOU rates. Via a software application, the full profile can be viewed of the power traversing the local grid including the battery system, the battery state-of-charge (SOC), the local load needs, and the generated power of the PV system. At present, the software applications available via the user interface include temporal controls, solar self-use, and standby power [35].

### **2.3: Diesel Generator**

The DG set consists of an engine coupled to a pancake brushless generator with the engine being a 4-cycle, 3-cylinder, liquid radiated engine with an attached generator rated at 20 kVA at 0.8 PF, constructed as a 4 pole, 3-phase, 12 lead system. The AVR is supplied electrical power from the single-phase auxiliary stator winding, illustrated in Figure 2.3, which allows the AVR to control the generators output voltage via a brushless excitation system. To close the feedback loop for the AVR, it monitors a single phase of the 3-phase voltage output of the generator and adjusts the excitation current as needed. The AVR can either be operated in isochronous or droop control modes. The auxiliary winding generator advantages are found in reduced equipment compared to other systems which reduce production costs and can make for compact axial generators. While the output power can affect the supply voltage of the AVR, which usually insignificant, it is a design that rarely fails and can withstand repeated abuses. The auxiliary winding design minimizes its mutual inductance with the primary windings and thereby and distortions found in the main outputs will have meniscal effects on the AVR's operation. The



generators 12 leads are configured for a parallel-star arrangement with an output voltage of 208Y/120 V, its electrical specifications are found in Appendices 3 and 4.

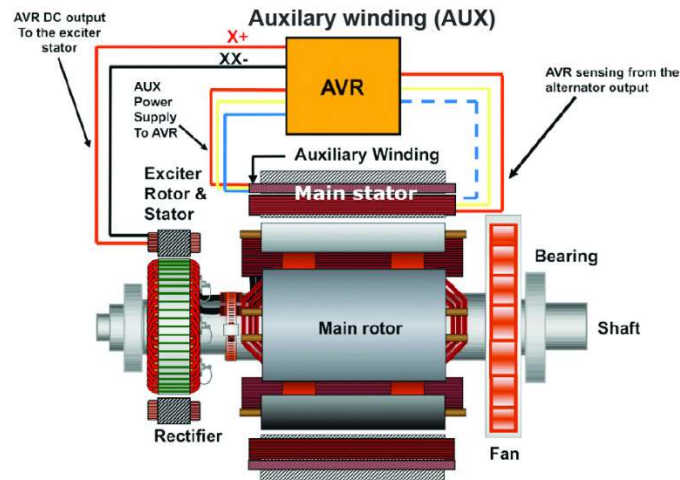


Figure 2.3 Diagram of Generator Excitation System [36].

## 2.4: Load Banks

The loads consist of three separate units with discrete manually adjustable steps, the first being a resistive (30 kW), an inductive bank (9 kVAR), and a capacitive bank (2.7 kVAR). The reactive load bank was designed and built-in house to be a switchable bank that is configured in a delta connection. Each leg of the delta consists of 3 inductors in parallel, and their specifications are found in Appendix 7. A small capacitor and resistor are added parallel with each inductor to provide safety during switching. Finally, the utility power is from a local

substation via an underground distribution feeder rated at 12.47 kV to a 75 kVA transformer connected to the microgrid.

## **2.5: Generator and Inverter Controls**

*Inverter Controls* – A separate controller from the inverter manufacture allows the user to gain access to the inverter software controls and provides system monitoring and data recording. The inverter tested in this experiment can only be connected via a controller which provides an interphase to the inverter software which allows for system monitoring and recording data. The controller uses a communication protocol widely used in the solar industry called Modbus but can be controlled via TCP/IP. To change various parameters found in the software of the inverter, a code was needed which the manufacturer of the inverter supplied. Inverter communication is achieved wirelessly by means of a router that assigns an IP address to the controller. The controller in turn communicates with the inverter via an Ethernet cable. An image of the controller and a communications diagram are shown in Figure 2.4 and Figure 2.5, respectively.



Figure 2.4 Image of Inverter Controller with Router.

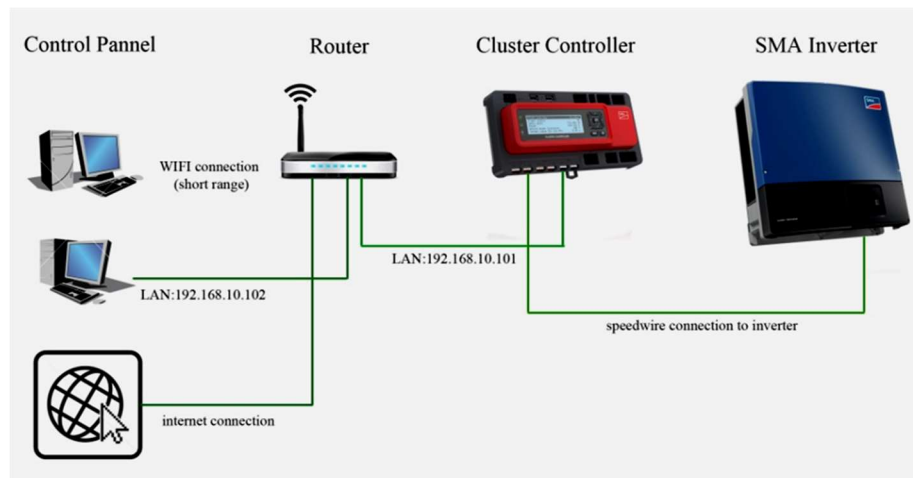


Figure 2.5 Communication with Smart PV Inverter.

*Diesel Generator Synchronizing Module* – The investigator used an Auto Mains (Utility) Failure Control Module (model DSE8620) that is suitable for paralleling multiple generators

(diesel or gas) with the utility grid. The DSE8620 is designed to control the DG to match the utility grid's voltage, frequency, and phase automatically before connection to the microgrid or it can switch from utility to generator supply all while providing an electricity service with no interruptions. The DSE8620 can detect utility disconnect via both "Vector Shift " and "Rate-of-Change-of-Frequency" methods and can control the decoupling grid switch when detected. A SEL700G is also installed for additional protection, it allows for the monitoring of electrical power amounts and compares the amounts to setpoints and parallel timing thresholds to which it can then control the connect/disconnect relay. More data on this module is found in Appendix 4.

*Diesel Generator AVR Module* - The diesel power synchronous generators' original analog AVR was replaced with a DESA106 digital closed loop AVR powered by either a shunt or a stator auxiliary winding that can operate in either a droop control mode or isolated isochronous control mode. This advanced AVR has many abilities which include a connection for a quadrature CT for droop tuning, remote voltage tuning, and soft start power ramping. The speed controls of the DG have also been modified from OEM by changing the analog nonprogrammable governor to a digital programmable governor. This governor uses a magnetic pick-up (MPU) sensor to senses the engine rpm via the engine's flywheel and is well-suited for paralleling generators due to its load-share and droop functionalities. The AVR specifications are found in Appendix 5.

*Diesel Generator Governor Control Module* – A Woodward digital governor controller (model DPG-2201-001), the speed control device of the engine, can govern engines fueled by either gas or diesel of motor generator sets. The digital controller uses a microprocessor that allows it to operate over a wide range of speeds and its embedded software has a user interface to allow access to all of the features of the controller. When this controller is properly tuned to the

motor generator set, speed or load changes will be rapidly delivered by the engine all the while providing stable isochronous operation. The controller response times are adjustable via distinct adjustable Proportional, Integral, and Derivative (PID) gains which proves a way to tailor a unique response to and motor generator set application. The controller software allows adjustment of acceleration and deceleration ramp rates, startup and torque limits, idle speed, and idle hold times. The governor specifications are found in Appendix 6.

*Voltage and Frequency Disturbance Controls* – The DG is designed to provide stable operation by use of its AVR and governor controllers, which are used to oppose and limit disturbances. Therefore, it is not possible to test the PV inverter's response to disturbances of frequency and voltage at the DG output terminals without modification of how the AVR and governor received control signals and feedback. Consequently, their inputs that they use for control had to be modified by a custom-built microprocessor-based controller which allowed for the repeatable manipulation of their control signals. By use of a variac, the sensing input voltage for the AVR could be bucked or boosted allowing for externally biasing the set-point control. To accomplish this change, the microcontroller circuit energizes several relays to switch in the variac that allows for the modification of the sensing input with the original sensing path being disconnected. Control of the governor is again manipulated by the microcontroller circuit by means of a relay, which applies a signal to the governor which forces the controller to use its secondary speed setting. Figure 2.6 below is an image of the controller.



Figure 2.6 Frequency and Voltage Disturbances Controller.

## **Chapter 3: Diesel Generator Modeling and Testing**

The diesel generator consists of the diesel engine and the electric synchronous generator (SG), and these are coupled through a mechanical drive train, depicted by a block diagram in Figure 3.1 below [37]. The figure also shows the mathematical model of both mechanical and electrical subsystems including speed governor, fuel actuator, combustion, engine rotating parts, automatic voltage regulator, exciter, and synchronous generator. The DG's dynamic reaction to rapid load variations is dictated by the exciter and governor control loops which include the mechanical and electrical parameters of DG subsystems. While the generator electrical parameters are known, those associated with the AVR and speed control loops are often unknown. To develop a simulation, some of these unknown parameters of the AVR and speed control loops need to be estimated, which can be accomplished by certain tests given the right test set-up conditions. [38]. The same procedure proposed in this latter reference is to estimate the values of the governor and voltage regulator parameters; namely, (a) preparing a number of the experimental tests on the DG under various load conditions, (b) performing these tests and recording the system response in terms of frequency and voltage deviations, (c) developing a computer model of the DG set using Matlab-Simulink software, (d) simulating the tests defined above and adjusting the associated parameter values until the simulated curves closely match the measured ones.

### **3.1: Generator Dynamic Model**

The block diagram of the generator is shown in Figure 3.1 and consists of two main parts, the diesel engine, and the driven synchronous generator. Linked by a shaft, the electrical frequency of the generator is a function of the engine's speed and rotor pole pairs.

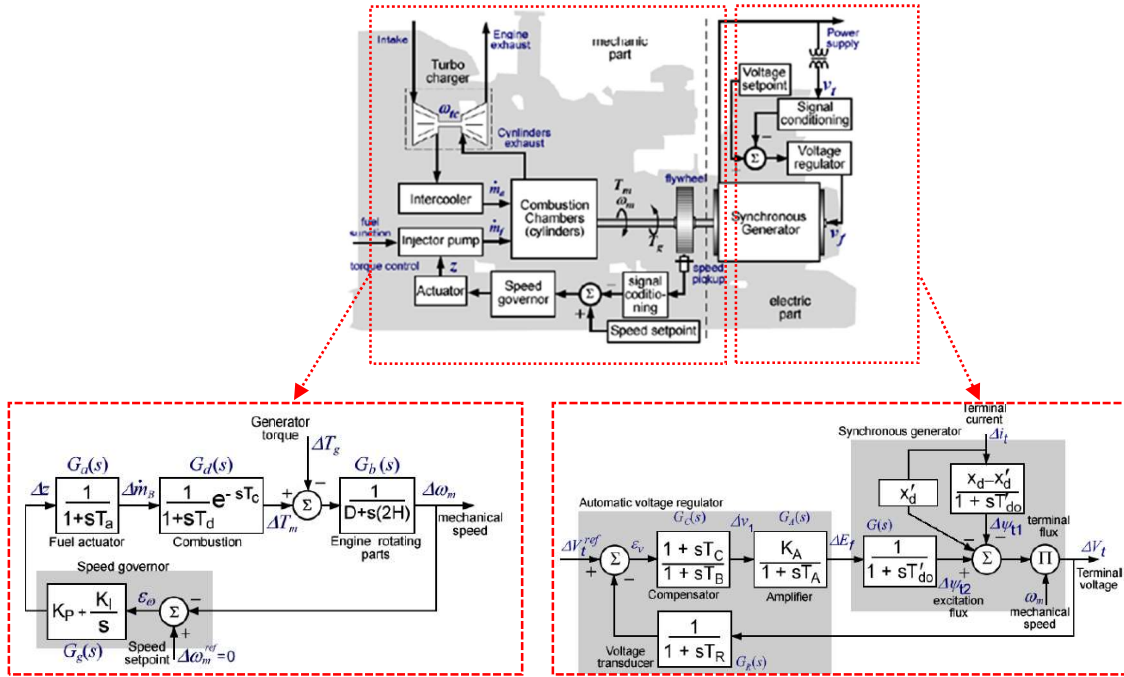


Figure 3.1 Diesel Generator Block Diagram with Mechanical and Electric Subsystem [37].

$$2\pi f_e = n_p \omega_n \quad (3.1)$$

To maintain a constant mechanical engine speed ( $\omega_m$ ), therefore a constant electrical frequency ( $f_e$ ), the governor applies or removes fuel via a throttle body fuel actuator. The speed that the governor tries to maintain is set by the user via software and is detected via a fly wheel sensor, which counts the number of teeth passing by it in a set time interval.

The synchronous generator is a three-phase generator with an AVR which measures the terminal voltage, sampled on phase A, and will decrease or increase the field voltage ( $V_f$ ) to maintain the phase voltages, the voltage set in the AVR. As the load varies, it will induce a



voltage and speed change in the generator and motor to which the governor and AVR will vary fuel and field voltage to maintain a constant frequency and voltage. The parameters from the manufacturer of the generator and motor are used in the following models, found in appendix 3.

### 3.2: Automatic Voltage Regulator Model

With the field connections hard to access, the ability to measure  $V_f$  directly is problematic, therefore tests are chosen to isolate certain parameters that control the predominant transient behaviors in the AVR, and therefore we can indirectly measure the quantities of the AVR, gain ( $K_A$ ), time constant ( $T_A$ ) [37].

Using the approximations of the round rotor, constant field current, balanced phase voltages and currents, then the q-axis voltage  $V_q$  is the stator voltage, or the terminal voltage.

$$v_q = \frac{\omega}{\omega_s} V_E - R_a i_q - (L_s \frac{d}{dt} i_q + \omega L_s i_d) \quad (3.2)$$

If the load of the generator is a purely reactive load, then  $i_q$  will be zero further reducing the equation to

$$v_q = V_t = \frac{\omega}{\omega_s} V_E - \omega L_s i_d \quad (3.3)$$

Where  $i_d$  is the phase current which when the load changes will cause a  $\Delta V_t$  with no  $\Delta \omega$ . The  $\Delta V_t$  will be sensed by the AVR and produce a  $\Delta V_E$  via the field voltage and field current.

$$V_E = \omega_s L_{af} I_f \quad (3.4)$$

The AVR modulates  $V_f$  to try and maintain a fixed terminal voltage ( $V_t$ ). Physical inspection of this device and the data sheet, the AVR is a rectifier, with a proportional and integral

amplifier. The voltage at the terminal and the reference voltage is compared and the difference error is used to produce a correcting field voltage, ( $\Delta V_f$ ). Examining the IEEE standard 421.5 [39], the model that most closely represents the AVR is the ST1C type, a DC excitation system. A simplified diagram is presented in Figure 3.2 with the power stabilizer and field current/voltage limiters ignored. During testing the system transient must not exceed any limiter for the simplified model. The time constants  $T_R$  and  $T_A$  are also neglected by assuming a fast operation of the AVR, thousands of a cycle, and the compensator block is removed due to the AVR not having it present in its design. The rectifier/amplifier is modeled by a Proportional Integral (PI) controller with a static gain  $K_A$ ,  $K_I$ , and a time constant  $T_A$ .

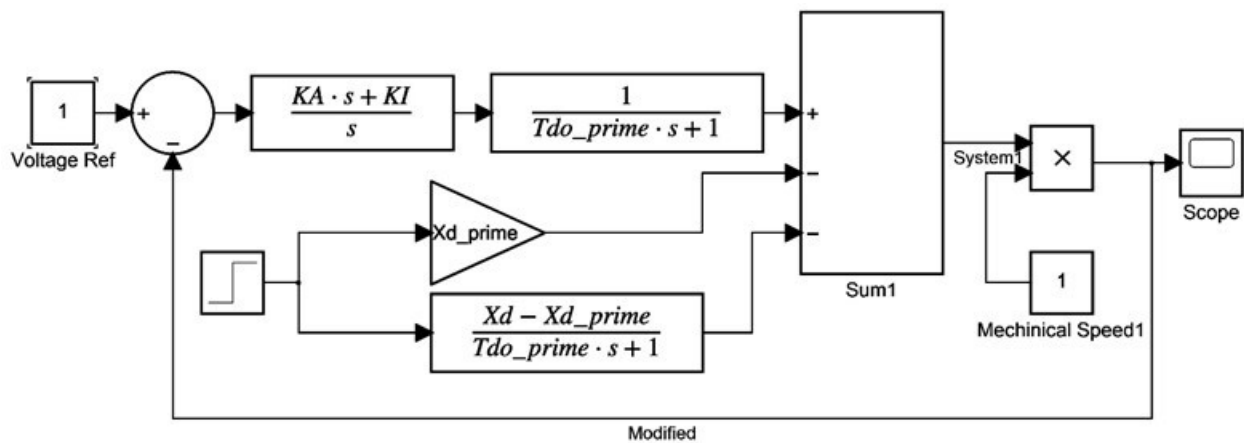


Figure 3.2 Automatic Voltage Control Model.

### 3.3: Governor Control Model

Figure 3.1 shows a simplified model that represents most of the dynamic performance of a diesel engine taking into account the following. The throttle actuation, the combustion cycle, the engine's moving parts, and the governor.

The fuelling actuator is modeled as a first-order transfer function with a time constant.

$$\frac{1}{T_a s + 1} \quad (3.5)$$

The engine's combustion process is modeled by the time delay term which represents the average time between a fuel flow actuation and the subsequent power stroke.

$$\frac{e^{-sT_c}}{T_d s + 1} \quad (3.6)$$

To derive a simplified model of the combustion process,  $T_d$  representing between fuel addition and combustion, a zero-order Padé approximation of the combustion term as given by

$$e^{-sT_c} \approx 1 \quad (3.7)$$

$$\frac{e^{-sT_c}}{T_d s + 1} \approx \frac{1}{(T_d s + 1)} \quad (3.8)$$

The rotating parts model is driven using a droopless model, represented by  $D=0$ , for the small system, with  $H$  representing the inertia of the rotating parts, a value easily obtained from the engine manufacturer, the block of the rotating parts can be simplified to

$$\frac{1}{D + s(2H)} = \frac{1}{s(2H)} \quad (3.9)$$

This leads to the following block model shown in Figure 3.3,

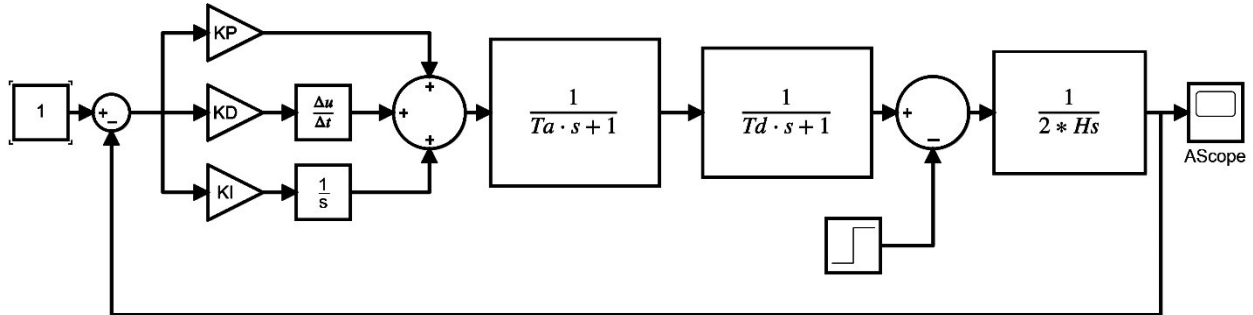


Figure 3.3 Governor Control Model.

The governor, the speed control device, of the diesel engine is a Woodward DPG-2223-001. It is a microprocessor-based, digital controller and allows adjustment of all the controller functions. To provide isochronous operation, the governor senses and reacts quickly to speed changes. The governor is a Proportional( $K_P$ ), Integral( $K_I$ ), and Derivative( $K_D$ ) (PID) gain device and includes the setting for idle speed and hold time, engine ramp rates of acceleration and deceleration, and startup and torque limits. The characteristic equation for the engine speed sensor, the throttle solenoid and governor (PID) is given by the following equation.

$$\frac{K_D s^2 + K_P s + K_I}{s} \quad (3.10)$$

$T_a$  and  $T_d$  are the response times of the solenoid and sensor and  $K_p$ ,  $K_d$ , and  $K_i$  are the gains of the PID controller. From figure 3.2 we can develop the characteristic equation for this feed back loop.

$$2T_a T_d H s^4 + 2H(T_a + T_d)s^3 + (2H + K_d)s^2 + K_p s + K_i \quad (3.11)$$

This is a 4 order system in which a fast response is required for stability and some overshoot and oscillation is acceptable. Therefore all the poles need to be located in the right-hand plane with the 2 dominant poles being located near the axis.

Figure 3.4 shows the governor model with both governor and AVR models included controlling a synchronous generator model.

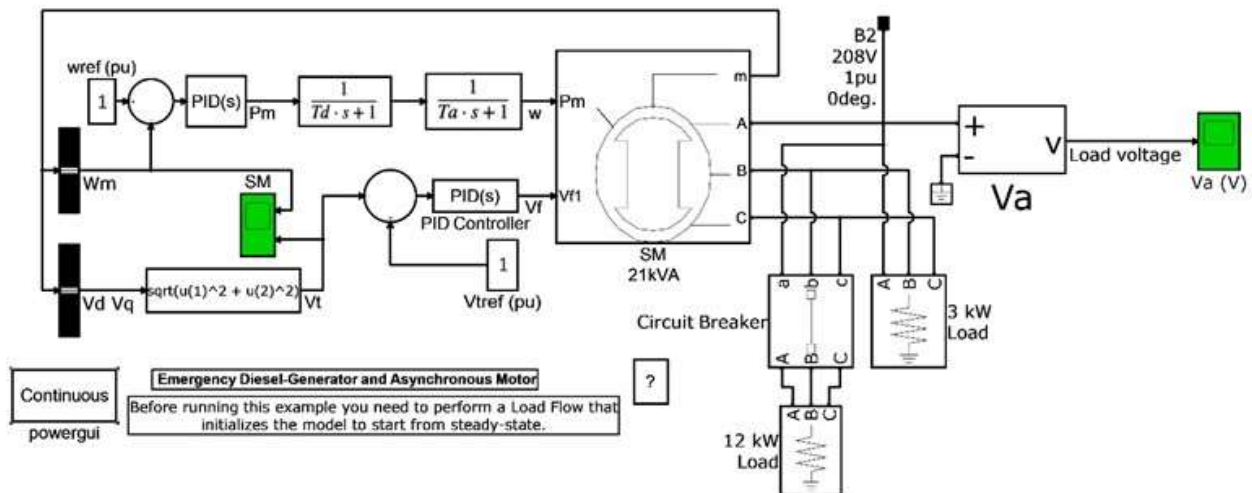


Figure 3.4 Complete Generator Model with Controls.

### 3.4: Generator Response to Load Acceptance and Rejection

Covered in this section is how when the load changes what frequency and voltage deviations will occur when the generator is in stand-alone mode, no other sources or utility grid, the load is supplied entirely by the generator. The stability of this system is expected if the electric power use is less than the rated output of the DG. Sudden load changes will exhibit the mechanical and electrical characteristics of the motor generator sets components which include the voltage exciter and speed governor control loops. To ascertain how a PV system will react to sudden load changes, it is critical to know and understand the frequency and voltage deviations. The frequency and voltage deviations from a 12kW load rejection (loss of load) are shown below in Figure 3.5 with the axis scale in 60 Hz cycles. Consider that the voltage first rises to a maximum of 140 V (16.6% above nominal) while during the same time the frequency jumped by 2.5%, due to lack of mechanical load, before dipping by 1.5% of nominal, these variations are due to the governor characteristics as it tries to maintain 60 Hz operation. The PV inverter would probably disconnect due to these significant deviations in both voltage and frequency. A 9 kVAR load acceptance (gain of load) is shown in Figure 3.6 below, in which the frequency deviation was small, due to small real power consumption of the load, but the dip in the phase voltage was 33% of nominal (40V) during the sub transient period and by 16% of nominal (20V) during the transient period.

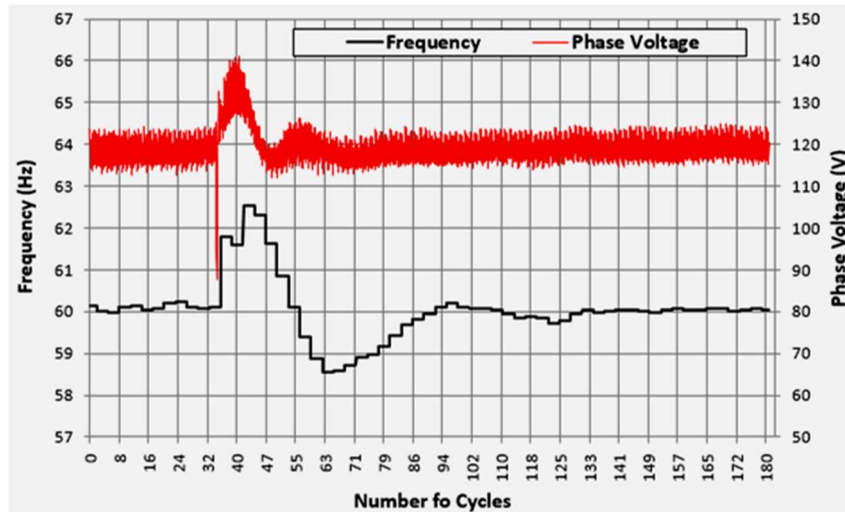


Figure 3.5 Frequency and Voltage Deviations Due to 12 kW Resistive Load Elimination [33]

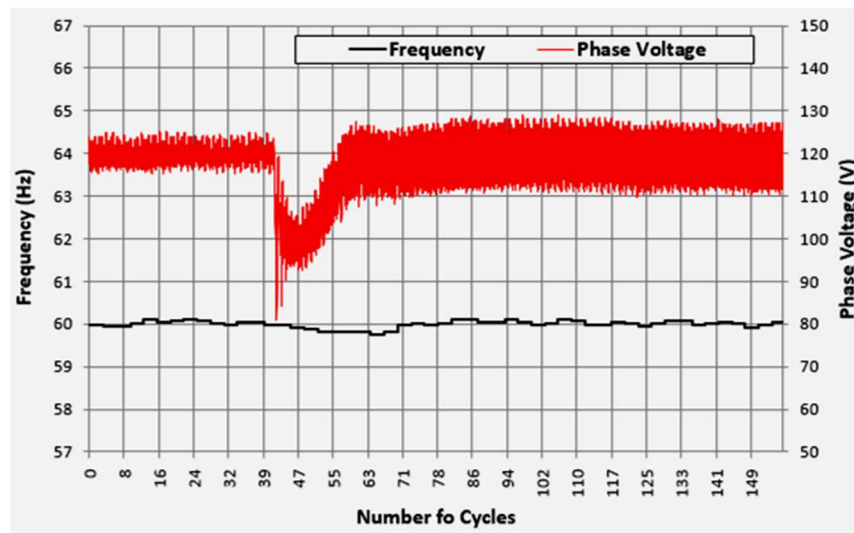


Figure 3.6 Frequency and Voltage Changes Due to 9 kVAR Inductive Load Addition [33]

Figure 3.7 shows both the simulated and measured voltage for a 12kW load rejection. The output of the system shows an underdamped step response, a damping ratio to be less than 1, with a settling time of .9 second and an overshoot of 4%.

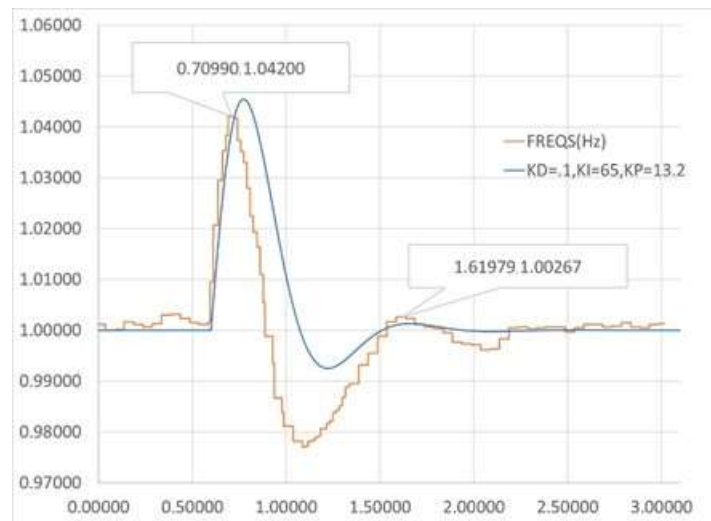


Figure 3.7 Simulated and measured voltage for 12 kW resistive load rejection.

Using the equations for settling time ( $T_s$ ) and natural frequency ( $\omega_n$ )

$$T_s = \frac{4}{\zeta * \omega_n} \quad (3.12)$$

$$\omega_d = \omega_n \sqrt{1 - \zeta^2} \quad (3.13)$$

We calculate the following values, which will give the correct general response.



$$\omega_n = 8.14 \text{ and } \zeta = .53 \quad (3.14)$$

Giving the placement for the two dominating poles as

$$s = -\sigma \pm j\omega_d = -4.36 \pm j6.98 \quad (3.15)$$

For the 4 poles to be in the right-hand plane the following conditions must be met,

$$\frac{K_p(T_a + T_d)(2H + K_d) - K_p T_a T_d - 2H(T_a + T_d)K_i}{(T_a + T_d)(2H + K_d) - T_a T_d K_p} > 0 \quad (3.16)$$

$$2HT_a T_d > 0 \quad (3.17)$$

$$2H(T_a + T_d) > 0 \quad (3.18)$$

$$K_i > 0 \quad (3.19)$$

To calculate  $T_d$ , we must look at the four-stroke engine and the way the engine converts fuel into mechanical power. The engine fundamental frequency is determined by half of the number of engine rotations since each cylinder is fired once for every two rotations of the crankshaft, it can be shown that engine fundamental frequency is given by:

$$\omega_n = \frac{\text{rotation speed}}{2} * 3 \text{ cylinders} \quad (3.20)$$

With 60 rpm = 1 revolution per second, or 1 Hz, an engine connected to a 4-pole generator trying to maintain 60Hz with a speed of 1,800rpm. Therefore, the  $T_d$  time constant is given by

$$T_d = \frac{1800rpm * 3 cylinders}{2 * 60rpm} = 45Hz \text{ or a period of } 22.2 \text{ milliseconds} \quad (3.21)$$

From the fuel actuator used in the design, we get a value for  $T_a$  as 45 milliseconds, this is the time listed for 64% of travel length, from the data sheet.

Using the simplified block model diagram, Figure 3.2, of the engine used to compare the data.

With the following parameters,  $K_i = 65$ ,  $K_d = 0.1$ , and  $K_p = 13.2$ , set into the Woodward governor, represented by the PID controller, the graph in Figure 3.7 was able to closely match the collected data for the case of a 9 kVAR load acceptance. The discrepancies are easily described by items not modeled, the parasitic losses in the system, and throttle body restrictions. The output of the system shows an almost critically damped step response, a damping ratio slightly less than one, with a peak time of 56 milliseconds and an overshoot of 4%.

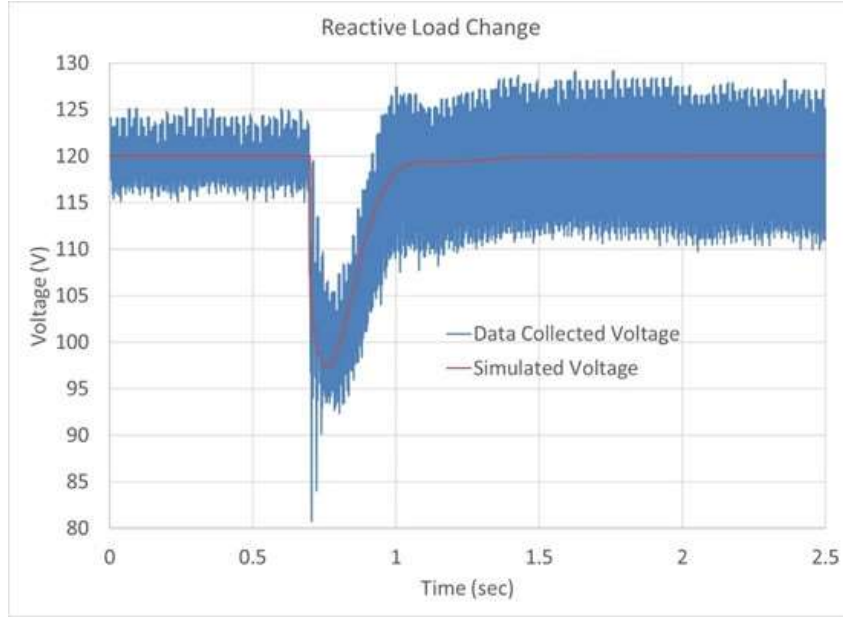


Figure 3.7 Measure and Simulated Voltage for 9 kVAR Load Acceptance.

The transfer function for the model is derived to be

$$V_t(s) = \frac{(K_A s + K_I) - I_D(s)[x'_d \cdot s \cdot (T'_{do} s + 1) + s(x_d - x'_d)]}{T'_{do} s^2 + (K_A + 1)s + K_I} \quad (3.22)$$

We can see that the characteristic equation for this feed back loop is

$$s^2 + \frac{(K_A + 1)}{T'_{do}} s + \frac{K_I}{T'_{do}} \quad (3.23)$$

With

$$\omega_n^2 = \frac{K_I}{T'_{do}} \quad (3.24)$$

And

$$2\zeta\omega_n = \frac{(K_A + 1)}{T'_{do}} \quad (3.25)$$

Using the methods in the paper referenced, the user manual for the AVR, and the manufacturer's data for the generator, the gains for  $K_A$  and  $K_I$  were found to be 15 and 73 respectively.

## Chapter 4: PV System Modeling and Testing of Inverter Autonomous Functions

This chapter summarizes more advanced inverter experimental test results and several of its autonomous functionalities including *dynamic Volt/VAR control*, *soft-reconnect*, *non-unity PF*, *OUF ride through*, and *OUV ride through*. Since PV and grid simulators were not available at the test site, the investigator used physically built and fielded PV system with local generation for testing. Section 1 is a brief review of the PV array and circuit models with Section 2 covering grid interconnection standards. The experimental setup and test plan are addressed in Section 3 with Section 4 describing how the inverter parameters are adjusted. Section 5 describes the reason and method of the five functionalities above along with the test results.

### 4.1: Photovoltaic System and Inverter Model

A model of an ideal solar cell uses an ideal current source  $I_L$  and a diode in parallel but to represent the non-ideal aspects of the solar cell, a series resistor and shunt resistor are added to the ideal model. The ideal source represents the photo-generated current of the solar cell while the diode represents the p-n junction of the solar cell, this circuit is shown in Figure 4.1 below [40].

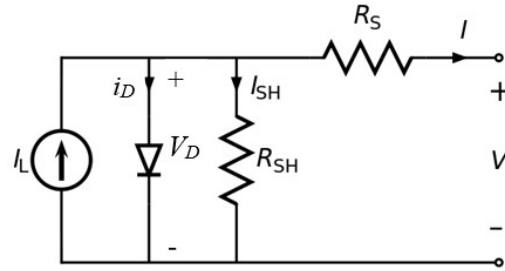


Figure 4.1 A Solar Cells Equivalent Circuit.

Herein,

- $V$  = the solar cells terminal voltage,
- $I$  = the solar cells terminal current,
- $I_L$  = photo-generated current,
- $V_D$  = voltage across the diode,
- $I_D$  = the current through the diode,
- $I_{SH}$  = current through the shunt resistor,
- $R_{SH}$  = shunt resistor,
- $R_S$  = series resistance.

It is evident from the equivalent circuit above that the solar cells' current output is the photo-generated current minus the diode current and shunt resistor current:

$$I = I_L - I_D - I_{SH} \quad (4.1)$$

Using Ohm's Law, the relationship of the cells diode and terminal voltage related to the shunt and series resistors currents is given by:

$$I_{SH} = \frac{V_D}{R_{SH}}, \quad V_D - V = IR_S \quad (4.2)$$

Finally, substituting equations (4.2) into (4.1) one can derive the solar cells characteristic equation:

$$I = I_L - I_o \left( e^{\frac{q(V+IR_S)}{nkT}} - 1 \right) - \frac{V + IR_S}{R_{SH}} \quad (4.3)$$

Note that the above equation has no general analytical solution (i.e., transcendental function) due to cell current being on both sides of the equation but by using a numerical method, it is solvable.

Not connecting the solar cell terminals to any electrical circuit, it is said to be open-circuited, i.e., when  $I = 0$ , with the corresponding voltage at the solar cells terminals defined as the *open-circuit voltage* ( $V_{OC}$ ). The second term found in the right-hand side of equation (4.3) above can be neglected since it is relatively small when compared to the first term and by utilizing this simplification, the open-circuit voltage value is given by:

$$V_{OC} \approx \frac{nkT}{q} \ln \left( \frac{I_L}{I_o} + 1 \right) \quad (4.4)$$

When a short is placed across the outputs of the solar cell,  $V = 0$ , the current through the short is defined as the *short-circuit current* ( $I_{SC}$ ). For solar cells that are of high quality, it can be shown that the short-circuit current  $I_{SC}$ , due to a low  $R_S$  and  $I_o$  and a high  $R_{SH}$ , is approximately equal to the photo-generated current:

$$I_{SC} \approx I_L \quad (4.5)$$

The solar cell terminal current-voltage curve, or I-V curve, is defined by the relationship of 6 variables as defined above (i.e.,  $I_L$ ,  $T$ ,  $R_S$ ,  $R_{SH}$ ,  $I_o$ , and  $n$ ). These parameters depend on the design of the solar cell and the solar irradiance powering the solar cell. The effect on the I-V curve for each parameter is well documented.

One solar cell produces only a few watts of power at a voltage of 0.5-0.6 V. By wiring cells in series to form a PV module, a larger voltage with the same current as a single solar cell is achievable. Today's PV modules can generate over 400 W of power under Standard Test Condition (STC). Multiple PV modules can be wired in parallel to increase the output current or can be wired in series to increase the output voltage and form a PV array of any desired size. The voltage of an array that is composed of  $m$  series-connected modules, each containing  $n$  cells is determined by

$$V_{string} = m \cdot n \cdot (V_D - IR_S) \quad (4.6)$$

The grid-tied inverter converts the DC power produced by a PV array into AC power and in addition to DC-to-AC power conversion, the inverter performs numerous other functions including tracking and operating at maximum power, providing a sinusoidal current waveform with limited distortion, and synchronizing with the grid voltage supply and disconnecting in case of disturbances in the electrical grid. Figure 4.2 shows a typical circuit diagram of a single-phase inverter that consists of a capacitive filter on the DC side, a modified square-wave inverter, a transformer designed for high-frequencies which is used for voltage amplification and galvanic isolation, a full wave bridge rectifier, a DC link capacitor bank for smoothing the rectified



voltage, a sinusoidal PWM inverter, and finally filtering of the high-frequency harmonic components by use of a low-pass filter. For simplicity, the control circuitry, EMI filters, and protection devices are not shown in this diagram.

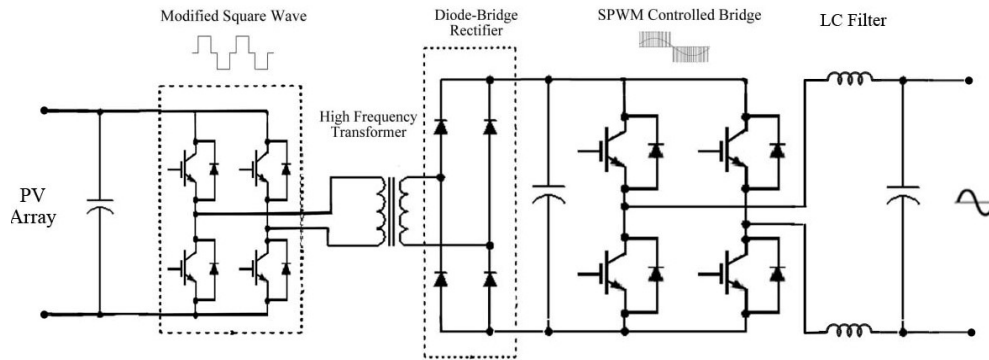


Figure 4.2 Typical Circuit Diagram of Single-Phase Grid-Tied Inverter.

A ratio of peak-to-peak voltage ripple ( $\Delta V_C$ ) to average capacitor voltage ( $V_C$ ) to in DC section of the inverter, after the rectifier, is related to the value of the capacitor ( $C$ ), the AC supplies angular frequency ( $\omega$ ), and the generated output power ( $P$ ) by the following relationship [40].

$$\frac{\Delta V_C}{V_C} = \frac{P}{\omega C V_C^2} \quad (4.7)$$

The above ripple is typically limited to less than 5% and the pulse-width-modulated waveform switching frequency is in the range between 10 kHz and 25 kHz. The resulting AC side

current waveform contains unwanted frequency components and large voltage “spikes” because of fast transition rates,  $dv/dt$ , during switching. These unwanted artifacts caused by the AC waveform generation are filtered out by low-pass and Electromagnetic interference (EMI) filters, as required by interconnection standards, before entering the grid and are reviewed in the subsection that follows. The inverter contains a Maximum Power Point Tracker (MPPT) which allows for maximizing power production based on current solar and weather conditions. Numerous MPPT techniques are available in the literature [41], [42] and the most common ones include perturb-and-observe and incremental conductance methods.

#### **4.2: Review of Interconnection Standards**

Conventional grid-tied PV inverters were originally designed according to IEEE Standard 1547-2003 which was developed under the assumption that such distributed resources represent just a small fraction of the load. These inverters were not allowed to ride through disturbances in the utility voltage or frequency and were not allowed assist in voltage regulation through reactive power generation/absorption at the point of common coupling (PCC). However, PV penetration is reaching a significant level in some distribution systems throughout the US, especially in some parts of the State of California. Such large numbers of PV systems are placed in unplanned locations, and their fluctuating responses to weather conditions are having a noticeable impact on distribution system operation and service reliability. This has led to a universal call to include new inverter capabilities and functions that will allow inverters to support distribution grid operations and update the interconnection standard under high PV penetration [20]–[23]. Table 4.1 below lists the new default as well as adjustable clearing times for voltage deviations of the new PV inverters. Table 4.2 lists the corresponding clearing times for frequency deviations.

Table 4.1 Original and Revised Interconnection Standard Dealing with Ride Through Times to Irregular Voltages [20].

| Default settings <sup>a</sup>                   |                   |   |
|---|-------------------|---|
| Voltage range (% of base voltage <sup>b</sup> ) | Clearing time (s) | Clearing time: adjustable up to and including (s) |
| $V < 45$  | 0.16              | 0.16  |
| $45 \leq V < 60$                                | 1                 | 11  |
| $60 \leq V < 88$                                | 2                 | 21  |
| $110 < V < 120$                                 | 1                 | 13  |
| $V \geq 120$                                    | 0.16              | 0.16  |

<sup>a</sup> Under mutual agreement between the EPS and DR operators, other static or dynamic voltage and clearing time trip settings shall be permitted

<sup>b</sup> Base voltages are the nominal system voltages stated in ANSI C84.1-2011, Table 1.

Table 4.2 Original and Revised Interconnection Standard Dealing with Ride Through Times to Irregular Frequencies [20].

| Function | Default settings |                   | Ranges of adjustability |  |
|----------|------------------|-------------------|-------------------------|--|
|          | Frequency (Hz)   | Clearing time (s) | Frequency (Hz)          | Clearing time (s) adjustable up to and including |
| UF1      | < 57             | 0.16              | 56 – 60                 | 10   |
| UF2      | < 59.5           | 2                 | 56 – 60                 | 300  |
| OF1      | > 60.5           | 2                 | 60 – 64                 | 300  |
| OF2      | > 62             | 0.16              | 60 – 64                 | 10   |

IEEE Std. 1547-2018 describes inverter advanced functions including Volt/VAR control, frequency/watt control, dynamic reactive power support, and ramp rates. It also addresses best practices when operating with numerous inverters and microgrids, advanced controls of

inverters, transmitted/received data by inverters supporting the grid, offers the newest information for Distributed Energy Resource (DER) group conduct, interactions with grid hardware/software, and the interconnected system reaction to irregular conditions.

Prior to the publication of the above IEEE Standard, the 3 major investor-owned utilities in the state formed a Smart Inverter Working Group (SIWG) to develop quickly the practical steps needed to improve how distributed energy generation is to support the operation of the distribution system while upholding the standards of dependable and safe service [22]. SIWG proposed the following inverter response to abnormal voltage deviations in Table 4.3 and frequency deviations in Table 4.4.

Table 4.3 CA Rule 21 Inverter Response to Abnormal Voltages [22].

| Lim | Voltage Level Multiplier of Nominal Voltage | Stay Connected Until                      | Lim | Voltage Level Multiplier of Nominal Voltage | Disconnect by     |
|-----|---|---|-----|---|-------------------|
| c   |   |   | d   | >1.2  | < 0.16 sec.       |
| c   | 1.09-1.17                                   | 12 sec.                                   | d   | 1.1 - 1.2                                   | 13 sec.           |
|     | 0.92-1.09                                   | Indefinite                                |     | 0.88 – 1.1                                  | Do not disconnect |
| b   | 0.7 – 0.92                                  | 20 sec.                                   | a   | 0.6 – 0.88                                  | 21 sec.           |
| b   | 0.5 – 0.7                                   | 10 sec.                                   | a   | 0.45 – 0.6                                  | 11 sec.           |
| b   | 0 – 0.5                                     | 1.0 sec. (range between 0.16 to 2.0 sec.) | a   | 0 – 0.45                                    | 2.5 sec.          |

Table 4.4 CA Rule 21 Inverter Response to Abnormal Frequencies [22].

| System frequency     | Default Frequency settings (Hz) | Range of adjustability (Hz) | Default clearing time (s) | Range of adjustability (s) |
|----------------------|---------------------------------|-----------------------------|---------------------------|----------------------------|
| $f > 62$             | $> 62$                          | 62 - 64                     | 0.16                      | 0 - 300                    |
| $60.0 < f \leq 62$   | 60.5                            | 60 - 62                     | 300                       | 0 - 300                    |
| $58.5 < 60.5$        | indefinite                      |                             |                           |                            |
| $57.0 < f \leq 58.5$ | 58.5                            | 57 - 60                     | 300                       | 0 - 600                    |
| $f \leq 57.0$        | 57                              | 53 - 57                     | 0.16                      | 0 - 5                      |

For the autonomous *Volt/VAr control* function, several dynamic variables denote the change required in absorption/generation of VARs in response to changes in the local voltage measured at the PCC have been proposed. One piece-wise linear curve with a dead-band that is commonly used for this application is shown in Figure 4.3 below. Hysteresis can be added to such a curve to provide different return routes and dampen unnecessary swings. CA Rule 21 proposed the establishment of Volt/VAR default settings according to the values listed in Table 4.5 where  $\%VAR_{Aval}$  represents the percentage of VARs available from the inverter.

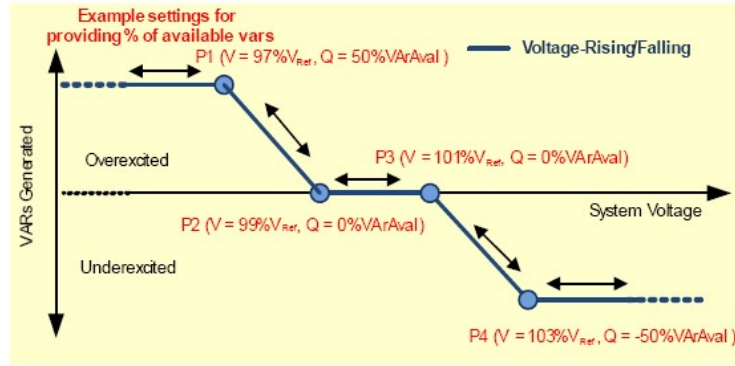


Figure 4.3 Common of Volt/VAR Using Piece-Wise Linear Curve [22].

Table 4.5 CA Rule 21 Default Volt/VAR Control Settings [22]

| Voltage Array<br>(% VRef <sup>20</sup> ) |     | VAr Array<br>(% VArAval <sup>21</sup> ) |      | Settings  | Default Values  |
|--|-----|---|------|---|-----------------|
| V1                                       | 88  | Q1                                      | 100  | VAR Ramp Rate Limit – fastest allowed decrease in VAR output in response to either power or voltage changes | 50 [%VArAval/s] |
| V2                                       | 99  | Q2                                      | 0    | VAR Ramp Rate Limit – fastest allowed increase in VAR output in response to either power or voltage changes | 50 [%VArAval/s] |
| V3                                       | 101 | Q3                                      | 0    | Randomization Interval – time window over which mode or setting changes are to be made effective            | 60 s            |
| V4                                       | 110 | Q4                                      | -100 |   |                 |

### 4.3: Test Plan and Experimental Setup

Testing of an advanced or “smart” inverter generally requires a well-equipped laboratory with PV array simulators, utility grid simulators, and Real Time Digital Power System Simulator (RTDS). In our case, the tests were conducted locally at the microgrid facility described in

Chapter 2 above, which is equipped with real power generation systems instead of simulators. The local test depended on whether or not the inverter can be “fooled” such that it will treat the DG like a local grid. The “smart” inverter that was chosen for testing is SMA’s Sunny Tripower (Model STP12000TL-US) which is equipped with a number of grid management functions which includes the following, abnormal frequency ride-through, abnormal voltage ride-through, reactive power control, ramp rate control, etc. Some technical challenges when using actual PV and generation systems include the following:

- Unlike the PV simulator, the power production of a real PV system depends on weather conditions which change continuously.
- Unlike the grid simulator, a real synchronous generator cannot absorb real power, thus requiring a local load bank. Furthermore, the inverter may not synch to such a weak microgrid due to its advanced anti-islanding techniques.
- The active and reactive powers drawn by a constant impedance load bank depend on both voltage and frequency. Hence, causing a disturbance in the voltage will affect the frequency and vice versa.

In Figure 4.4 below, the experimental setup of the microgrid is shown as a block diagram, which is connected via a 3-phase circuit and contains the following key pieces of equipment:

- A diesel generator rated at 14 kVA, 208 V, 60 Hz, 1,800 rpm,
- A 3-phase advanced inverter rated at 408V and 12 kVA,
- A PV array rated at 12 kW DC rating based on STC,
- A transformer rated at 480V/208 V and 30 kVA, ,
- An inductive load bank (discrete step adjustable) rated at 9 kVAr,

- A resistive load bank (discrete step adjustable) rated at 15 kW
- Utility grid rated at 208 V.

To isolate or connect parts of the circuit or equipment, switches (S1-S4) are used, to record and measure various power quantities (i.e., AC voltage and current in each phase, frequency, the inverters active power generated, and the inverters reactive power generated/absorbed) a power recorder is connected at the transformer on the 208 V side, the microgrid side. The sampling period of the recording device is 500 milliseconds (30 cycles) and an image of the test equipment is shown in Figure 4.5.

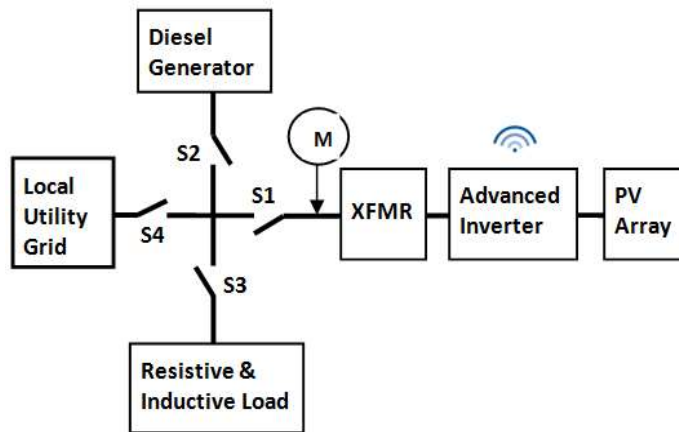


Figure 4.4 Experimental Setup Block Diagram.





Figure 4.5 An Image of the Advanced Inverters Experimental Test Setup.

Contingent on the capabilities of the inverter to be tested, the DG (off-grid) or with the utility grid (grid-tied) can be synched to the PV systems inverter. Inverter tests that do not require frequency or voltage disturbances will dictate the inverter be grid-tied (S1 and S4 in the contact made position, while S2 and S3 in contact break position) which allows for the testing of the *non-unity PF operation* and *soft reconnect* capabilities. Inverter tests that do require frequency or voltage instabilities will dictate the inverter be disconnected from the utility (S1, S2, and S3 in the contact made position, while S4 in contact break position) which allows for the testing of the *Volt/VAr control*, *OUF ride through*, and *OUV ride through* capabilities. The latter operation can be referred to as a “microgrid” or “islanded” operation since the PV system, generator and load form a small electrical system that operates independently from the local utility distribution system.

The inverter parameters are modified by accessing its embedded software settings as described in Section 5 of Chapter 2 and for the five tests mentioned above, parameters associated with each are modifiable over a predefined range, shown in Table 4.6 below, with a discussion of each to follow in the section below.

#### **4.4: Test Procedure and Results**

The purpose, test procedure, and test results of each of the five tests mentioned above are summarized in this section. Due to limited space, test results at different parameter values that had similar results have been omitted.

##### *4.4.1: Soft Reconnect*

*Purpose:* Following a utility outage, if numerous inverter-based generation systems recover concurrently (typically takes seconds to reach maximum power available at that time), they result in a sizeable intake of real power being injected into the utility grid. The aforementioned systems will then cause the feeder to experience an abrupt decline in load as the PV systems go back to nominal operation. The result of this will lead to over-voltages that compromise the stability of the grid, particularly when demand is minimal and when PV generation is elevated. In order to deter this grid disruption from transpiring, system personnel can utilize the functionality of soft reconnect found in advanced inverters which allows for the programming of an offset reconnection in distributed PV systems on a lone feeder circuit. Lengthening the rise time for the maximum real output of a PV plant will allow the systems voltage-controlled equipment the ability to react properly. An alternative way to ameliorate such a sharp transition is to assign different delay times between power restoration and the reconnection, to the different PV

systems on the distribution feeders (instead of having a common delay time with a default of 5 minutes).

Table 4.6 Inverter Software Settings (Parameter, Range, Clearing Times) [29]

| <i>Variable</i>               | <i>Parameter</i>          | <i>Range</i> | <i>Clearing time (sec)</i> |
|-------------------------------|---------------------------|--------------|----------------------------|
| Soft Start                    | <i>Power Rate of Rise</i> | 1%-10,000%   | n/a                        |
| <i>Non-Unity Power Factor</i> | <i>Under-excited</i>      | - 80% – 100% | n/a                        |
|                               | <i>Over-excited</i>       | +80% – 100%  | n/a                        |
| <i>Voltage Ride through</i>   | <i>Upper Voltage</i>      | 277-332.4    | 0.1-60                     |
|                               | <i>Lower Voltage</i>      | 138.5-277    | 0.1-10                     |
| <i>Freq. Ride through</i>     | <i>Upper Freq.</i>        | 60-65        | 0.1-10                     |
|                               | <i>Lower Freq.</i>        | 44-60        | 0.1-300                    |
| <i>Volt/Var Control</i>       | <i>Dead Band</i>          | 1%-2%        | n/a                        |
|                               | <i>Var Limit</i>          | ±40%         | n/a                        |
|                               | <i>Q/V Gradient</i>       | 1%-10%       | n/a                        |

It is worth pointing out that “soft reconnect” is a subset of the inverter’s ramp “*ramp rate*” function. While generating fluctuating power due to moving clouds, the PV inverter ramp-up can be slowed down (as the cloud shade starts to clear the PV arrays), but ramp-down (when cloud shade starts to cover the PV array) cannot be achieved unless it is equipped with an energy storage system. The idea behind the establishment of the ramp-up and ramp-down rates is to assist the utility or local grid smooth its change from one power level to another.

Test Procedure: To verify the ramp-up rate setting of the inverter, the subsequent test procedure will be utilized, which consists of two basic steps. Prior to power generation, a value will be entered into the software of the inverter followed by the activation of the inverter connected to the grid to examine if the selected value matches the power generation rise rate measured. Utilizing the available range in the software, repeat the process for different quantities. For the tested inverter, this ranges in the software between 1% - 1,000% of its rated power for each second (this will be from 0.002 kW/sec. and 2 kW/sec.).

Test Results: Figure 4.6 illustrated below captures the PV real power (kW) production and the variation in the nominal voltage (per unit) in which multiple tests were performed utilizing different output power gradients (ramp rate). In the first part of the figure, it shows the inverter coming online with the inverters software output power gradient parameter set to 10%, 1.2 kW/min, and the maximum power of 8.2 kW was obtained in approximately 7 minutes. The middle part of the figure reveals the inverter coming online after a shutdown of the inverter was performed and the output power gradient was adjusted to 100% or equivalent to 12 kW/min, and it should be noted that it took less than sixty seconds to attain the steady value of 8.2 kW. The last part of the figure depicts the inverter coming online after the output power gradient was adjusted to 1,000%, 120 kW/min, in which the inverter reached 8.5 kW in several seconds. In conclusion, the output power gradient control of the inverter worked as expected, the measure ramp rates matched the software parameter settings.

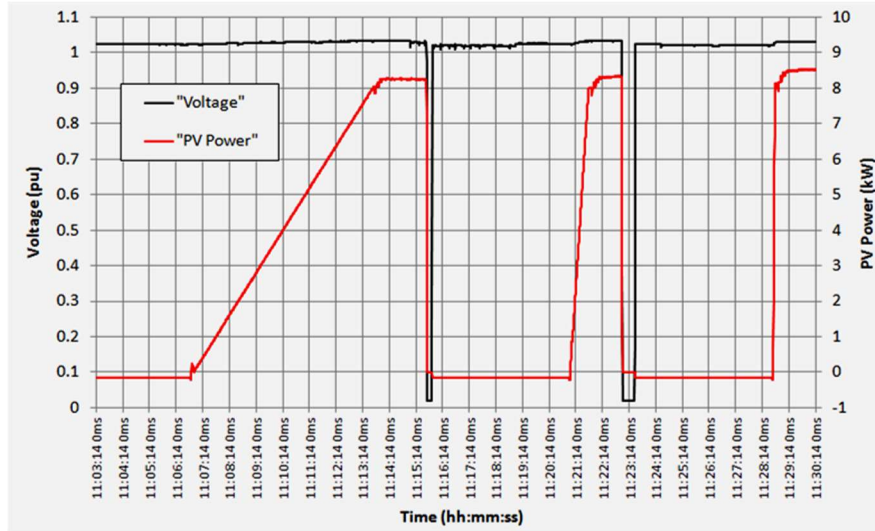


Figure 4.6 Ramp-Up Adjustment (10%, 100%, 1,000%) of Soft-Start Function [29].

#### 4.4.2: Non-unity PF

Purpose: First generation PV inverters were designed to function at a PF of one, however, with their increased use, distribution systems started operating at lower PFs, but with lower losses due to the PV power generation being located close to the load. By shifting the generation of power close to the end of the distribution system, it led to a smaller voltage drop across feeder conductors due to less real power transiting the resistive portion of the feeder, this led to an over-voltage at the head of the distribution feeders. This is due to the system being designed to take the voltage drop into consideration. Overall, this will negatively impact the distribution system operation (less than optimum). Using the PV inverters with a PF less than one (a setting in the inverter) allows for the inverter to help the distribution circuit PF reach unity and assist the utility in voltage support by either absorbing or injecting reactive power.

Test Procedure: The performed tests were comprised of selecting the PF of the inverter between 80% lead (under excited) and 80% lag (over excited). After several minutes of operation at unity PF, the inverter's PF was set to 90% leading followed by successive PF settings at 80% leading, 90% lagging, 80% lagging, and ending in the unity setting.

Test Results: The recorded data are shown below, Figure 4.7, illustrates the generated real power (approximately 8 kW) and the reactive power, negative during absorption (leading) or positive during generation (lagging), and the resulting PF of the tests. Initially, the inverter was configured to operate at unity power but as depicted in the figure, there was approximately 1 kVAR absorbed reactive power. This is found to be due to the probe placement for the test, the reactive power shown was not consumed by the inverter but was consumed by the transformer magnetizing and leakage reactances. The transformer reactive power issue led to recorded PFs being different than the inverter's software settings, but if the component of the transformer's reactive power is removed, the PF parameter adjustment functioned as anticipated.

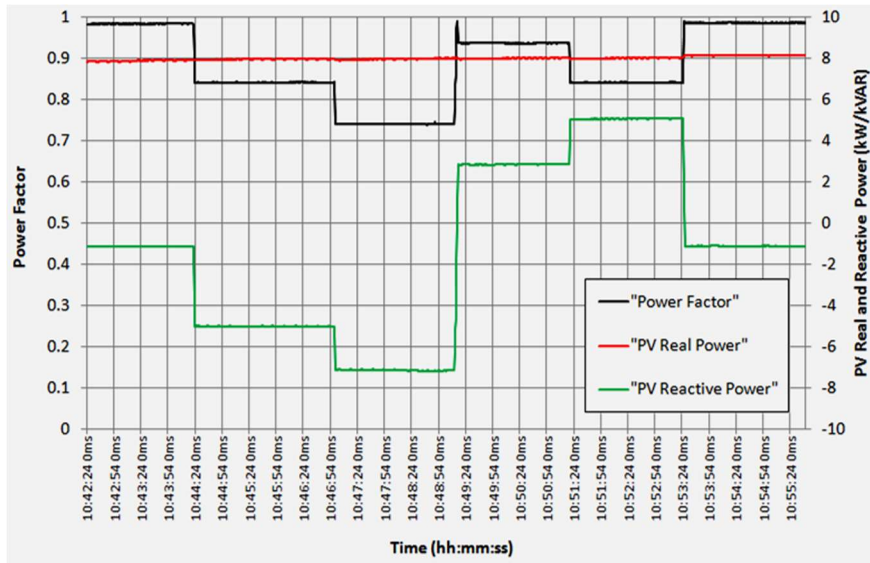


Figure 4.7 PF Adjustment (100%, 90% and 80% Under-Excited and Over-Excited).

#### 4.4.3: Over- and Under-Voltage Ride Through

Purpose: Sudden load changes will cause voltage fluctuations which can result in the voltage to rise/drop beyond regulated nominal voltage limits. While these fluctuations are of short duration, PV systems will be disconnected by such disturbances, as previously required by IEEE Std. 1547. With the sudden loss of PV generation on the feeder, the voltage may be incapable of returning to the nominal value in the regulated time limit resulting in unwarranted power outages. Advanced grid-tied inverters will be able to take advantage of the proposed new ride through time limits regarding high and low voltages or frequency deviations thus reducing the unnecessary disconnects of PV systems and their associated power outages. Therefore, using the amended interconnection standard, the operator can use the voltage-time settings in advanced inverters to best fit their system and provide for increased stability.

Test Procedure: By changing the taps of under-load tap changing transformer (ULTC) voltage disturbances can be induced, however, this type of transformer is typically available at power company distribution substations and obtaining authorization to cause that type of disturbances is highly improbable to be granted since it will impact the local consumer, while they are connected to the same transformer. Consequently, the local grid is emulated by utilizing a 14-kW DG and the load banks, which must be set to utilize more power than is produced by the PV system. The Automatic Voltage Regulator (AVR) experiment set-point is biased, via an external variac, by bucking or increasing the input of the voltage to be detected at the controller. According to IEEE std. 1547, the default values of inverter OUV were set, and its response to different magnitudes and periods of voltage deviations were noted. After disconnecting, the OUV time was enlarged, and once again the experiment was repeated to ascertain whether the inverter will be able to tolerate the disturbances. Table 4.6 delineates the clear times for the voltage levels, lowest and highest, for the tested inverter.

Test Results: The inverter response shown in Figure 4.8 depicts its performance during an eight-second period, in an under-voltage condition of 82%. The inverter tripped immediately with the default setting upon its first disturbance, within 500 milliseconds, then after increasing the inverter ride through time to 15 seconds and under the same voltage conditions, the inverter did not trip. The inverter continued to be online as demonstrated in Figure 4.9 when the voltage is increased or decreased by 90% and 108% of nominal value. The inverter response depicted in Figure 4.10, shows an over-voltage condition duration of 10 seconds that is 112% above nominal. The inverter was defaulted back to its original settings and received a similar response. The initial trip of the inverter transpired right after the disturbance was initiated but after modifying the inverter's ride through time to 15 seconds, it rode through the same disturbance.



Employing the same procedure, the inverter was reset to its default settings, and in Figure 4.11 one can see a similar response to a 117% over-voltage disturbance, therefore, the expected response for the inverter was observed to voltage disturbances.

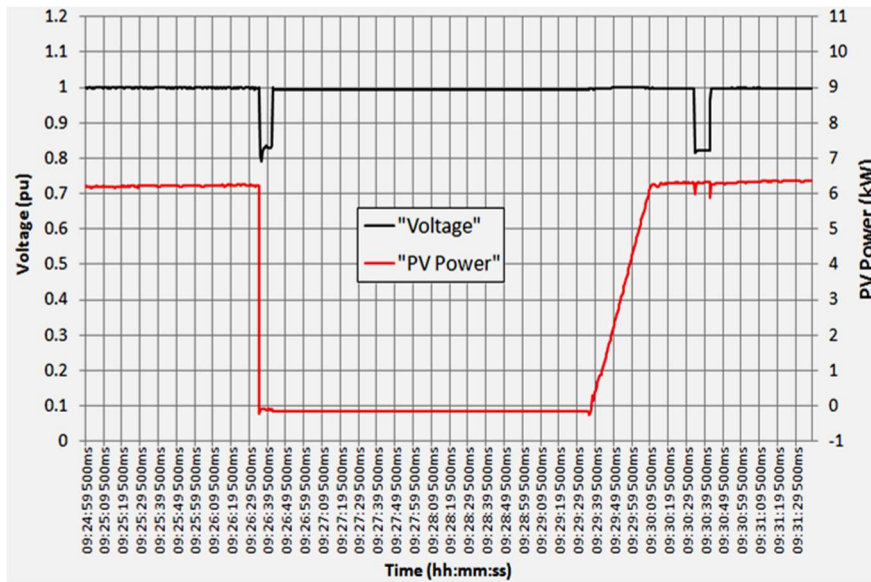


Figure 4.8 Temporary 82% Under-Voltage.

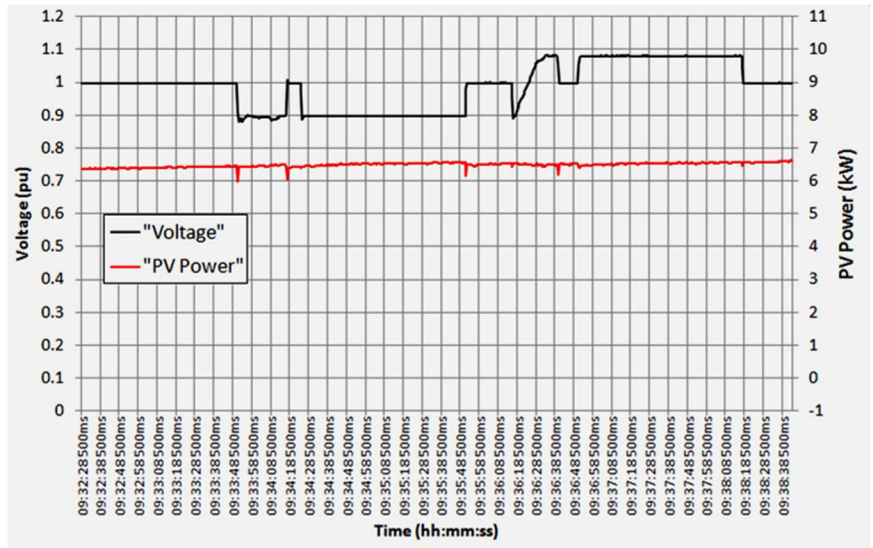


Figure 4.9 Voltage Variation between 90% and 108%.

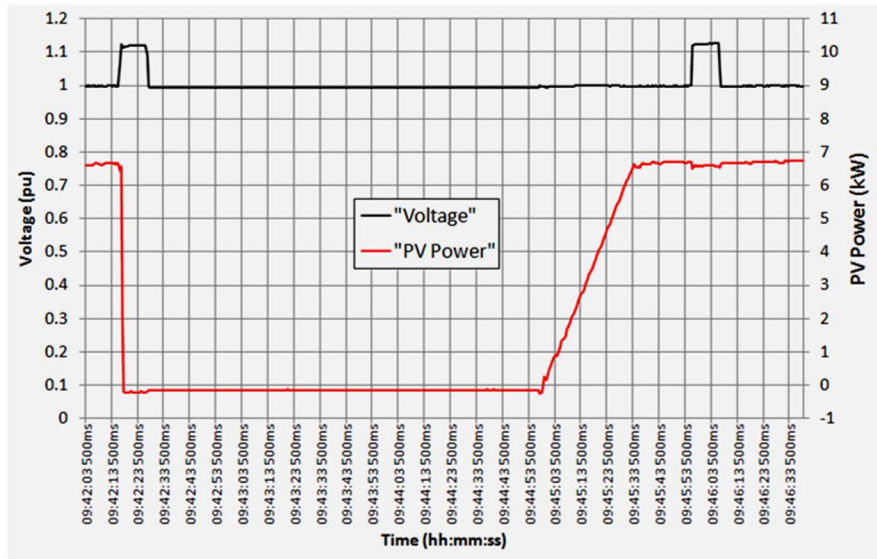


Figure 4.10 Temporary 112% Over-Voltage.

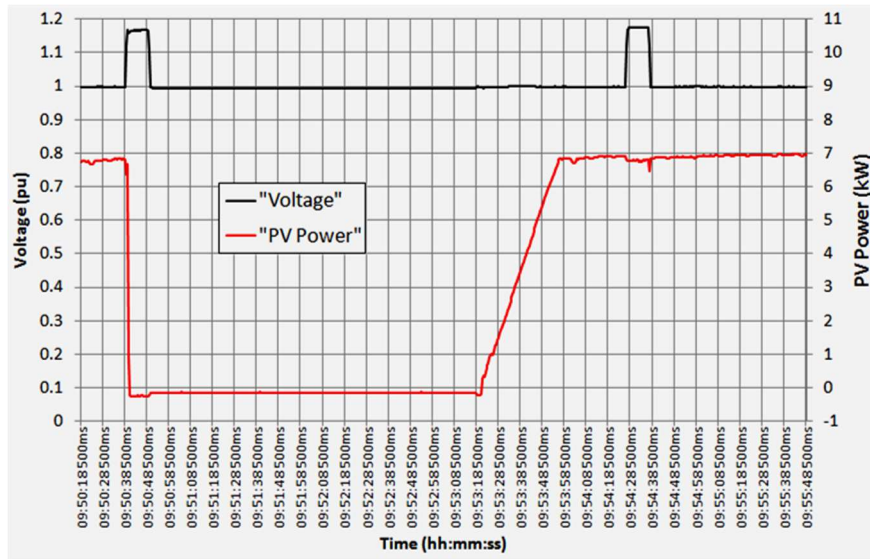


Figure 4.11 Temporary 117% Over-Voltage.

#### 4.4.4: Over/Under Frequency Ride Through

Purpose: The direct cause of under or over frequency deviations is the difference between load and power generation, produced by a variety of reasons that include sudden loss of generated power or an increase/decrease in load. The primary reason of OUF ride through is like the OUV ride through, to allow PV systems to operate during frequency deviations for longer times as specified in [20].

Test Procedure: The test setup is to generate frequency disturbances, and this is accomplished by the use of the micro-controller circuit as described by externally triggering the governor of the diesel generator via a DC control signal which enables the governors second sync speed. The inverters software is set to its default settings, and the inverter response is recorded to a frequency deviation. Using the inverters software, the clearing time was increased

to a value in the allowable range specified in reference and repeated was the same disturbance as before, magnitude and duration.

*Test Results:* The inverters response to a 15 second 58 Hz under-frequency condition is shown in Figure 4.12, the inverter tripped immediately as soon as the deviation was applied to the microgrid. Increasing the inverter's ride through time to 20 seconds, the inverter did not trip to the same disturbance. With the same 20 second inverter software settings, setting the frequency range to 60.5 Hz - 59.5 Hz, the inverter rides through the frequency deviations, Figure 4.13 shows the recorded test results. A 400 millisecond over-frequency condition of 61.5 Hz and the inverters response is shown in Figure 4.14 shows the inverter response, the first half of the figure is the response when the inverter is set to its 2 second default condition and the second half is the inverters response after changing the ride through time to 5 seconds. Similar inverter responses are noted for an over-frequency disturbance of 62.5 Hz as shown in Figure 4.15, with the multiple tests showing that the inverter responds to the software inputted parameter setting regarding frequency ride through time

#### *4.4.5: Dynamic Volt/VAR Control*

*Purpose:* Now that PV inverters are allowed to regulate the voltage through their ability to generate or absorb reactive power, the VAR output can be controlled in many different ways, such as defining a time-based schedule to vary the VAR output, or a function based on the active power output, or a function based on the local voltage. The latter method, referred to as "Dynamic Volt/VAR Control", appears to be most effective and hence attracted a lot of attention for use in areas of high PV usage [43]–[46]. It permits the inverter to either absorb or supply VARs (hence, PF) independently and dynamically to assist in the feeder's voltage regulation and in some applications to help with maintaining Conservation Voltage Reduction (CVR) levels.

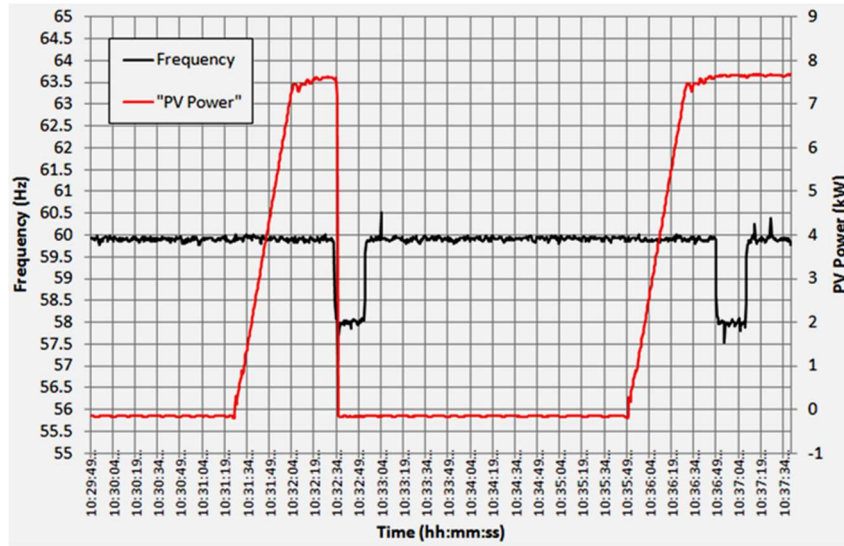


Figure 4.12 Temporary 58 Hz Under-Frequency.

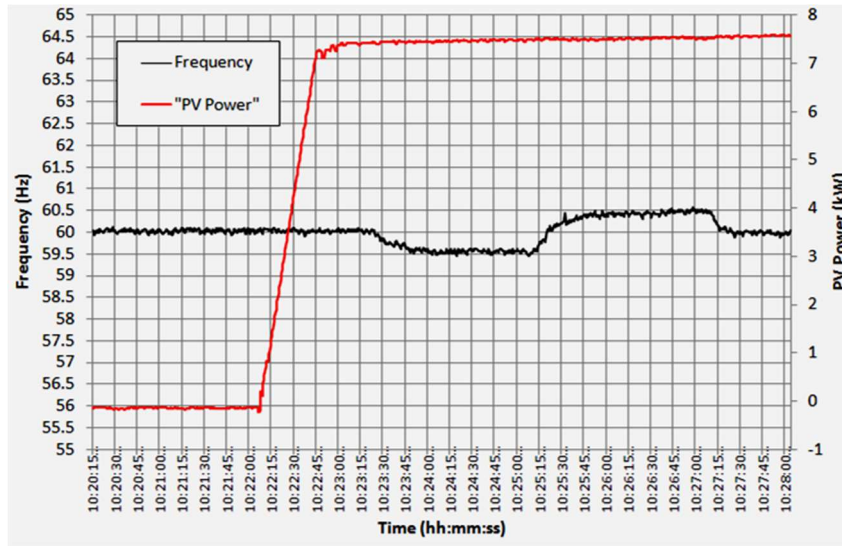


Figure 4.13 Frequency Deviation between 59.5 Hz and 60.5 Hz.

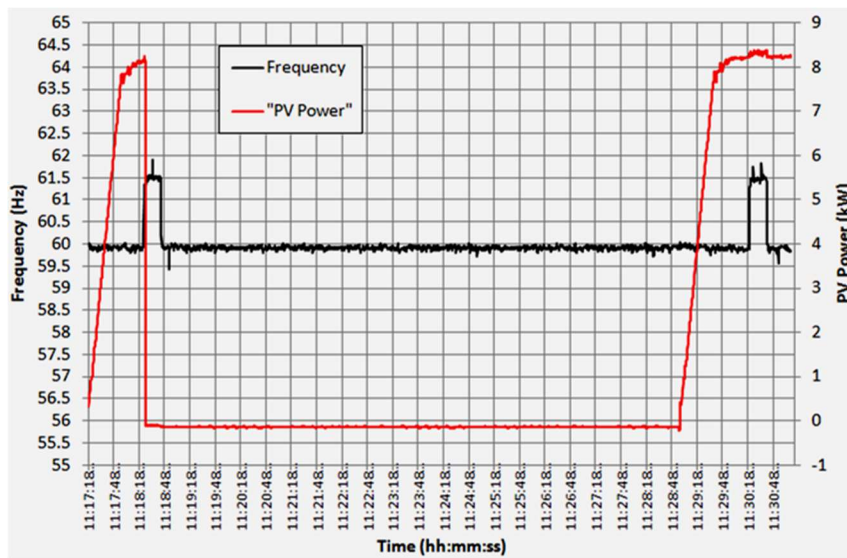


Figure 4.14 Temporary 61.5 Hz Over-Frequency

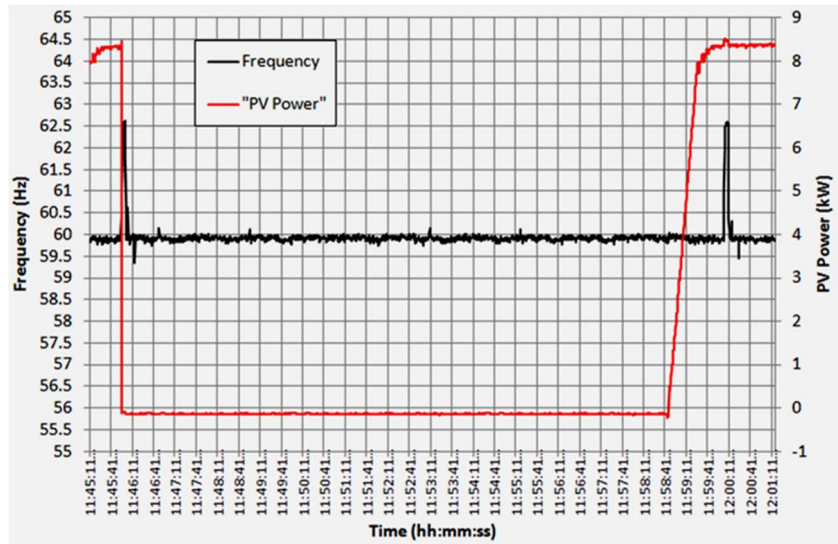


Figure 4.15 Temporary 62.5 Hz Over-Frequency

Dynamic Volt/VAR characteristic “curves” that specify absorption/generation of VARs in response to changes in the local voltage measured by the inverter are well established. Herein, the amount of reactive power is often defined, as to not affect active power production, as a percentage of the “available” VARs. To define how much the reactive power will change as a function of voltage change, the gradient of the curve (Q/V%) is also specified. An area around the nominal voltage is defined as the dead band and is often included in the curve - sometimes with hysteresis - to reduce unnecessary fluctuations.

*Test Procedure:* To test the advanced inverter dynamic Volt/VAR control, the parameter settings in the inverter software were programmed to generate the following volt/VAR curve, dead band =  $\pm 1\%$  of nominal voltage, the slope of the VAR-to-voltage curve set to 4%, and of the available reactive power = 50%. The inverter generating 8 kW during the test, makes 9 kVARs of reactive power available, so the 50% setting limited the maximum reactive power generation

to  $\pm 4.5$  kVARs. With the slope set to 4%, it meant that 0.35 kVARs would be produced for each 1% deviation of voltage beyond nominal, and the dead band would mean the voltage have to reach either .98 or 1.02 pu before reactive power would be generated. To verify the Volt/Var control feature was working as programmed, the voltage of the DG would be increased and decreased in 1% increments via the microcontroller circuit, while the VARs being generated or absorbed by the inverter would be recorded.

Test Results: Shown in Figure 4.16 is the inverters response to a voltage change and the reactive power absorbed or supplied by the inverter, the voltage was raised to 1.065 pu, and the reactive power decreasing down to -3.7 kVARs. Then the voltage was lowered to 0.89 pu with the reactive power increasing to +2 kVARs and by removing the reactive power consumed by the transformer, the test results have an agreement between the programmed and measured values. As shown in Figure 4.17, the inverter VARs in reaction to a burst of over- and under-voltages that last nearly 20 seconds, where the inverter responded almost instantaneously by injecting or absorbing reactive power to compensate for such voltage deviations. The above compensation did not affect the voltage in this particular setting since the impedance of the cable connecting the two sources is nearly zero.



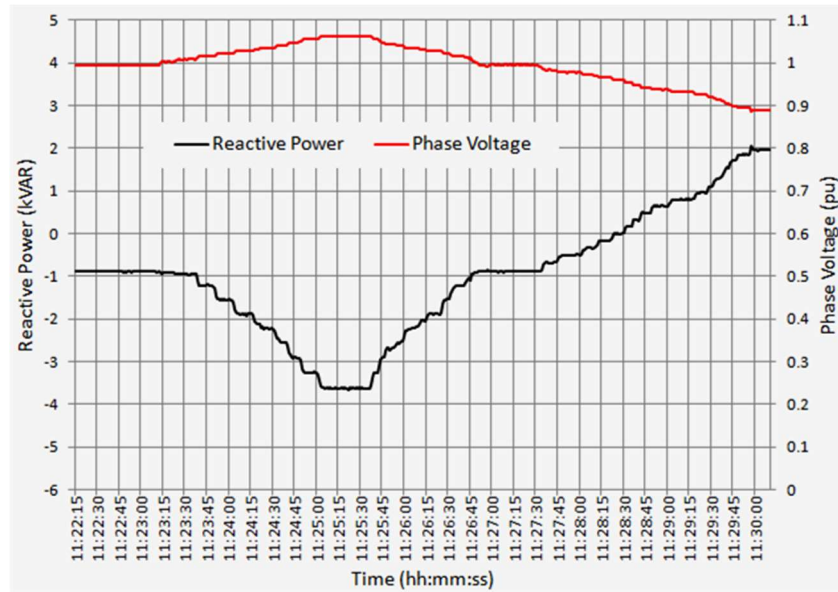


Figure 4.16 Dynamic Volt/VAR Baseline Test with Gradual Voltage Changes [29].

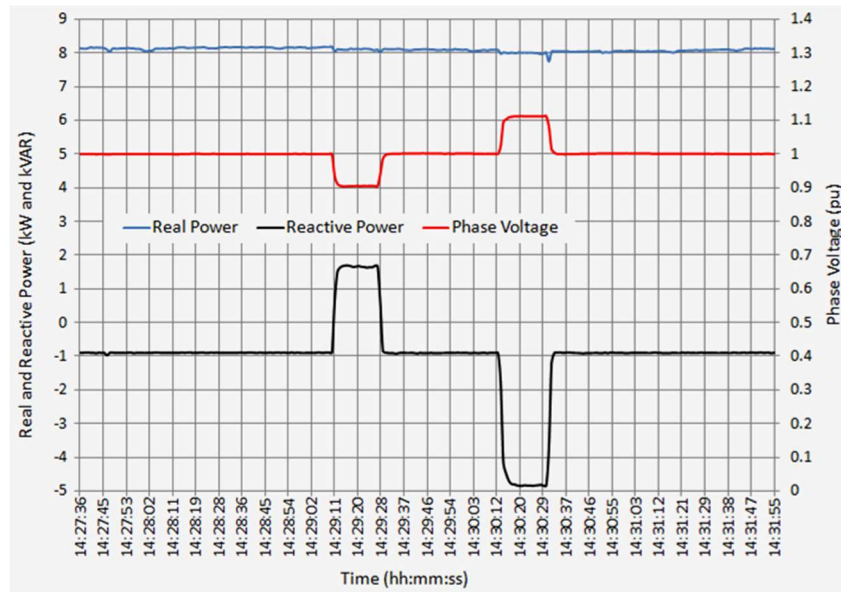


Figure 4.17 Dynamic Volt/VAR Baseline Test with Fast and Temporary Voltage Changes [29].

## Chapter 5: Islanding Test of Advanced Inverter

For safety considerations, grid-tied inverters are constantly looking for indications of grid disconnect because they are prohibited to generate power in an islanded condition and therefore must shut off immediately. To detect utility outage the inverter monitors the voltage (magnitude and frequency) at the inverter connections. During a utility outage, the voltage (magnitude and frequency) generally deviates up or down by several percent from the nominal values, depending on the conditions of local power generation and local load. According to IEEE Std. 1547-2018, inverters are mandated to shutoff within 10 cycles, or 160 milliseconds, if the voltage rises above 120% or drops below 45% of its nominal value, as specified in Table 4.1 above. If the frequency goes above 62 Hz or goes below 57 Hz (refer to Table 4.2), the identical clearing time pertains. The expansion of the clearing time to 1 second is allowed if the voltage rises to a value between 110% - 120% or drops within 45% - 60% of the rated value. Finally, the 2 second clearing time is for frequency variations between 60.5 Hz - 62 Hz or 57 Hz - 59.5 Hz, or if the voltage declines between 60% - 88% of the rated value. With an agreed upon contract between distributed generator owner and the local utility company, the 1 second and 2 second clearing times can be increased, specified in Table 4.1 and Table 4.2 of the updated interconnection standards.

### 5.1: Potential Interference of Autonomous Functions with Islanding Detection Schemes

Several active and passive methods are used to prevent islanding conditions [47]–[53]. There are the classical methods of OUF and OUV detection used by conventional inverters. Figure 5.1 shows the microgrid with a load and PV system connected and to simplify the load, it is regarded as a constant impedance load, a parallel connected  $R-L-C$  circuit. To have the transformer shunt impedance as a portion of the parallel connected  $R-L-C$  load, the insignificance of the series impedance of the transformer and connection cables are ignored. Denoting the PV system active

and reactive powers produced as  $P_{DR}$  and  $Q_{DR}$ , respectively, and  $P_G$  and  $Q_G$  be the portions of  $P_{DR}$  and  $Q_{DR}$  that are supplied to the grid. To represent the differences between local active and reactive power generation by the PV system and the local load demand, the following quantities can be represented by  $P_G/P_{DR} = \alpha$ , and  $Q_G/Q_{DR} = \beta$  and can be expressed by

$$P_{DR}(1 - \alpha) = \frac{V_{old}^2}{R} \quad (5.1)$$

$$Q_{DR}(1 - \beta) = \frac{V_{old}^2}{\omega_{old}L} (1 - \omega_{old}^2LC) \quad (5.2)$$

where  $V_{old}$  and  $\omega_{old}$  are the grid voltage and the grid angular frequency at the interconnection point before grid disconnect, simply shown by the switch closed and the grid is present.

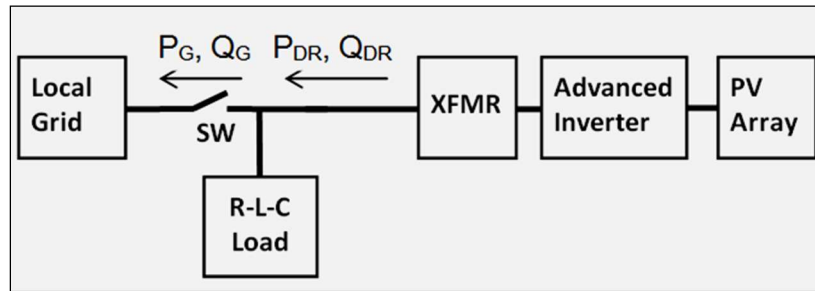


Figure 5.1 Circuit Block Diagram of the Utility Grid, PV System, and Local Load [33].

$P_G$  and  $Q_G$  will become zero after the utility separates, with the assumption that PV system generated powers will remain unvarying. The voltage and frequency will change and start

towards new steady state values ( $V_{new}$ ,  $\omega_{new}$ ), these new variables can be associated with the old ones as follows:

$$\frac{V_{new}}{V_{old}} = \frac{1}{\sqrt{1-\alpha}} = \sqrt{\frac{P_{DR}}{P_{load}}} \quad (5.3)$$

$$\frac{\omega_{new}}{\omega_{old}} = \frac{-b + \sqrt{b^2 + 4d}}{2d} \quad (5.4)$$

were

$$P_{load} = P_{DR} - P_G \quad (5.5)$$

And

$$b = (1-d) \frac{1-\alpha}{1-\beta}, \quad d = \omega_{old}^2 LC \quad (5.6)$$

The frequency relationship in Eqn. (5.4) shortens by ignoring the capacitive component of the load

$$\frac{\omega_{new}}{\omega_{old}} = \frac{1-\beta}{1-\alpha} \quad (5.7)$$

Four relays usually make up the standard passive islanding protection, which is the under-frequency relay, over-frequency relay, under-voltage relay, and the over-voltage relay of a grid-connected PV system under most circumstances, will usually prevent islanding. Frequency and voltage deviations depend on the overall power flow supplied/absorbed by the grid (magnitude and direction), as shown in the expressions above. When local demand nearly matches the local

generation, comparing a utility grid outage versus the typical fluctuations in the grid during normal operation of the grid will be difficult as frequency and/or voltage changes will be minor. This makes it difficult to distinguish between the two, they will have values that will be considered in the Non-Detection Zone (NDZ), and the trip levels cannot be set so small for the 4 relays or nuisance trips will disconnect the PV system. Therefore, additional active or passive schemes are often needed to reduce the probability of an island to occur [47], [54].

The following popular *passive schemes* are undetectable in the current and voltage output waveforms and therefore are impossible to measure and study under regular operating conditions:

- Phase Jump Detection (PJD), the inverter monitors the voltage at its terminals, specifically measuring the voltage's phase, if a sudden change or 'jump' is detected the inverter will disconnect.
- Voltage Harmonic Monitoring (VHM), the grid voltage is monitored at the inverter and if the total harmonic distortion is greater than the software setting, the inverter will disconnect.
- Slide-Mode Frequency Shift (SMFS), where the grid's frequency is a function of the current-voltage phase angle. This function will report unstable, and the inverter will disconnect if the phase of the grid voltage at the inverter increases quicker than the phase of the inverter's current.

Some *active schemes* try to change the frequency or voltage from their nominal values to detect a utility disconnect by actively trying to change the frequency for voltage. These active processes will result in deviations of the voltage and current, thus make it possible to detect their use by recording specific power-quality values and below is a list of the two of the most frequent used schemes:

*Impedance Measurement (IM) method:* In this method, the inverter will agitate periodically the current supplied which will produce a change in the grid voltage which can be detected if the utility is disconnected, which will then shut down the inverter. The name of this method is derived due to the inverter changing the current to see a change in the voltage which is  $dv/di$ , and if the inverter is using this method, you will measure periodic waveform distortions in the output current.

*Active Frequency Drift (AFD) method:* This method has the PV inverter generate a current that every half cycle will cause a chopping, or zero current for part of the voltage waveform. The current initiates at the voltage zero point and reaches zero before the next voltage zero point, remaining there until the voltage crosses zero again. This process will cause the frequency to drift down or up if there is a utility outage and therefore if it is being used, its detection can be accomplished by measuring the current's waveform.

The above active inverter schemes try to determine if the grid is connected or possibly disconnected by changing the voltage and/or frequency of the inverter and measuring how these values change. If minimal to no change is measured then the grid is “stiff”, not islanded, or if a significant change is measured then the grid is “movable”, possibly islanded. Each active scheme has its advantages and disadvantages in terms of cost, effectiveness, trip threshold, power quality, and ease of implementation. Manufacturers of commercial inverters do not have a standardized test for the detection and prevention of unintentional islands, and they rarely share how they accomplish this.

In advanced inverters there are several grid support functions available, due to the ability to assist the energy company with local voltage management, the most popular is the *Volt/VAR control*. The *Hz/Watt control* function is the second most popular/important function because it

helps control the grid's frequency, it has its limitation since PV power generation is not infinite and is limited to the solar panels and current climate conditions. To accomplish a power delivery above the maximum, systems can incorporate an energy storage system allowing the system to provide power above the current operating maximum. When the grid support functions are activated, the inverter measures the frequency and voltage deviations at the connections of the inverter. The inverter then modifies the real and reactive powers generated,  $P_{DR}$  and  $Q_{DR}$ , to try and reduce irregular grid conditions. Changes in frequency and voltage will cause a response in the inverter proportional to the programmed voltage/reactive power ( $V-Q$ ) and frequency/power ( $F-P$ ) curves along with the responsiveness of the control circuitry. Figure 5.2 shows a typical piece-wise linear curve that represents how the inverter will adjust the generation power, real and reactive, to voltage and/or frequency variations.

To illustrate this point, the curves in Figure 5.2 show  $Q_{DR}$  as a function of voltage,  $g(V)$ , and  $P_{DR}$  as a function of frequency,  $h(f)$ . A new voltage and frequency will occur after utility disconnect and as defined in (5.3) and (5.4) which will lead to a new real inverter power,  $Q_{DR,new} = g(V_{new})$ , and a new reactive inverter power,  $P_{DR,new} = h(f_{new})$ . This process will reiterate until a new steady state real and reactive power is reached. The inverter tested in this experiment lacks the functionality of the Frequency-Watt control and therefore it was excluded from the test procedure. Another method for the inverter to detect utility disconnect and therefore islanded operation is to use a method of active frequency drift (Sandia frequency shift) [55]. The frequency drift method constantly attempts frequency deviations to detect utility disconnect raising the concern that these grid support functions, when working, try and destabilize the grid and can result in a worse grid performance and possible unacceptable islanded operation.

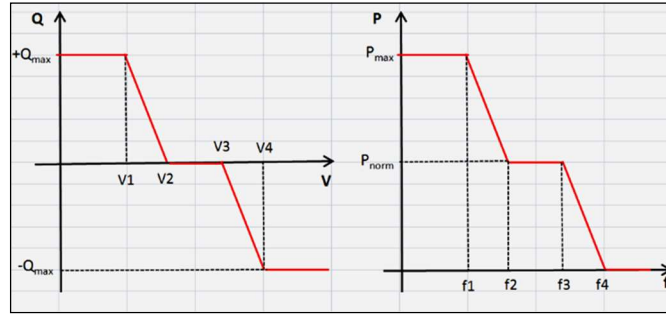


Figure 5.2 Characteristic Volt/VAR and Watt/Hz Inverter Contour [32].

## 5.2: Experimental Setup

The experimental setup contains the following major pieces of equipment that are connected as shown in Figure 5.1:

- local grid supply rate at 120/208 V,
- PV array rated at 12 kW (based on STC),
- Transformer rated at 480V /208 V, 30 kVA ( $Z = 4\%$ ,  $I_{ex} = 2.5\%$ ),
- Advanced 3-phase inverter rated at, 480 V, 12 kVA,
- Adjustable load banks rated at (25 kW resistive, 9 kVAR inductive, and 1.8 kVAR capacitive)
- A switch to connect/disconnect the load banks and PV system from the grid
- To record active and reactive powers, two non-transient power monitors, one connected to measure supplied/absorbed by the utility ( $P_G$ ,  $Q_G$ ) and the other connected to measure the PV systems generated powers ( $P_{DR}$ ,  $Q_{DR}$ ).



- To record the current and voltage waveforms during transition, a transient power monitor.

The non-transient power monitors have a sampling rate of 500 milliseconds or every 30 cycles, and any type of abnormality will trigger the transient recorder automatically.

The test entails the subsequent steps:

- 1) To achieve the desired power flow discrepancy between  $P_{DR}$ ,  $Q_{DR}$  and  $P_G$ ,  $Q_G$ , change the local load demand,
- 2) In the inverter software, enable and/or adjust the variables that control/set the desired function of grid support,
- 3) Using the switch, disconnect the utility and
- 4) Record the ride time ( $\Delta t$ ) before the inverter shuts off due to utility disconnect.

The time that allows for the smallest deviations by the PV system in respect to real power is near solar noon, on clear days. Since the individual elements of the load are not adjustable in a continuous fashion but can only be varied in discrete steps, the possibility of achieving zero mismatches, i.e.,  $P_G=0$  and  $Q_G=0$ , extremely difficult. Therefore, every effort was made to trying to make  $P_G$  and  $Q_G$  as close to zero as possible.

### **5.3: Test Findings**

The differences in inverter operation/response to a grid disconnect are presented in this section with default settings and various inverter parameter modifications and were recorded after minimization of  $P_G$  and  $Q_G$ . The parameters in the inverter include those associated with *Dynamic Volt/Var Control*, *Non-Unity PF Operation*, and *UOV and OUF Ride Through*.

#### *5.3.1: Operation at Unity PF*

Case 1 Table 5.1 below, was used to build a baseline case, therefore the default settings of the inverter (refer to Table 4.1 and Table 4.2) were used in its operation of this case. With the inverter on and producing 4.7 kW and consuming 260 VARS, the transformer magnetizing and series reactances account for the reactive power as the inverter was set to unity PF. A resistive load bank and a capacitive load bank consumed/produced an equal but opposite amount of real and reactive power produced/consumed by the inverter. Case1 turned out to be unique, the test was able to achieve a situation where  $P_G=0$  and  $Q_G=0$ . When the grid disconnected, this matched load/generation situation led to no voltage and frequency changes, thereby forcing the inverter to cease operation by use of its active islanding detection scheme. This scheme is unknown and not listed in any documentation.

Figure 5.3 shows Case 1 and displays a phase voltage during the time from grid separation (red arrow) to inverter cut off and shows a ride time of over just over 1 second. As can be seen, the voltage does not drop instantly due to  $P_G$  and  $Q_G$  being near zero but drops near the end of the figure to nearly 70% of nominal value, in the final 8 milliseconds before the tripping the over-voltage relay, the voltage surged to 140% of its nominal value.

To see if the result was repeatable, the experiment was reperformed after a few minutes, even though it was approximately the same solar time, conditions had changed. This proved that duplicating experiments on real life systems is difficult and can lead to significantly different outcomes. During this test, there was a slight reactive power mismatch as shown in Table 5.1, Case 2. The real power was balanced ( $P_G=0W$ ), but reactive power was being imported from the grid leading to a mismatch of reactive power ( $Q_G=130$  Vars). The instantaneous phase voltage of this event is shown in Figure 5.4, and the mismatch of  $Q_G$  led to significant frequency deviations

within 65 milliseconds of grid disconnect (red arrow), which in turn triggered the under-frequency relay and disconnected the inverter, shutting it off.

Table 5.1 Parameter Values Used in Islanding Tests [32].

| <i>Case No.</i> | <i>PDR/QDR<br/>(kW/kVAr)</i> | <i>PF<br/>(%)</i> | <i>PG/QG<br/>(kW/kVAr)</i> | <i><math>\alpha</math></i> | <i><math>\beta</math></i> | <i><math>\Delta t</math><br/>(ms)</i> |
|-----------------|------------------------------|-------------------|----------------------------|----------------------------|---------------------------|---------------------------------------|
| 1               | 4.70/-0.26                   | 99.8              | 0.00/0.00                  | 0                          | 0                         | 1,020                                 |
| 2               | 4.78/-0.28                   | 99.8              | 0.00/-0.13                 | 0                          | 0.46                      | 65                                    |
| 3               | 4.65/-0.27                   | 99.8              | -0.08/-0.03                | -0.02                      | 0.11                      | 715                                   |
| 4               | 3.90/2.35                    | 85.6              | 0.15/-0.02                 | 0.04                       | -0.01                     | 200                                   |
| 5               | 5.35/1.35                    | 97.0              | -0.22/0.16                 | -0.04                      | 0.12                      | 114                                   |
| 6               | 5.30/-1.72 <sup>†</sup>      | 95.0 <sup>†</sup> | 0.12/-0.10                 | 0.02                       | 0.06                      | 3,330                                 |

(<sup>†</sup>) Automatically set prior to utility disconnect.

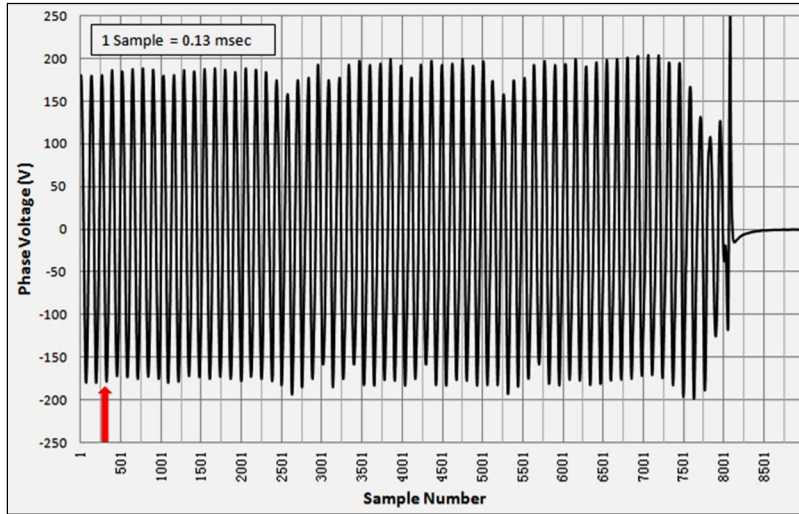


Figure 5.3 Case 1 ( $P_G=0, Q_G=0$ ) Unity PF Operation of Inverter [32].

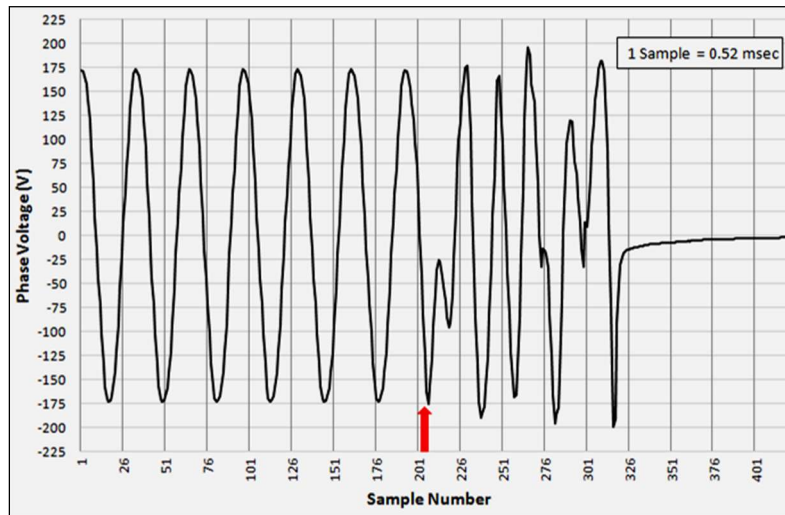


Figure 5.4 Case 2 ( $P_G=0, Q_G=130$ ) Unity PF Operation of Inverter [32].

### 5.3.2: Over- and Under-Voltage and Frequency Ride Through

Advanced inverters have additional features such as extend frequency -time and -voltage time ride through settings to minimize the number of needless PV system shut-offs and are specified in the amended interconnection standard. Case 3 of the testing is a modification of the setup for Case 1, by using the inverter software to change the trip set-points, voltage, and frequency, to the extreme permissible bounds as detailed in Table 4.1 and Table 4.2. Case 3's main question is, what is the effect of changing the settings in the inverter to increase the ride through time. Table 5.1, Case 3 shows the local power generated as well as the imported/absorbed power by the grid with the resulting voltage waveform, Figure 5.5, of how the system performed to grid disconnect. As in before, the conditions in Cases 1 and 2 could not be duplicated due to the reasons stated above and the local power load can only be controlled in discrete increments. Even though the investigators tried to match local demand to local generation right before utility disconnect, at the time of utility disconnect the grid was supplying trivial quantities of active and reactive powers ( $P_G=80$  W and  $Q_G=30$  VAr). Local generations' small discrepancy when compared to local load caused deviations in both frequency and voltage but the inverter did stay active and only shut off after 715 milliseconds. While the inverter did not stay connected for the same amount of time as in Case 1, 70% less of the time but when compared to Case 2, it was an increase by a factor of 11. The results from Case 3 are non-conclusive because Case 1 test conditions could not be duplicated. Even a slight difference in  $P_G$ ,  $Q_G$  can have a significant effect on  $\Delta t$ .

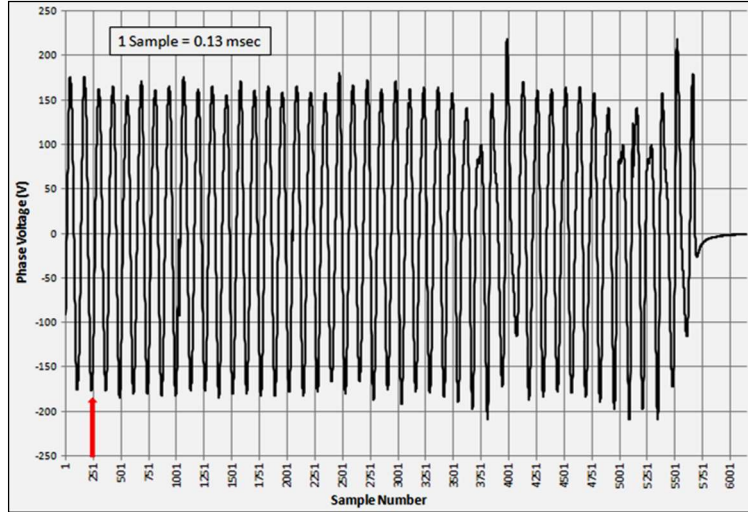


Figure 5.5 Case 3 (Ride Through Activated of OUV and OUF Conditions) with the Inverter Operating at Unity PF [32].

### 5.3.3: Inverter Operation with a Setting of Non-unity PF

For test Cases 4 and 5 in Table 5.1, the inverter software was changed to make the inverter function in the non-unity PF mode, to have a PF of 85.6% and 97% relative. The reason to allow a PV inverter to operate in this condition is to have the inverter absorb or inject reactive power to help control the local voltage and thereby compensate the overall feeder PF. To absorb the reactive power supplied by the inverter, an inductive load replaced the capacitive load and the OUV and OUF settings (Table 4.1 and Table 4.2) were unchanged from Case 3. Again, efforts were made to make  $P_G$  and  $Q_G$  near zero but unsuccessful, and the measured quantities are shown in Table 5.1 at the time of utility disconnect.

For Cases 4 and 5, Figure 5.6 and Figure 5.7 respectively show the phase voltage waveform of the tests during utility disconnect, showing ride times of 200 milliseconds and 114

milliseconds before inverter shut off. These tests were performed repeatedly with minor differences in  $P_G$  and  $Q_G$ , always trying to minimize  $P_G$  and  $Q_G$  but the ride time after utility disconnect never exceeded 220 milliseconds. With these tests showing the inverter shut off well before the 2-second default time limit, it is concluded from the results that using the advanced inverter OUV and OUF settings had no effect on a utility disconnect. Although with a lesser amount of confidence, since the inverter shut off the quickest in Case 4 and Case 5, it can be concluded that the inverter operating in a non-unity PF mode will lead to quick shutdown times.

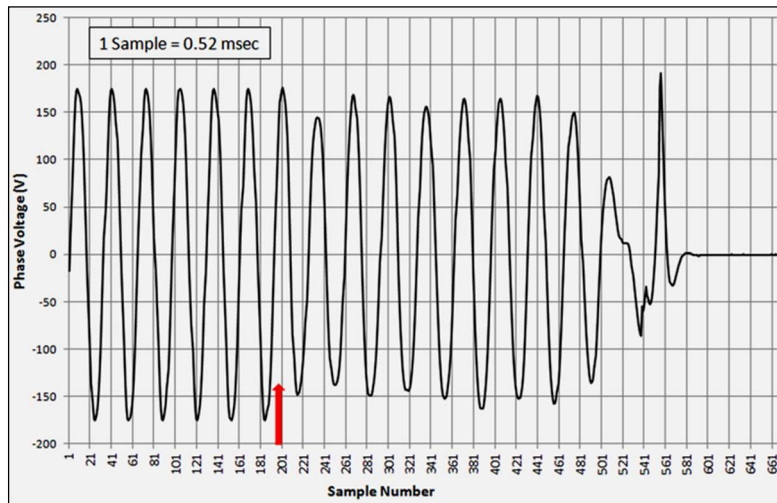


Figure 5.6 Case 4 Non-unity PF (85.6%) Operation of Inverter [32].

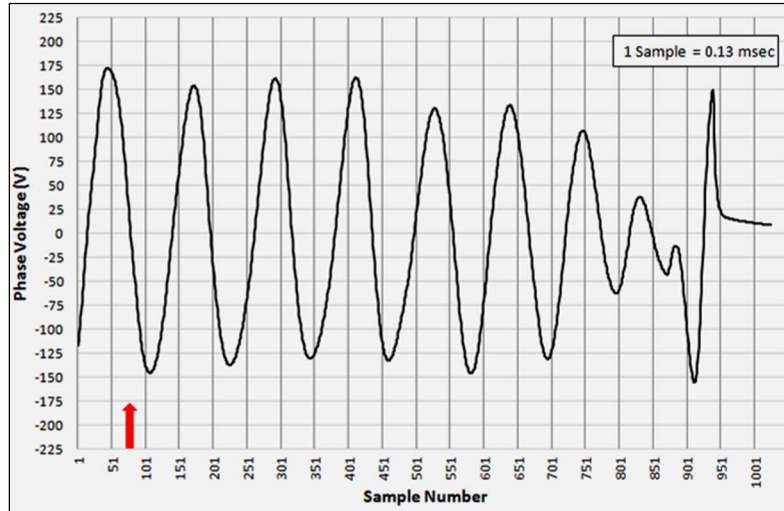


Figure 5.7 Case 4 Non-unity PF (97%) Operation of Inverter [32].

#### 5.3.4: Operation under Dynamic Volt/VAR Control

For Case 6 of Table 5.1, inverter software variables would have to be changed to best represent the curve shown in Figure 5.2, the Volt/VAR curve. The variables needed to be set in a way where real power generation is unaffected, inverter software variables that set the Volt/VAR curve are as follows. The voltage dead band =  $\pm 1\%$  of nominal value, of available reactive power only use 50%, and the slope of the line segments (reactive power-to-voltage gradient) set to a 10 to 1 ratio. The 10 to 1 ratio is used outside of the dead band and states that for a 1% nominal change in voltage, the inverter will absorb or supply 10% of its available reactive power. With the inverter synchronized to the grid and producing a real power constant at 5.3 kW and the grid having a voltage 2.8% greater than the rated value, it produced - 1.7 VARs which is approximately 15% of the available reactive power.



Case 6 of the experiment had the longest recorded inverter ride time after utility disconnect. As in previous test cases, an effort was made to minimize  $P_G$  and  $Q_G$ , but a zero value could never be reached. For over three seconds the inverter operated in Case 6 before shutting down and Figure 5.8 shows a single phase of the system and the related changes in both voltage and current after utility disconnect. Note due to the long period of time before inverter shut down, relative to previous test cases, RMS values are displayed rather than instantaneous values. The figure shows an oscillation of the current and voltage between +3% and -8% of their average output values, except for a noticeable momentary event, a dip in the voltage of nearly 50%, that occurred at 700 milliseconds mark after utility disconnect, this oscillation continued until the inverter eventually shut down.

The long ride through time of Case 6 led to the belief that activating the Volt/VAR control functionality in the inverter software, had degraded the ability of the inverter to detect grid disconnect. To test this thought, several attempts were made to duplicate the long ride time after utility disconnect, each time minimizing  $P_G$  and  $Q_G$ , but the inverter shutdown time was never recorded greater than 500 milliseconds. Therefore, the long ride time of Case 6 is most likely caused by several unknown factors that may include the frequency of the MPPT procedure and how it is implemented in the inverter, the processing time of Volt/VAR function, and the method(s) the inverter detects utility disconnect.

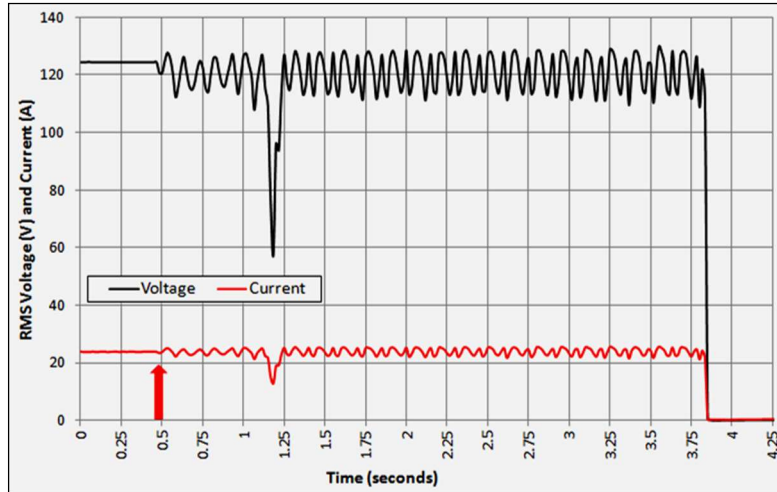


Figure 5.8 Islanding During Dynamic Volt/VAR Control [32].

A main concern over the dynamic operation of the Volt/VAR control of advanced inverter is the possibility that this function might interfere with the detection of an islanded situation. Attempts have been made to learn about the islanding detection schemes embedded in the inverter under test and to create an islanded operation. Many methods are well-known for grid-tied PV inverters to detect utility grid disconnect, but the manufacturers of inverters believe these are trade secrets and therefore do not make literature available describing the methods used in the company's products.

## Chapter 6: Unintentional Islanding of Diesel Generator – PV Microgrid

This chapter analyzes the microgrid operation dynamically, where the DG is working in combination with the PV system to serve the local load whilst on islanded mode while connected to the grid. Reference [56] conducted a similar study but only through computer simulations. In our case, experiments are conducted on a real system where the outcome desired is that the microgrid remains functioning after grid disconnection due to an outage. For simplicity, the islanding detection mechanism implanted in the synchronizing module was deactivated for the DG, and to reduce the nuisance produced by the continual tripping of the inverter, its ride through times were expanded for frequency and voltage deviations to the largest settings delineated per the revised interconnection standard [20]. In the grid-connected mode illustrated in Figure 6.1 below, the microgrid can either be importing or exporting real and reactive power. As indicated in Chapter 2, the generator is outfitted with a module capable of synchronization to the utility, load sharing and detection of grid disconnect. The microgrid is also comprised of a backup detection module, the SEL700G. This can measure electrical quantities for display and use in the time in and connection of the microgrid to the utility. If the SEL module detects undesirable conditions, it can control switches to disconnect the utility and shut down the DG set along with activating the appropriately distributed control system alarms.

Two sections of the chapter: Section 1 details the response of the microgrid to an intentional utility disconnect (i.e., islanding) with the microgrid operating at different mismatched conditions in local generation and load, along with the inverter set to operate with different settings. Section 2 evaluates how the inverter responds in real time to rapid changes in load while isolated from the grid.

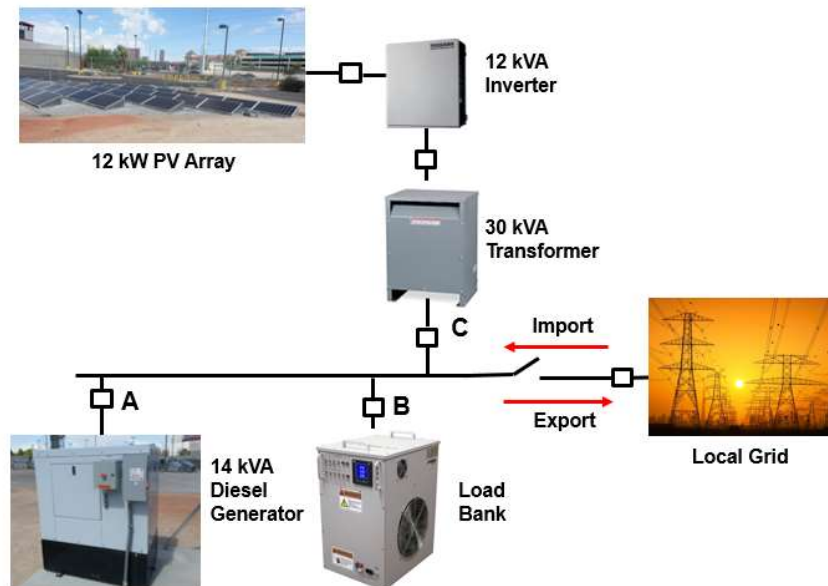


Figure 6.1 The Microgrid and its Components under Study.

## 6.1: Unintentional Islanding of Operational Microgrid

Describe in this section is the microgrid's capability to continue function after intentional utility disconnect while operating at various microgrid power import levels. The inverter software settings were set up to a default value, as stated in IEEE 1547-2003, at the inverter the frequency, voltage, and power were recorded at the different mismatched conditions of local generation and local load demand. Similarly, a test was conducted, where the inverter software setting was altered to allow a longer voltage and frequency disturbance ride through voltage per Reference [20].

### 6.1.1: Inverter Operation under Default Settings

With the inverter software set per IEEE 1547-2003 and with the load was consuming 10 kW, under all power matched or mismatched conditions, whether importing or exporting, the inverter detached from the microgrid. Figure 6.2 illustrates the operation of the PV inverter's voltage and power after utility disconnects, such as the one at 55 seconds with the utility grid supplying 1 kW or another at 135 seconds in which there was no flow of power between the utility and the microgrid. In the initial case, 3.75 kW is the output of the PV system which immediately turns off at utility disconnect. However, in the subsequent case, in an islanded mode and with the diesel generator providing the supply voltage for the inverter, the inverter operated for 25 seconds after utility disconnect. As projected, the generator was able to provide the supply voltage and the difference in power for the load, until the inverter shut down overloading the generator causing it to shut down.

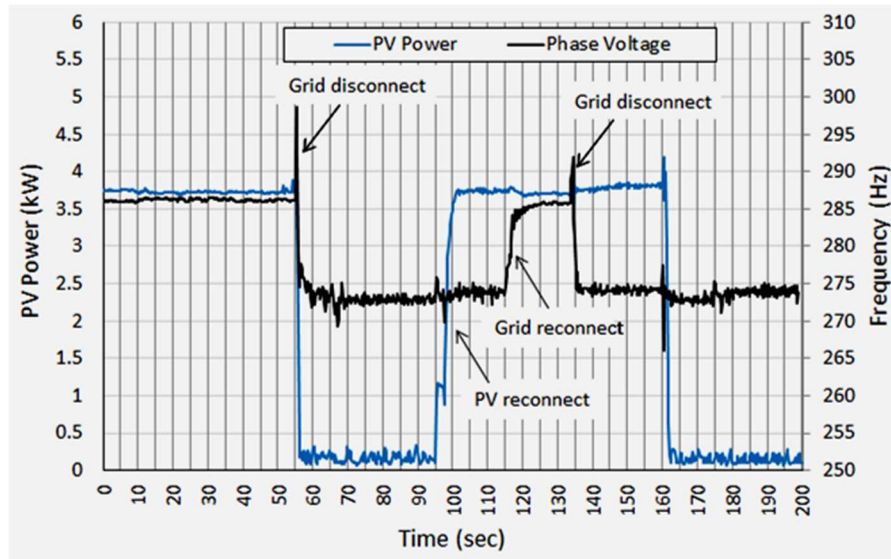


Figure 6.2 Advanced Inverters Voltage and Power Response to Utility Disconnect, Utility Supplying 1 kW and 0 kW (250ms Sample Period) [29].

Due to the microgrid facility being located across the street from the electric power companies' substation, the voltage is at the upper limit of the permissible value, and therefore when the utility disconnects the voltage instantaneously dropped from 286 V to 274 V, which is the voltage set point of the DG. The frequency changes corresponding to the tests described above are shown in Figure 6.3 and the frequency deviation immediately following utility disconnect, the frequency is severe when importing 1 kW of power and infinitesimal when the is zero power is imported and exported. With zero power imported/exported the inverter took some time to detect the utility disconnect using its active anti-islanding scheme.

Captured in Figure 6.4 is the inverter current, which is noticeably distorted due to low solar irradiance, but it continued to produce power and stay on for thirty seconds following grid disconnect [57] with a rapid decline in voltage following the inverter shut down.

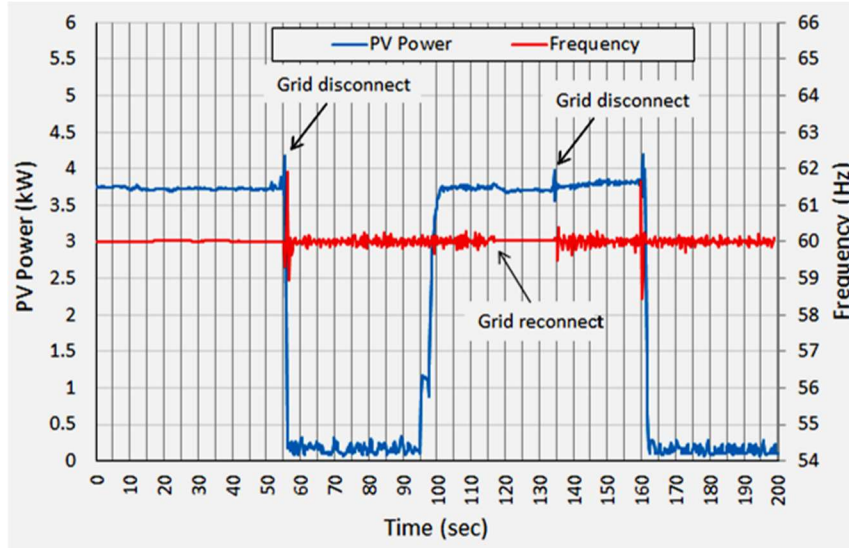


Figure 6.3 Advanced Inverters Voltage and Power Response to Utility Disconnect, Utility Supplying 1 kW and 0 kW (250ms Sample Period) [30].

### 6.1.2: Inverter Operation under Advanced Settings

The deliberate utility disconnect was tested following the widening of the inverter software ride through times regarding frequency and voltage disturbances, the time was set to the maximum amount permissible per IEEE 1547a. In this scenario the PV system and DG set were producing a combined 20 kW, 8 kW PV, and 12 kW diesel, with a local load of 18 kW, and importation of 2 kW. Upon utility disconnect, Figure 6.5 shows how the system collapsed, by examining both the current and voltage supplied in the figure, it shows the inverter disconnected

immediately upon utility disconnect to which the synchronous generator was shut down due to the overload protection scheme.

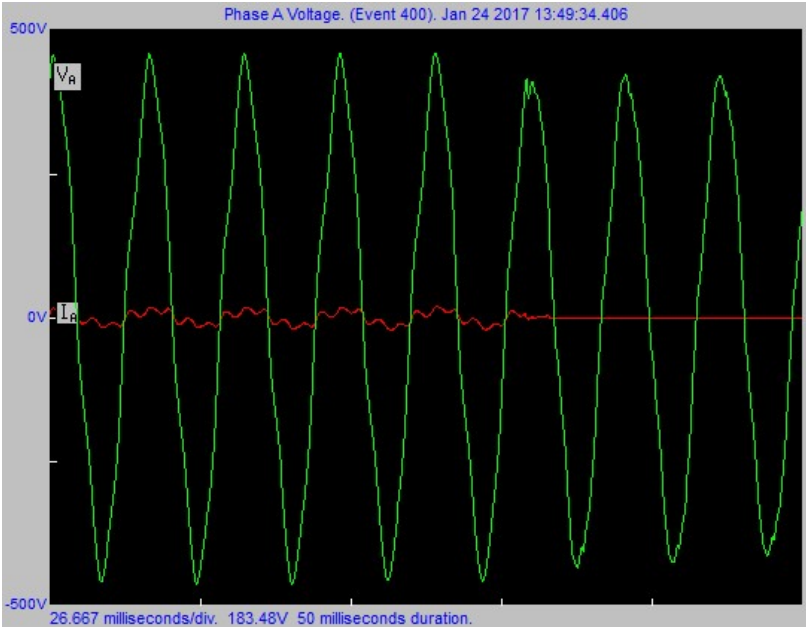


Figure 6.4 Advanced Inverters Current and Voltage Waveforms Response to Utility Disconnect [29].

To ascertain the microgrid stability in different conditions of import/export power after disconnect from the utility supply is the test shown in Figure 6.6. The figure displays the continual power generated by the PV inverter and the deviations in the microgrid voltage during utility disconnect with the conditions of 1 kW export (75 seconds), 0 kW (340 seconds), and 1 kW import (630 seconds). Figure 6.7 depicts the corresponding frequency deviations for the



same test conditions and procedures as above. Easily seen in the figure is the stable 60 Hz frequency value while the microgrid is attached to the electric power grid, and the slight fluctuating frequency value during utility grid disconnection, this fluctuation is a condition that DG's exhibit when operating in standalone mode, and as shown in both figures, the inverter did not disconnect during these disturbances but rode through as programmed.

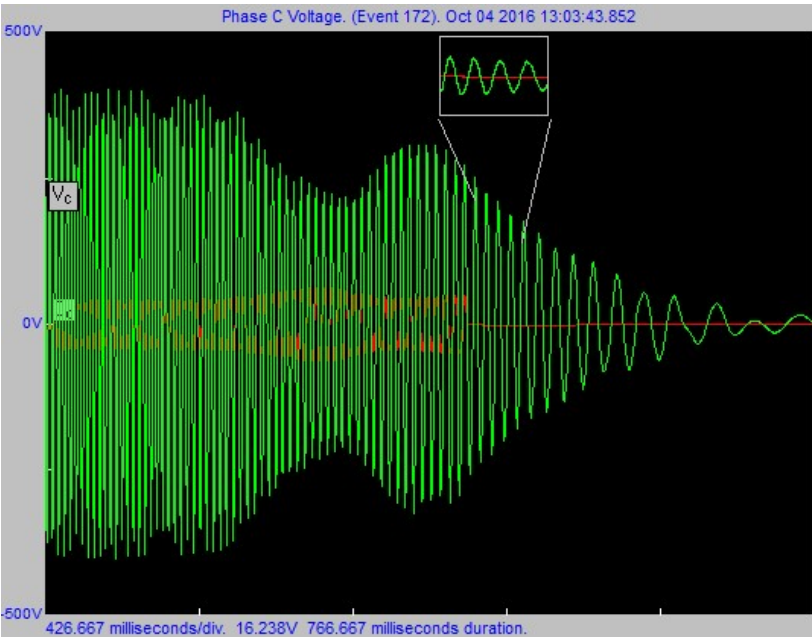


Figure 6.5 Advanced Inverters Current (Red) and Voltage (Green) Response to Utility Disconnect, Utility Absorbing 2 kW.

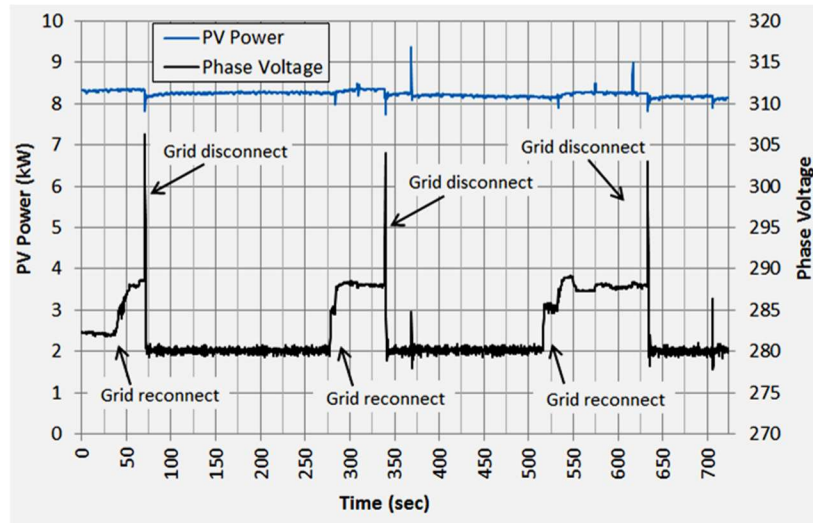


Figure 6.6 Advanced Inverters Voltage and Power Response to Utility Disconnect, Utility Absorbing 1 kW and 0 kW (250ms Sample Period).

The final portion of this test was comprised the same as the last test above, but with the change of setting the microgrid to import/export 2 kW during utility disconnect. The case where the microgrid was exporting power at utility disconnect resulted in an immediate collapse of the microgrid while in the case where the microgrid was importing power, the inverter ran for some time before shutoff. As shown in Figure 6.8 below, the inverter stayed connected through the utility disconnect deviations for almost 50 seconds until it disconnected, while Figure 6.9 shows the same test but displays the inverters instantaneous phase current and voltage during grid disconnect which occurred at the 97 second mark.

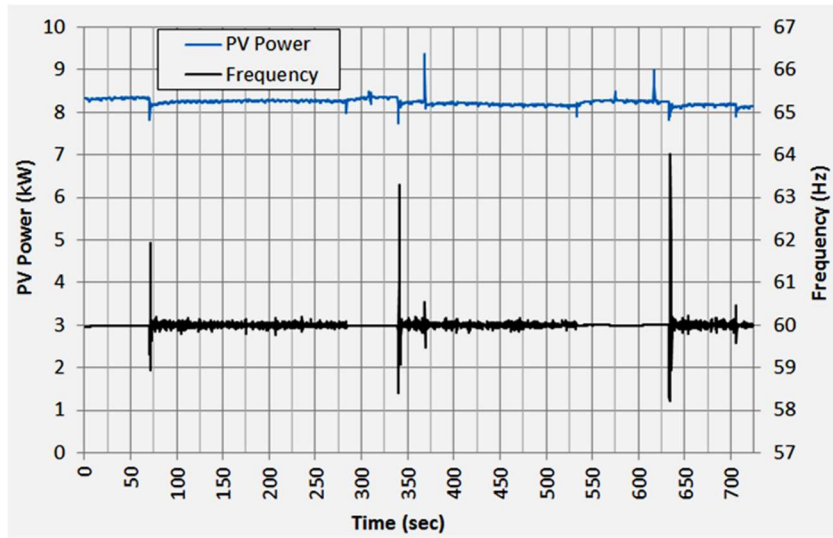


Figure 6.7 Advanced Inverters Frequency and Power Response to Utility Disconnect, Utility Absorbing 1 kW, 0 kW, and Utility Supplying 1 kW (250ms Sample Period)

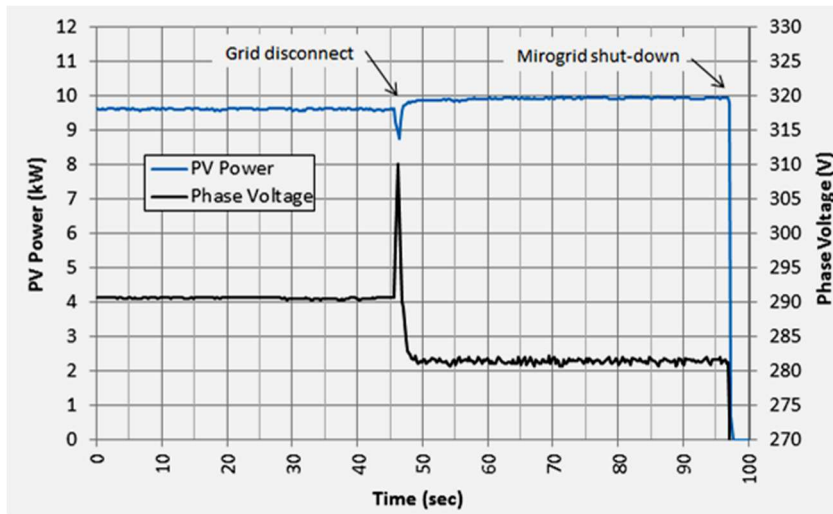


Figure 6.8 Advanced Inverters Voltage and Power Response to Utility Disconnect, Importing 2 kW (250ms Sampling Period).

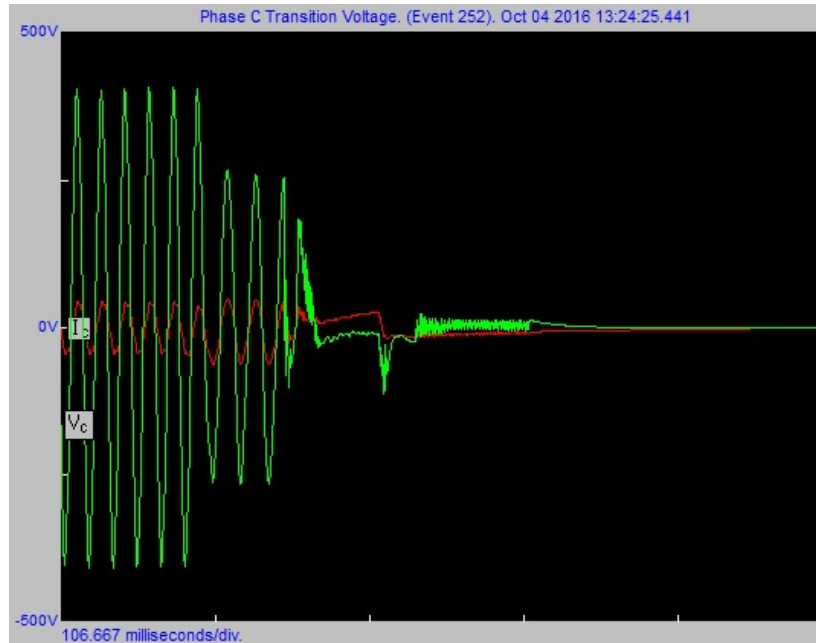


Figure 6.9 Advanced Inverters Current (Red) and Voltage (Green) Response to Utility Disconnect, Utility Supplying 2 kW.

## 6.2: Microgrid Operation in Islanded Mode

With the utility disconnected, islanded mode, and to keep the microgrid operational, the DG must provide the grid voltage to allow operation on the PV inverter. For a particular solar irradiance, a function of the sun's position relative to the solar panels and attenuated by weather, the PV system will produce the maximum power possible. The DG must provide the difference in power to meet the current load with the load always being greater than the PV system power provided. The reason for this restriction is to stop the generator from disconnecting due to a reverse power condition, the diesel engine can only convert chemical energy to mechanical power and cannot convert mechanical power to chemical energy, if the generator disconnects, the microgrid will collapse in islanded mode. Figure 6.10 below shows the sharing of the load

between the PV system and DG by displaying the powers generated by each system for the fixed load, which in the particular test was 12.25 kW. The 12.25 kW load sharing test is with the PV inverters software programmed to replicate IEEE Std. 1547-2003, which is the inverters software's default settings. The test starts with the DG servicing the entire load, as seen in the figure, and supplying the microgrid voltage to which allowed the microgrid to activate and start to provide power, shown at the 80-second mark. A partial overcast for the day of the test is responsible for the gradual power changes shown in the PV systems output and due to the DG's frequency characters and power variations, the frequency deviated about the nominal 60 Hz by  $\pm 50$  milli-hertz, and the voltage fluctuated by  $\pm 1$  volt.

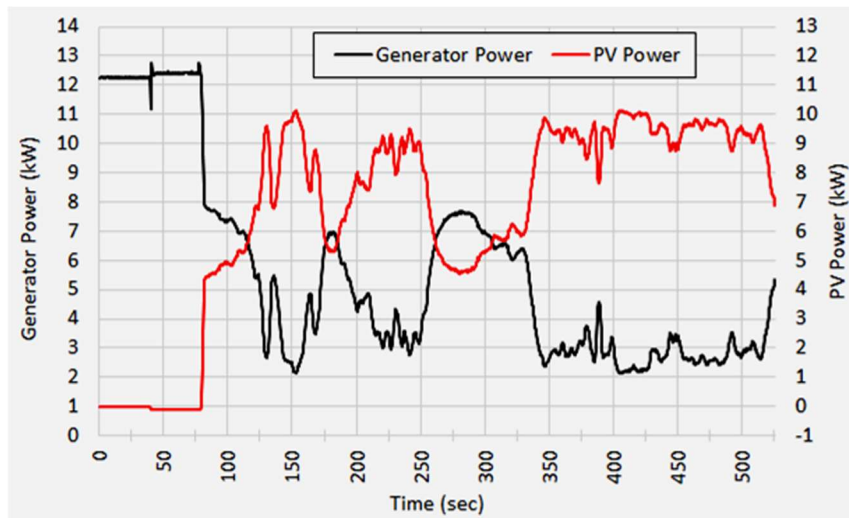


Figure 6.10 DG and PV System (Low Solar Irradiance) Load Sharing.

Figure 6.11 shows the powers generated by each system during sudden load changes and therefore the figure displays how the load is shared between the PV system and the DG during islanded operation. Initially, there was an 8 kW load and at the 80 second mark, an additional 2 kW of load was added, then removed at the 90 second mark which was then followed by an adding of 4 kW of load at the 100 second mark and then removed at the 160 second mark. The final changes to the load were an increase of 4 kW to the load at the 220 second mark followed by an 8 kW reduction to the load at the 280 second mark, and the microgrids frequency and voltage changes caused by the sudden load changes are shown in Figure 6.12 and Figure 6.13. Initially, 3.5 kW was supplied to the 8 kW load by the PV system due to weather conditions limiting solar irradiance and with the sudden load change of 2 kW, Figure 6.12 shows that the voltage did not deviate from the nominal value by more than 3%. This deviation did not activate the under voltage or over voltage relays of the inverter as they are set to accept a voltage of 12% above nominal or 12% below nominal. Figure 6.13 shows frequency deviations of the microgrid did exceed the range of  $60 \pm 0.5$  Hz during sudden load changes of 4 kW or greater, this is why the inverter did not disconnect from the microgrid due to sudden load changes of 2 kW but shut-off during the greater sudden load changes.

From the above response of the inverter to frequency changes, it is apparent that the updated interconnection standard [20] that allows for an increased time of the *OUF ride through* function will allow advanced inverters the ability to help increase the stability of microgrids when experiencing sudden large load changes. To prove this, the next test on the islanded microgrid was with the advanced inverter's software changed to increase the ride through time to frequency deviations, Figure 6.14 below shows the results of these tests. The test shows that the inverter did

not disconnect even with sudden load changes of 8 kW, in fact, no sudden load change affected the inverter as long the load was kept greater than the power generated by the inverter.

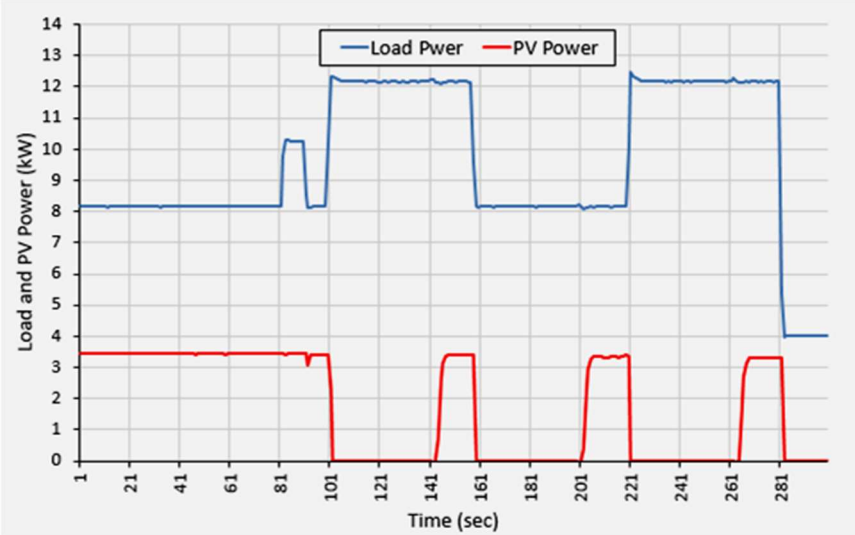


Figure 6.11 Advanced Inverters Power Production Response to Rapid Changes in Load (Inverter Software - Default Values).

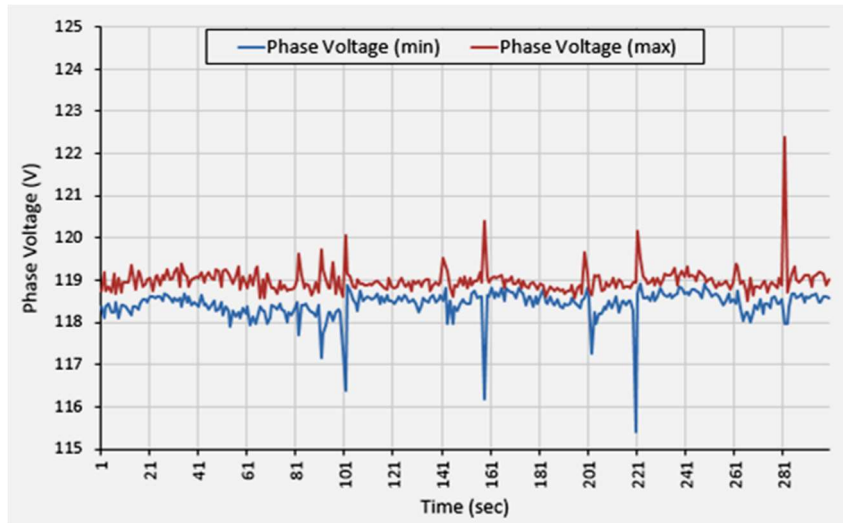


Figure 6.12 Disturbances in Voltage Due to Rapid Changes in Load Shown in Fig. 6.11.

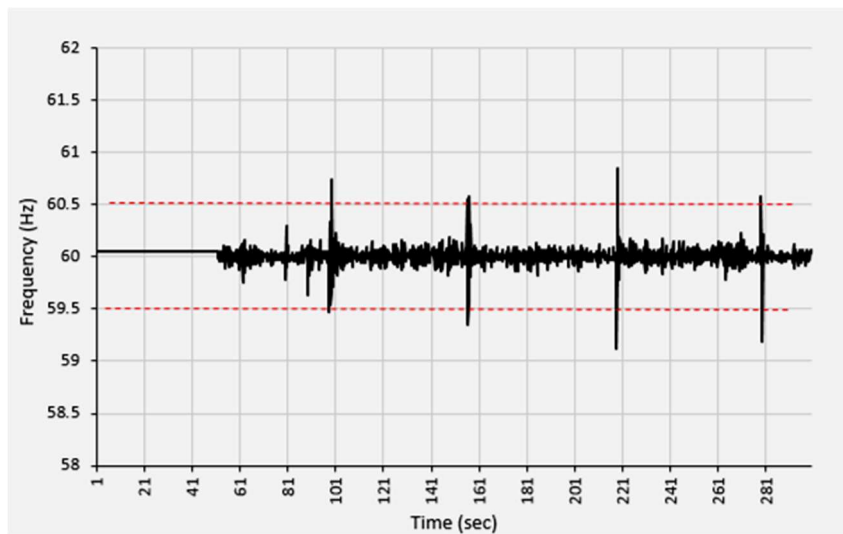


Figure 6.13 Disturbances in Frequency Due to Rapid Changes in Load Shown in Fig. 6.11



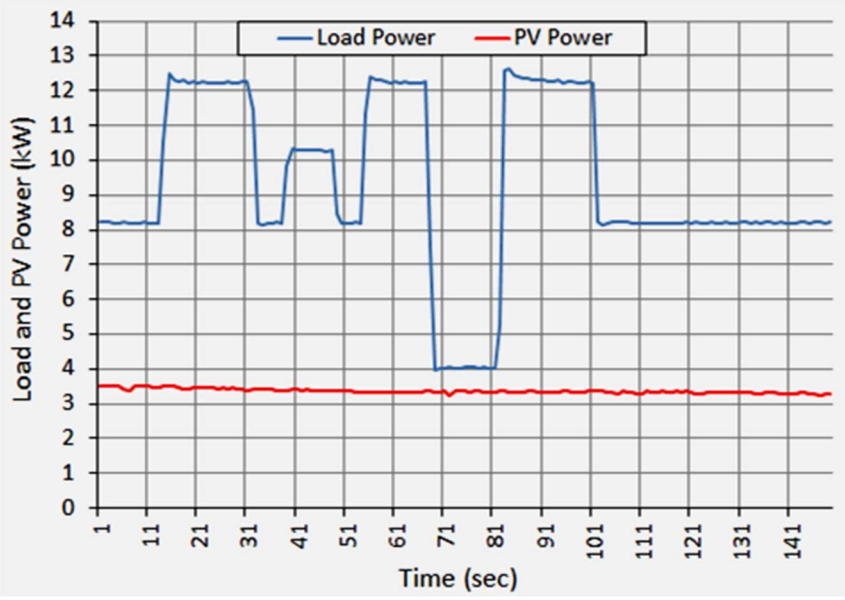


Figure 6.14 Advanced Inverters Power Production Response to Rapid Load Changes (Inverter Software - Modified Values).

## **Chapter 7: Pairing a Battery Energy Storage System (BESS) with PV**

Due to its unique flexibility, a BESS can provide over a dozen types of electricity services depending on its placement within an electrical grid [58]. On the customer side of the meter, by pairing a home BESS with a PV system in regions that offer ToU electricity rates, one can store solar energy when utility rates are low then use the stored energy when rates are highest, or in areas that provide incentives for maximizing self-consumption or reducing demand charges [59]. Several recent papers examined the influence of different parameters on the ability to generate revenue for the customer-sited PV+BES systems, such as optimal BES sizing [60]–[62], demand charge, and energy consumption cost reduction [63]–[65]. Others allowed the BESS to charge during nighttime when the electricity rates are lowest and discharge during on-peak hours [66], but such practice does not qualify for local and federal incentives. In Ref. [67], the net present value of a BES is evaluated for different grid interconnection rules, net-metering schemes, and PV and BESS sizes.

In this investigation, a set of experimental tests allowed for an analysis of an actual BESS system integrated with a PV system, with the focus being on the BESS's operation during steady state and transient conditions. The test on the BESS as a standby power source was to measure its dynamic response to a utility outage and the quality of voltage quality during islanded mode operation. A description of the experimental set-up is in Section 1 with a configuration of the associated hardware, where a presentation of the test results is in Section 2, which shows the BESS's response in terms of its voltage quality to sudden load changes, to a utility outage and when operating in islanded mode. A case study in Section 3 shows an evaluation of a BESS combined with a domestic PV system, the purpose of which is to show possibilities of improved management of electricity use thereby reducing costs.

## 7.1: Experimental Setup for BESS Testing

The experimental analysis includes the following main components, a commercial BESS with its related hardware, a grid-tie inverter with its PV array, the utility supply, circuit breakers housed in an electrical panel, a load bank, and measuring instruments as shown in Figure 7.1. The BESS, which is the item under study, is an AC-coupled system that was described in Chapter 2. Its characteristics are briefly repeated here for convenience. It contains an integrated bidirectional inverter and liquid cooling system and has a useable capacity of 13.5 kWh. The BESS has a continuous power charge/discharge limit of 5 kW with an efficiency of 90%, round-trip, when in an environmental temperature of 77° F while at a 3.3 kW continuous power charge/discharge rate [35]. The Tesla Powerwall 2™ is a complete package that can detect a utility disconnect by the voltage and current of the device, activate its communication and control protocols to disconnect from the grid by use of a switch, and restore power to the local grid. All this can be accomplished in a fraction of a second but the Tesla Powerwall 2™ also assists utilities in stopping utility customers that own the system from recycling grid electricity by prohibiting its use as a revenue generator which would be possible by arbitraging grid electricity via TOU rates and NEM [68]. Via a software application, the full profile can be viewed of the power traversing the local grid including the battery system, the generated power of the PV system, the local load demand, and the SOC. Also, in the user interface of the software application, a user has access to temporal controls, solar self-use, and standby power [35].

The PV system contains 4 parallel strings of PV panels, with the panels rated for 270 W (STC) with each string containing 11 panels connected in series. It is ground mounted with a tilt angle of 25° facing south and this configuration makes it a 12-kW array and it is available for this experiment. In this study, only two strings of the PV array will be connected to build a 6 kW

PV array which is connected to a 6 kVA non-transformer, single phase, grid-tied inverter which operates at the 240 V grid supply. A resistive bank will represent the local load, it is adjustable in 1kW steps to a maximum load of 10 kW. To record the desired grid quantities the following was used, Fluke-3 Model 1735 power analyzer (numerous quantities measured/recorded including harmonics), AEMC Power Meter Model 8220 (records waveforms of the current and voltage, including their steady state harmonic conditions), and a Reliable Power Meter (records current and voltage transients of sudden load changes).

## **7.2: Test Results**

BESS test findings are listed in this section and include the voltage quality supplied by the BESS without the PV system operating and it in standby mode, and the dynamic response of the battery to utility outages and sudden changes in load while operating with different conditions of power mismatch.

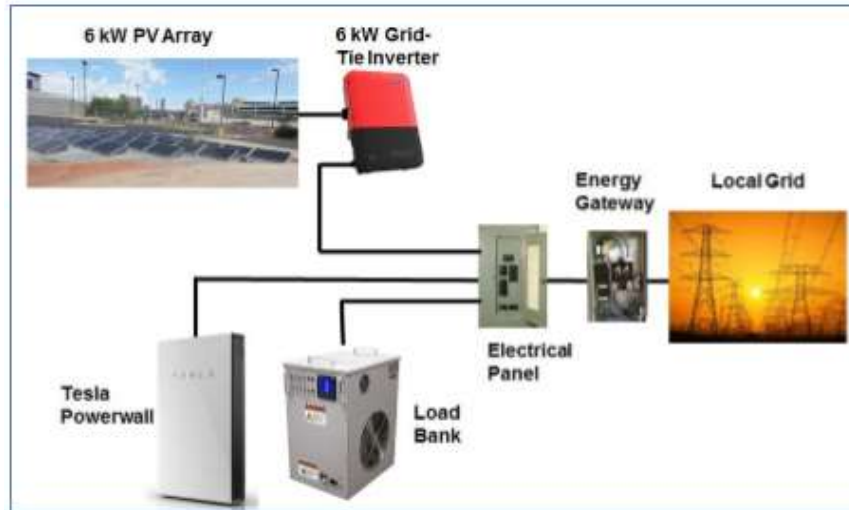


Figure 7.1 Experimental Test Setup for PV + BESS.

### 7.2.1: Power Quality Test

The utility grid imposes the operational frequency and voltage at the junction box of the synched BESS and the PV system, given there is enough solar irradiance available. During a utility grid outage, the BESS will operate in islanded mode and if the solar irradiance available, the PV system will operate in conjunction with the BESS. Therefore, while the BESS and PV system works together, it is important to understand the voltage waveform, the current distortion, and the power flow of the combined systems.

To create a baseline for the tests, hours of data was captured of the PV inverters current and the local grid voltage (240V) and then analyzed to which it was found that the utility voltage magnitude varied by 2.3%, while the 1.5% THD varied little, with the largest harmonic component being the 5th. The voltage and THD are within tolerance, voltage magnitude can vary by  $\pm 5\%$  from the rated voltage [ANSI C84.1] and the THD must be less than 8% [22].

Recommended by the interconnection standards, the THD limit is 5% and the datasheet for the PV inverter indications that at rated conditions, the current THD is less than 4% but operating the inverter in sub-rated conditions, the THD of the current can exceed the manufacture stated values [57].

Below are data captures of the current and voltage waveforms at the terminals of the BESS while it was operating in an islanded mode, Figure 7.2 specifically shows the BESS operating alone as the only power source to supply a 2.2kW resistive load. In the figure, the BESS generates a voltage magnitude that is 1.3% under the rated value, 236.8 V, and the THD is below 1%, which is obvious from the near a perfect sinusoid waveform. Since the BESS supplied a passive load, the current waveform is of the same quality, the only unexpected result was the current being 180° out of phase which was due to the probe being placed to measure current into the battery instead of out of the battery. Figure 7.3 shows the current and voltage waveforms for an islanded mode BESS and PV system operating simultaneously to supply a 7.4 kW load, with the PV system generating 4.6 kW of power and the BESS supplying 2.8 kW of power. This is possible due to the BESS operating in a mode that generates the voltage for the operation of the PV inverter, the BESS's "grid forming mode". In the figure, the combined system generates a voltage magnitude that is 1.25% above the rated value, 243 V, and the THD is below 1%, which is obvious from the near a perfect sinusoid waveform, but the current waveform has a noticeable distortion with a 3% THD approximately, caused exclusively by the operation of the PV inverter.

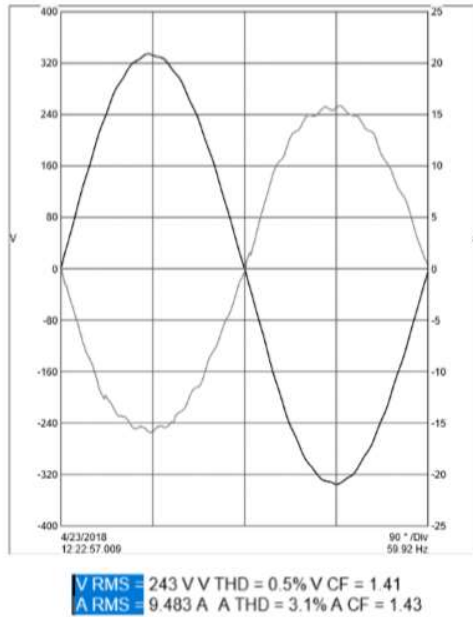


Figure 7.2 BESS Current and Voltage Waveforms When Load Sharing with the PV Inverter.

### 7.2.2: Dynamic Response Test

In this section, a recorder captured the current and voltage transients at the BESS's terminals to examine its responses to sudden changes including a utility outage with and without the PV system operating.

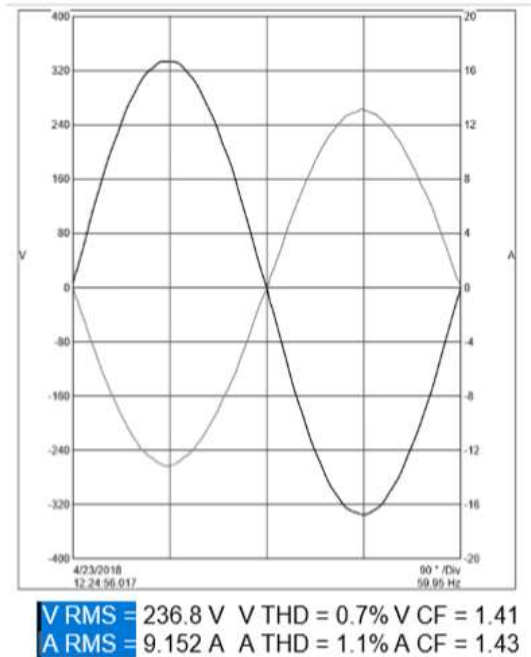


Figure 7.3 BESS Current and Voltage Waveforms to Resistive Load, No PV Generation.

- Without PV Present, the BESS's Response to a Utility Outage:* This test replicates a utility disconnect when the PV system is not operating due to the lack of solar irradiance, the initial state before utility disconnect was as follows, a 4.9 kW load supplied by the utility and the BESS in standby mode. Figure 7.4 and Figure 7.5 shows changes in both current and voltage RMS and instantaneous values of the BESS due to the transition from utility supply to the BESS supplying the load. Before the BESS could react and become the source of the load, a 2.5 cycle voltage collapse immediately followed by quarter cycle 30% over-voltage when the BESS started to provide power to the load.
- With PV Present, the BESS's Response to a Utility Outage:* This test replicates a utility disconnect while the PV system was generating power and there is no power interchange with



the local grid. Initially, the PV system was simultaneously supplying 2.5 kW to the load and charging the battery at a rate of 2.3 kW. The battery immediately shut down at the instant the grid disconnected, shown by the red arrow in Figure 7.6. After this instant, the PV system continued to supply the load but with a higher voltage that reached 120% of the nominal value within 4 cycles, after which it shut off as required by interconnection standards. After nearly 50 milliseconds, the battery switched back on to power the 2.5 kW load alone. Once the voltage stabilized after few dozen cycles (not shown in this Figure), the PV inverter resynched with the battery and started to deliver power.

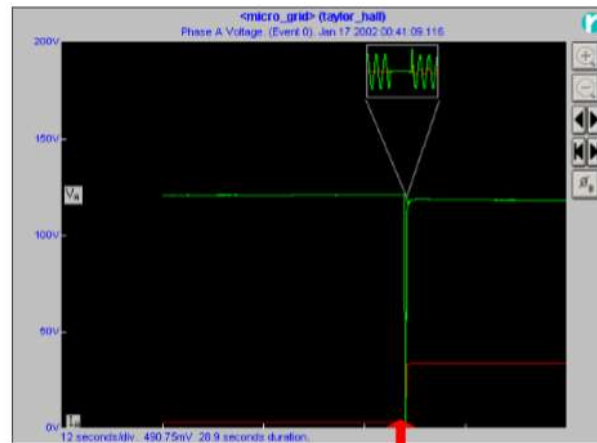


Figure 7.4 Battery Current and Voltage Response to Utility Disconnect, RMS Values, (No PV Generation).

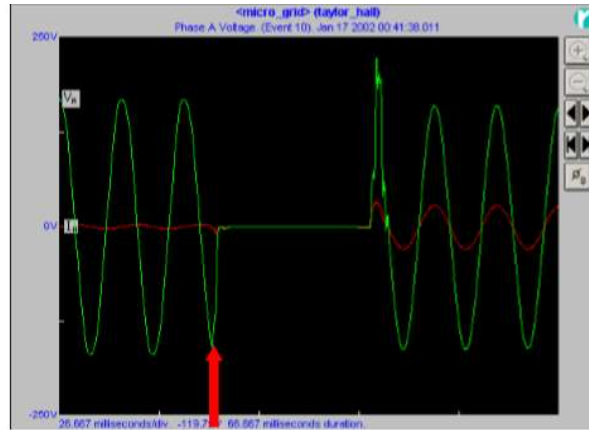


Figure 7.5 Battery Current and Voltage Response to Utility Disconnect, Instantaneous Values, (No PV Generation).

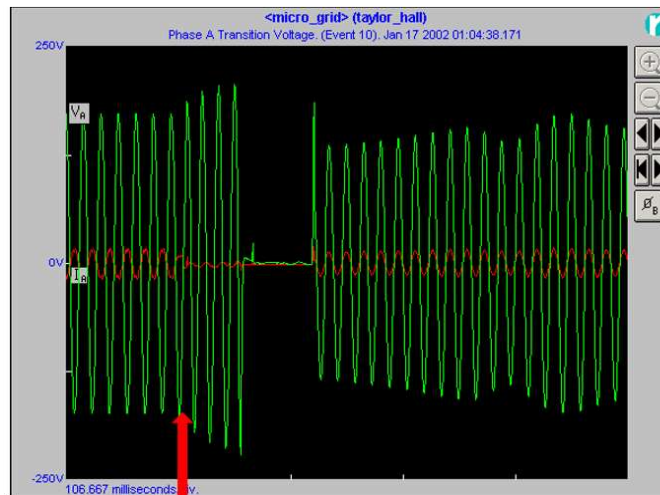


Figure 7.6 Battery Current and Voltage Response to Utility Disconnect, Instantaneous Values, (with PV Generation).

### 7.3: Residential Application

As indicated earlier in this chapter, several studies indicate that adding a BESS to deliver a primary service to a customer with a PV system can achieve significant operational revenue. But the payback period is considered too long due to the high investment cost, even when taking government rebates into account. In this section, an additional stacked BESS service, namely energy arbitrage, is sought to increase the revenue stream. The following are assumed to be in place in this analysis: coordination between the utility and BES aggregators; communication between the utility and distributed BESs to ensure instructions are received and executed in a timely and reliable manner; and regulatory barriers to customer-sited energy storage market participation are removed.

In areas where utility companies offer ToU rates, the cost of energy can be as much as one order of magnitude higher during the on-peak period than the off-peak period. Hence, shifting PV solar energy from morning to afternoon hours by means of a BES provides significant value. During off-peak periods, storing excess solar energy and shifting the stored energy so that it can be used during the night can add value in areas that either has no net metering or areas that provide incentives for self-consumption. In areas with net metering and with no incentives for self-consumption, however, performing such a shift is not encouraged as it results in loss of revenue. To generate additional revenue, this study examines the possibility to lease the BES to the local utility/aggregator in order to perform energy arbitrage in the regional EIM during the off-peak period. First, a mathematical formulation of the problem at hand is described, followed by a case study that analyzes a utility customer's power use profile, the PV system and BES characteristics, local electricity rates and incentives, simulation results, and discussion.

### *7.3.1: Solar Energy Shifting during Summer-on-Peak Period*

In this primary application, the BES is to be charged in the morning hours from the PV generated power and then discharged in the afternoon hours. The grids supply/absorption of power and BES are monitored and recorded by utility-grade energy meters. In addition, some mechanism that does not allow the BES system to charge from the grid is assumed to be in place. When the BES is charging in the morning hours, the power balance can be formulated as follows:

$$P_{grid,+} = (P^{batt,-} + P^{load}) - P^{pv} \quad (7.1)$$

$$P_{grid,-} = P^{pv} - (P^{batt,-} + P^{load}) \quad (7.2)$$

subject to the BES charging rate constraint,

$$P^{batt,-} \leq \min \{P^{pv}, C^{batt,-}\} \quad (7.3)$$

where  $P^{grid,+}$ ,  $P^{load}$ ,  $P^{pv}$ , and  $P^{batt,-}$  respectively represent the power from the utility, power used by the residential load, PV system generated power, and power supplied to the BES (when charging). Furthermore,  $C^{batt,-}$  and  $P^{grid,-}$  represent the BES charge rate limit and power flow into the grid.

Since the BES has limited capacity and incurs losses while charging, an additional constraint is imposed in order for it not to exceed its maximum State-of-Charge (SoC). This is achieved by monitoring its energy content and estimating its SoC. While charging at time interval  $i$ , the energy stored in the BES  $E_i$  and its  $SoC_i$  is determined by

$$E_i = E_{i-1} + \eta_c P_i^{batt,-} \Delta t, E_i \leq E_{rated} \quad (7.4)$$

$$SoC_i = SoC_{i-1} + 100 \frac{\eta_c P_i^{batt,-}}{E_{rated}} \Delta t, SoC_i \leq 100\% \quad (7.5)$$

where  $\Delta t$  is the sampling interval,  $E_{rated}$  is the BES rated capacity (in kWh), and  $\eta_c$  is the BES charge efficiency.

Similarly, when the BES is discharging in the afternoon hours, the balance equations are rewritten as follows:

$$P^{grid,+} = (P^{batt,+} + P^{load}) - P^{pv} \quad (7.6)$$

$$P^{grid,+} = P^{pv} - (P^{batt,+} + P^{load}) \quad (7.7)$$

Subject to the BESS discharge rate constraint,

$$P^{batt,+} \leq \min \{D^{batt,+}, (P^{load} - P^{pv})\} \quad (7.8)$$

where  $P^{batt,+}$  and  $D^{batt,+}$  respectively represent the power supplied by the BES and its maximum discharge rate. Its energy content and SoC and updated while discharging is computed by

$$E_i = E_{i-1} - \left(\frac{1}{\eta_d}\right) P_i^{batt,+} \Delta t, E_i \leq E_{rated} \quad (7.9)$$

$$SoC_i = SoC_{i-1} - 100 \left(\frac{P_i^{batt,-}}{\eta_d E_{rated}}\right) \Delta t, SoC_i \leq SoC_{min} \quad (7.10)$$

where  $E_{min}$  and  $SoC_{min}$  are the desired minimum stored energy and corresponding SoC, and  $\eta_d$  is the efficiency during discharge.

The customer energy cost after the BES installation is simply calculated by integrating grid power,  $P^{grid,+}$  and  $P^{grid,-}$ , over a period and multiplying these by the local electric energy rates. Herein, it is assumed that the load varies at a sampling rate  $\Delta t = 1$  hour, and the enforcement of ToU rate (as a pre-requisite for local BES rebate) which generally consists of 3 distinct time periods in a year: summer-on-peak, summer-off-peak, and rest-of-the-year, and a different electricity cost is assigned to each of these. Then the energy cost during for the entire year is determined by

$$EC_{\text{tou}} = \left[ \alpha_1 \sum_{i \in T_1} P_i^{\text{grid},+} + \alpha_2 \sum_{j \in T_2} P_j^{\text{grid},+} + \alpha_3 \sum_{k \in T_3} P_k^{\text{grid},+} - \alpha_n \sum_{m=1}^{8760} P_m^{\text{grid},-} \right] \Delta t \quad (7.11)$$

where  $(\alpha_1, T_1)$ ,  $(\alpha_2, T_2)$ ,  $(\alpha_3, T_3)$ , represent the electricity cost and time period for summer-on-peak, summer-off-peak, and rest-of-the-year, and  $\alpha_n$  is the net metering rate.

### 7.3.2: Additional BESS Services

This second service is applied in sequence during the rest of the year (outside the summer period). Note that unlike most studies that schedule stacked services simultaneously, the proposed scheme does not require complex co-optimization algorithms to implement. The real-time EIM is updated every 5 or 15 minutes and it is characterized by low Locational Marginal Price (LMP), but with significant uncertainties which favor energy arbitrage revenues, compared to Day-Ahead energy trading. In our case the local utility company which participates in this market is to purchase energy (charge a fleet of BTM batteries through aggregation) at a low price during the day where excess solar power occurs, then sell to its customers during the evening at the fixed rate schedule.

For arbitrage to be profitable, the ratio of sell/buy price must satisfy the following inequality:

$$\frac{F_r}{LMP_t} \geq \frac{1}{\eta} \quad (7.12)$$

where  $F_r$  is the fixed energy cost offered by the utility to its customer base (\$/kWh),  $LMP_t$  is the average locational marginal price published in the market during the time period  $t$ , and  $\eta$  is the BES round-trip efficiency. During the energy arbitrage period, the BES state is evaluated by a discrete energy flow model that updates its SoC as follows:

$$SoC_t = SoC_{t-1} + \frac{\left(\eta QC_t - \frac{QD_t}{\eta}\right)}{E_{rated}} \quad (7.13)$$

where  $SoC_t$  is the state-of-charge at time  $t$ ,  $QC_t$  is the quantity of energy charged and  $QD_t$  is the quantity of energy discharged. The yearly company profit from this energy arbitrage service is then determined by

$$EA_{profit} = F_r \sum_{i=1}^N (QD)_i - \sum_{j=1}^M LMP_j (QC)_j \quad (7.14)$$

where  $N$  and  $M$  are the number of discharges and charges made over the lease period. The BES owner will then be compensated either with a fixed amount or a variable amount that is based on performance. Depending on the contracted agreement, the payments can be made monthly or in one lump sum per year. The total yearly income generated by the BES installation is calculated by

$$EC_{save} = EC_{nb} - EC_{tou,wb} + EC_{ea} \quad (7.15)$$

where  $EC_{nb}$  is the customer's yearly energy cost prior to battery installation, and  $EC_{tou,wb}$  is the new yearly energy cost after battery installation (Eq. 7.11), and  $EC_{ea}$  is the yearly revenue generated from energy arbitrage.

The net cost of the battery energy storage system  $BESS_{cost}$  is determined by subtracting the rebate received  $C_{rebate}$  from its initial cost  $C_{battery}$ , and Federal Investment Tax Credit that is specified by a percentage rate  $FITC_{rate}$ ,

$$BESS_{cost} = (C_{battery} - C_{rebate})(1 - FITC_{rate}) \quad (7.16)$$

Finally, the project's economic feasibility can be generally assessed by its Net Present Value (NPV) that is computed by

$$NPV = \sum_{n=0}^N \frac{EC_{savings}^n (1+k)^n}{(1+i)^n} - BESS_{cost} \quad (7.17)$$

where  $i$  is the interest rate,  $n$  is the current year,  $N$  is the lifetime of the BES in years, and  $k$  is the yearly electric energy rate increase.

#### 7.4: Case Study

The mathematical formulation above is now applied to a local residential customer who has a roof-mounted 5.6 kW PV system and would like to conduct an economic analysis of the placement of a BES for solar energy shifting during the summer period and energy arbitrage during the rest of the year (through a lease agreement with the utility). A description of the local electricity rates, residential load profile, expected power generation from the PV system, and the characteristics of the BESS being considered follows.



#### *7.4.1: Local Energy Cost and Incentive Programs*

The State where the customer resides has an aggressive Renewable Portfolio Standard (RPS) that is among the highest in the US (50% by 2030). Due to concern over the future impact on grid operations, the local electric utility company now encourages customers with PV systems to install battery storage systems by providing a rebate which is recovered in electricity rates. The BESS incentive is capped at \$3,000 [69][72]. Battery installations when paired with new or existing solar systems also qualify for the Federal Investment Tax Credit (ITC), currently 30%, but the BESS cannot be charged by the utility, the only allowed method for BESS charging is from the PV system.

Two electricity rate choices are available for residential customers: flat (fixed) rate, and time-of-use (ToU) rate as shown in Table 7.1 below along with the net metering rate [70]. Presently, the incentive structure requires customers who wish to install a BES to sign up for the ToU rate in order to reduce utility peak demand.

Table 7.1 Local Electricity Rates for Single-Family Homes.

| Rate Type             | Month       | Time of Day                    | Time of Day |
|-----------------------|-------------|--------------------------------|-------------|
| Net Metering          | All year    | 1:00-24:00                     | -\$0.09     |
| Flat rate             | All year    | 1:00-24:00                     | \$0.11      |
| ToU Summer-on-peak    | June - Sept | 13:00-19:00<br>(Weekdays Only) | \$0.44      |
| ToU Summer-off-peak   | June - Sept | 19:00-13:00<br>+ Weekends      | \$0.06      |
| ToU Rest-of-the-year. | Oct - May   | All Day                        | \$0.05      |

#### 7.4.2: Residential Load

The residential electrical load consists of two HVAC units, pool pump, lighting, electronic loads, occasional use of oven/microwave, dishwasher, clothes washer/dryer (house heating and cooktops use natural gas). The region is characterized by two seasons: hot season (June-September) and cool season (November-April) with October and May being the transition (or shoulder) months. Consequently, the load demand is significantly higher during the hot season. Figures 7.7 and 7.8 show the hourly load and temperature variations of a typical cool day and a hot day. In the former, the average and peak powers are 1 kW and 3 kW (max temp. = 60°F), while in the latter, they rise to 4 kW and 9 kW, (max temp. = 100°F).

The hourly house load data for an entire year was obtained from the customer online electricity portal, and it is displayed in Figure 7.9 below. The house's total energy consumption is

17,290 kWh, with an average power consumption is 1.97 kW. The base yearly electric energy consumption and associated cost (without PV or BES) are listed in the first 2 columns Table 7.2.

Note the ToU rate is 2.8% higher than flat rate.

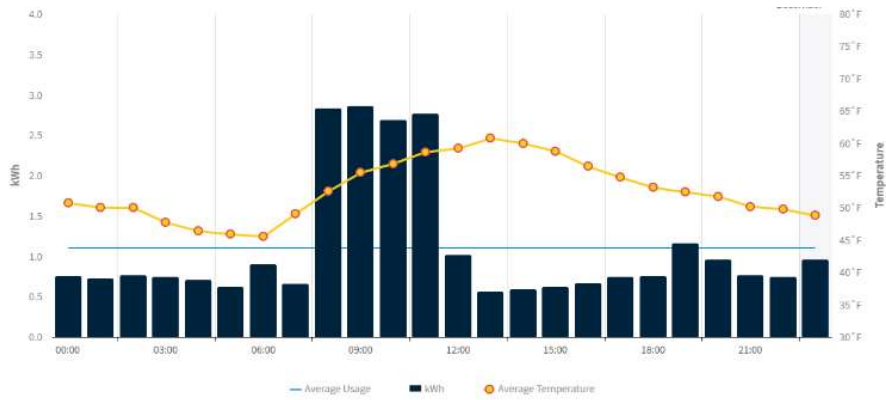


Figure 7.7 Daily Load During Cool Period

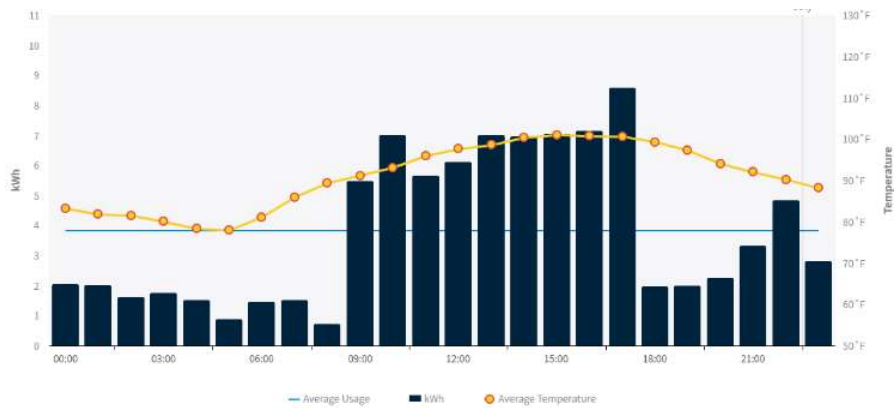


Figure 7.8 Daily Load During Hot Period

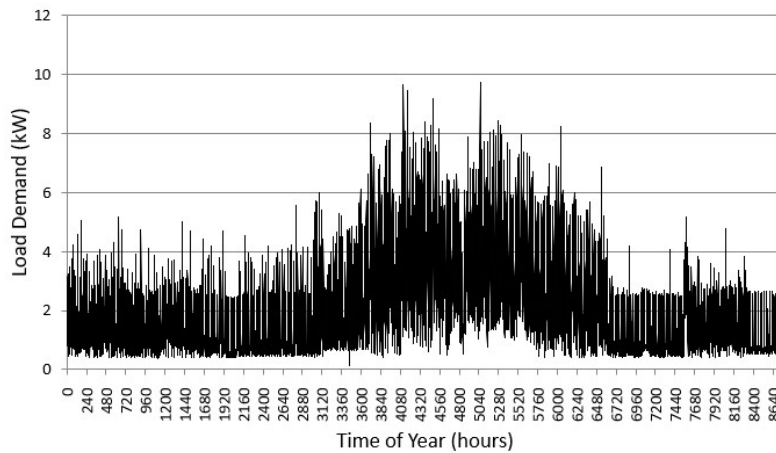


Figure 7.9 Hourly Residential Load Over One Year Period.

#### 7.4.3: PV System Addition

The PV system that is installed on the rooftop of the home has a DC nameplate rating of 5.6 kW, and it is made up of 2 parallel strings, each comprising 10 panels rated at 280 W (STC). A simulation tool (PVWatts) was used to estimate the hourly power production utilizing the following parameter values: local Latitude =  $36^{\circ}$  N, Longitude =  $-115^{\circ}$  W, array tilt =  $22^{\circ}$  and azimuth =  $180^{\circ}$ , system losses = 12%, inverter efficiency = 96%. The resulting hourly power production produced by the PV system is shown in Figure 7.10 below. The total energy produced over one year is estimated at 10,342 kWh - nearly 60% of the house energy consumption.

When combining the residential load profile and solar power production described above, one finds that 7,116 kWh of the solar energy produced was self-consumed (i.e., Self-Consumption Ratio SCR = 69%). Hence, the yearly electric energy drawn from and supplied to

the grid is respectively equal to 10,174 kWh and 3,227 kWh. The modified customer yearly electric energy consumption and associated cost are listed in the middle two columns of Table 7.2. Note that the ToU rate is now 9.3% higher than the flat rate after installing the PV system.

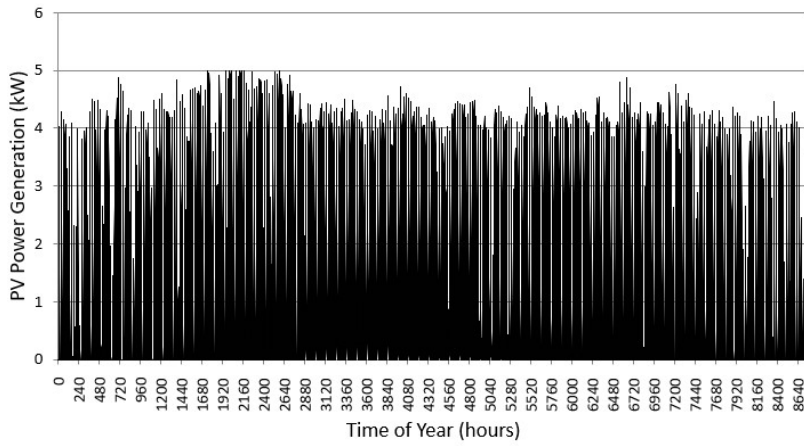


Figure 7.10 Estimated Hourly PV Power Generation Over One Typical Year.

Table 7.2 Customer Energy Cost Breakdown with PV and BESS.

| Utility Rate     | E <sub>0</sub> (kWh) | C <sub>0</sub> (\$) | E <sub>1</sub> (kWh) | C <sub>1</sub> (\$) | E <sub>2</sub> (kWh) | C <sub>2</sub> (\$) |
|------------------|----------------------|---------------------|----------------------|---------------------|----------------------|---------------------|
| Flat rate        | 17,290               | \$1,902             | 10,174               | \$1,119             |                      |                     |
| Net-Metering     |                      |                     | -3,227               | -\$290              | -2,919               | -\$263              |
| <b>Total</b>     | 17,290               | <b>\$1,902</b>      |                      | <b>\$829</b>        |                      |                     |
| Summer-on-peak   | 2,626                | \$1,155             | 1,655                | \$728               | 543                  | 239                 |
| Summer-off peak  | 6,654                | \$399               | 4291                 | \$257               | 5526                 | 332                 |
| Rest-of-the-year | 8,010                | \$401               | 4228                 | \$211               | 4228                 | 211                 |
| <b>Total</b>     | 17,290               | <b>\$1,955</b>      | 10,174               | <b>\$906</b>        | 10,297               | <b>\$519</b>        |

#### 7.4.4: BESS Addition

The BESS that is considered in this study is Tesla Powerwall 2<sup>TM</sup> which can be programmed to operate in time-based control mode, thus allowing solar energy shift during the summer period as well as energy arbitrage during the rest of the year. The unit’s initial cost is \$7,000, and after subtracting the utility rebate and Federal Investment Tax Credit, the net cost is reduced to \$2,800. The BES comes with a 10-year warranty and its technical specifications are as follows: Total/Usable Capacity = 13.5 kWh, Round-trip Efficiency = 90%, Depth-of-Discharge = 100%, Maximum Continuous Discharge Power = 5 kW.

The question now is whether installing a BESS will result in a sufficient amount of savings (from solar energy shift and energy arbitrage) that will justify such installation. During summer-on-peak periods, it makes economic sense to store any additional energy generated in the morning hours and utilize it in the afternoon. Unfortunately, the excess energy during the

summer period is found to be limited to only 308 kWhs due to high load demand. The 10% losses that occur when storing and releasing this block of energy results in 277 kWhs, which leads to a savings of only \$94/year.

Additional savings are achieved by storing PV energy in morning hours when the rates are low then utilizing it in afternoon hours when the rates are much higher. Ideally, the customer would want to eliminate the entire amount of energy imported during the summer-on-peak hours, i.e., 1,655 kWh. But the amount of energy shifting depends on a number of factors including PV energy available in the morning hours prior to 1:00 pm, net energy demand during peak hours (1:00 pm – 7:00 pm), battery capacity and its SoC just before requesting a charge command, and its maximum rate of charge and discharge. Figure 7.11 shows the daily PV energy that is produced in the morning hours and net energy demand during the summer-peak-hour period. While the total amount of PV energy available in the morning hours (1,456 kWh) can offset nearly 88% of the above imported amount, there are a number of days where the demand is higher than the available PV energy, and most importantly, the BESS's capacity is limited to 13.5 kWh (shown by the dotted green line).

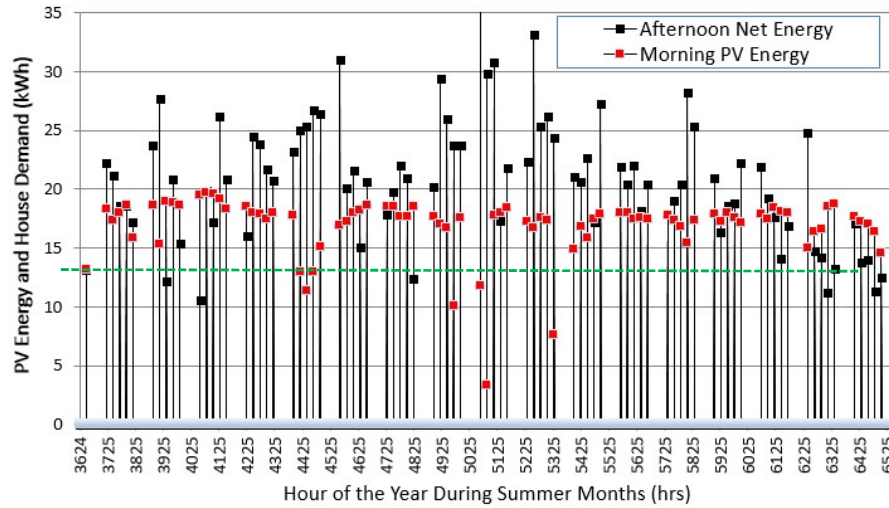


Figure 7.11 Morning PV Energy Available and Net Energy Demand in Afternoon Hours During the Summer-On-Peak Period.

Hourly simulations show that only 1,112 kWh, or 67% of the net energy demand, can be offset by the BES during the summer-on-peak period and this comes at the expense of storing 10% more of this amount (1,235 kWh) due to system losses. The resulting energy consumption and associated cost breakdown after installing a BES are listed in the last 2 columns of Table 7.2. The yearly energy cost savings is estimated at \$310/year, or 37.4%, of the cost without the energy storage system (using the fixed rate without BES as a base since it is more economical than the ToU rate).

Finally, the added value can be obtained through a contract with the local utility to utilize the BES for energy arbitrage by participating in the EIM. Presently, there is insufficient data to estimate such revenue (which depends on the type of agreement where compensation can be either a fixed monthly fee or a performance-based fee). Assuming a simple case where the fixed



lease price  $\$/month$  for a period of 9 months, one can perform some preliminary calculations on the Net Present Value (NPV) of the BES. Using the current interest rate of around 3.5% and typical rate increase in electricity cost of 2%, the NPV is calculated as a function of the number of years after BES installation; the results are shown in Figure 7.12 for  $L = \$0, \$10,$  and  $\$20$  per month. Note that without this second service, the NPV crosses from negative to positive territory just after 10 years, in time when the BES warranty expires. Positive NPV respectively occurs after 7.5 and 6 years for leases of  $\$10/month$  and  $\$20/month$ . The latter value is considered aggressive given the current EIM environment. This latter value corresponds to fully cycling the BES on a daily basis 75% of the time, an average LMP =  $\$20/MWh$ , and 2/3rd of the profit is transferred to the customer.

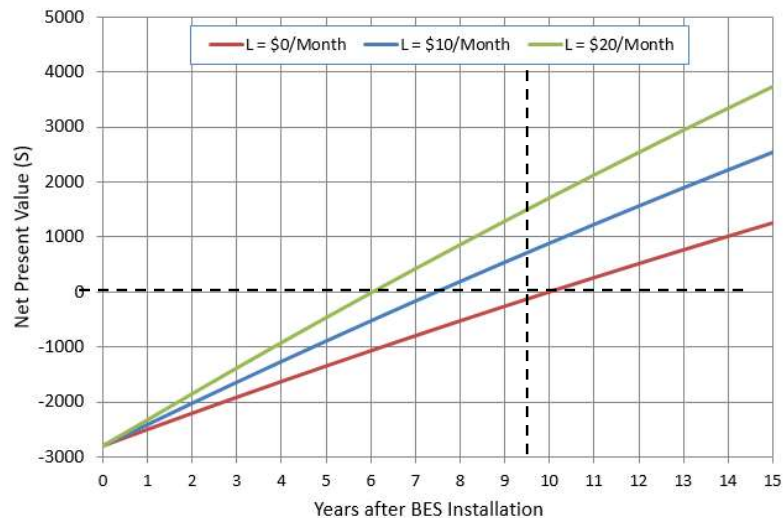


Figure 7.12 BES Net Present Value as Function of Years After Installation.

## Chapter 8: Conclusions

This dissertation presented the design, fabrication, and testing of a microgrid facility which comprises adjustable resistive and inductive loads, a diesel-powered generator, an advanced inverter PV system, a BESS, monitoring, protection, and control devices, built for both research and education purposes. Various experiments explored the application of advanced inverters and their advanced functionalities. The various experiments and results are summarized below.

To study operational challenges of a grid with a large percentage of power generated by PV inverters and how the autonomous functionalities found in advanced inverters can help alleviate some of the issues faced, experiments were performed at a facility with real power generation and a real PV system. These tests included the following functionalities, non-unity PF operation, dynamic Volt/VAr control, soft reconnect, OUV ride through, and OUV ride through. The recorded values produced by the experiments proved that the PV inverter functioned as programmed by the use of its software functions. Future interconnection requirements will undoubtedly require these advanced capabilities for all new distributed resources that are inverter-based.

The experiments performed while the microgrid was experiencing different conditions of power import/export, measured the dynamic response of the advanced inverter's performance due to intentional islanding of the microgrid. The results of the tests showed an advanced inverter and with an increased ride through times to anomalous frequency and voltages will provide reliability and power quality superior to a standard PV inverter, which lacks adjustability and has IEEE Std. 1547 defined tolerances.

Regarding the advanced inverter's impact on microgrid stability when comparing grid support functions and islanded detection functions, the data from the tests performed supported

no firm conclusions. This is due to inverter ride times varying inconsistently with conditions that were very similar but not exact and the unknown implementation of grid disconnect detection methods and grid support functions used in the inverter. These tests show that during a utility disconnect, it is difficult to project the disconnect time of the inverter. This is due to the absence of information with regards to the inverters power tracking methods, delay times of advanced functions commands, and how the inverters dynamic operation affects the active anti-islanding detection. However, analysis of the results from the test performed showed that where the utility disconnects within the 60 Hz cycle does have an impact disconnect time of the inverter.

Below are the electrical and operational characteristics of a residential BESS operating in conjunction with a PV system. Some of the major conclusions from the results of the tests conducted are as follows:

- The round-trip efficiency of the BESS that was calculated from several charge/discharge tests averaged nearly 90%, which is in line with the system specifications.
- The quality of the voltage waveform produced by the BESS when operating off-grid has a THD of less than 1% - that is of higher quality than that provided by the local grid.
- In the event of a power outage, the BESS backed up the load in less than 4 cycles of the 60 Hz frequency, or 50 milliseconds. The BESS's internal inverter also provided a reference voltage to the PV inverter, thus allowing it to generate power even under a grid outage.

An economic analysis for adding a battery energy storage system to a local residential home that is equipped with a PV system for the purpose of shifting solar energy during periods during high ToU rates while taking advantage of current State and Federal incentives. To increase revenue, the BES is leased to the local utility company for energy arbitrage in a regional energy imbalance market. This second which is applied in a stacked manner outside the peak summer

period (energy arbitrage through aggregation by the local utility company) can generate additional revenue. Numerical simulations indicate the BES can reduce the homeowner's energy bill by nearly 38%, but a most optimistic additional amount from this particular service will result in a positive NPV after no less than 6 years. The cost savings calculated in this study applies only to the local region and can differ significantly for other regions with different ToU rates, net metering rates, and local incentives for energy storage.

# Appendix

## 1. PV Module Technical Specs



### SW 270 mono / Version 2.5 Frame

SW-02-5160US 11-2012

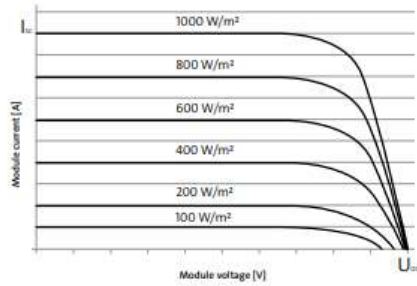
#### PERFORMANCE UNDER STANDARD TEST CONDITIONS (STC)\*

|                             |           | SW 270 |
|-----------------------------|-----------|--------|
| Maximum power               | $P_{max}$ | 270 Wp |
| Open circuit voltage        | $V_{oc}$  | 38.3 V |
| Maximum power point voltage | $V_{mp}$  | 32.1 V |
| Short circuit current       | $I_{sc}$  | 8.90 A |
| Maximum power point current | $I_{mp}$  | 8.42 A |

\*STC: 1000W/m<sup>2</sup>, 25°C, AM 1.5

#### THERMAL CHARACTERISTICS

|                       |               |
|-----------------------|---------------|
| NOCT                  | 46 °C         |
| TC $I_{sc}$           | 0.004 %/K     |
| TC $V_{oc}$           | -0.30 %/K     |
| TC $P_{mp}$           | -0.45 %/K     |
| Operating temperature | -40°C to 85°C |



#### PERFORMANCE AT 800 W/m<sup>2</sup>, NOCT, AM 1.5

|                             |           | SW 270   |
|-----------------------------|-----------|----------|
| Maximum power               | $P_{max}$ | 194.9 Wp |
| Open circuit voltage        | $V_{oc}$  | 34.5 V   |
| Maximum power point voltage | $V_{mp}$  | 28.9 V   |
| Short circuit current       | $I_{sc}$  | 7.19 A   |
| Maximum power point current | $I_{mp}$  | 6.74 A   |

Minor reduction in efficiency under partial load conditions at 25°C: at 200W/m<sup>2</sup>, 95% (+/-3%) of the STC efficiency (1000 W/m<sup>2</sup>) is achieved.

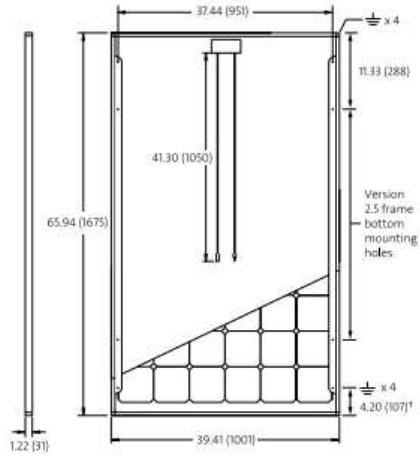
#### COMPONENT MATERIALS

|                  |                                     |
|------------------|-------------------------------------|
| Cells per module | 60                                  |
| Cell type        | Mono crystalline                    |
| Cell dimensions  | 6.14 in x 6.14 in (156 mm x 156 mm) |
| Front            | tempered glass (EN 12150)           |
| Frame            | Clear anodized aluminum             |
| Weight           | 46.7 lbs (21.2 kg)                  |

#### SYSTEM INTEGRATION PARAMETERS

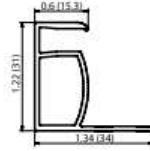
|                              |                   |                                   |
|------------------------------|-------------------|-----------------------------------|
| Maximum system voltage SC II | 1000 V            |                                   |
| Max. system voltage USA NEC  | 600 V             |                                   |
| Maximum reverse current      | 16 A              |                                   |
| Number of bypass diodes      | 3                 |                                   |
| UL Design Loads*             | Two rail system   | 113 psf downward<br>64 psf upward |
| UL Design Loads*             | Three rail system | 170 psf downward<br>64 psf upward |
| IEC Design Loads*            | Two rail system   | 113 psf downward<br>50 psf upward |

\*Please refer to the Sunmodule installation instructions for the details associated with these load cases.



#### ADDITIONAL DATA

|                             |               |
|-----------------------------|---------------|
| Power sorting <sup>1)</sup> | -0 Wp / +5 Wp |
| J-Box                       | IP65          |
| Connector                   | MC4 / KSK4    |
| Module efficiency           | 16.10 %       |
| Fire rating (UL 790)        | Class C       |



#### VERSION 2.5 FRAME

- Compatible with both "Top-Down" and "Bottom" mounting methods
- Grounding Locations:
  - 4 corners of the frame
  - 4 locations along the length of the module in the extended flange!

**NEW!**

Black & Veatch validated PAN files now available.  
Ask your account manager for more information.

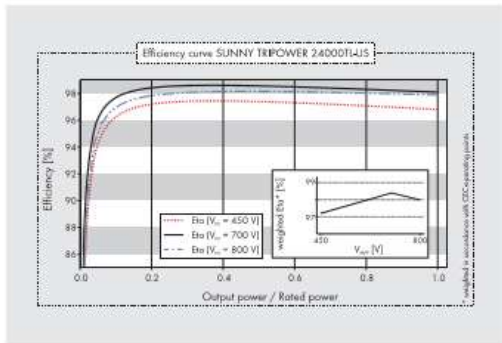
1) Sunmodules dedicated for the United States and Canada are tested to UL 1703 Standard and listed by a third party laboratory. The laboratory may vary by product and region. Check with your SolarWorld representative to confirm which laboratory has a listing for the product.

2) Measuring tolerance traceable to TUV Rheinland: +/- 2% (TUV Power Controlled).

3) All units provided are imperial. SI units provided in parentheses.

SolarWorld AG reserves the right to make specification changes without notice.

## 2. Inverter Technical Specs



### Accessories



RS485 interface  
DM-485CBUS-10



SMA Cluster Controller  
CLCON-10



Connection Unit  
CU 1000-US-10

● Standard features ○ Optional features – Not available  
Data at nominal conditions

| Technical data  | Sunny Tripower<br>12000TL-US  | Sunny Tripower<br>15000TL-US | Sunny Tripower<br>20000TL-US | Sunny Tripower<br>24000TL-US |
|---|-------------------------------|------------------------------|------------------------------|------------------------------|
| <b>Input (DC)</b>                                     |                               |                              |                              |                              |
| Max. usable DC power (@ $\cos \phi = 1$ )             | 12250 W                       | 15300 W                      | 20400 W                      | 24500 W                      |
| Max. DC voltage*                                      | 1000 V                        | 1000 V                       | 1000 V                       | 1000 V                       |
| Rated MPPT voltage range                              | 300 V...800 V                 | 300 V...800 V                | 380 V...800 V                | 450 V...800 V                |
| MPPT operating voltage range                          | 150 V...1000 V                | 150 V...1000 V               | 150 V...1000 V               | 150 V...1000 V               |
| Min. DC voltage / start voltage                       | 150 V / 188 V                 | 150 V / 188 V                | 150 V / 188 V                | 150 V / 188 V                |
| Number of MPPT tracker inputs                         | 2                             | 2                            | 2                            | 2                            |
| Max. input current / per MPPT tracker input           | 66 A / 33 A                   | 66 A / 33 A                  | 66 A / 33 A                  | 66 A / 33 A                  |
| <b>Output (AC)</b>                                    |                               |                              |                              |                              |
| AC nominal power                                      | 12000 W                       | 15000 W                      | 20000 W                      | 24000 W                      |
| Max. AC apparent power                                | 12000 VA                      | 15000 VA                     | 20000 VA                     | 24000 VA                     |
| Output phases / line connections                      | 3 / 3-N-PE                    |                              |                              |                              |
| Nominal AC voltage                                    | 480 / 277 V WYE               |                              |                              |                              |
| AC voltage range                                      | 244 V...305 V                 |                              |                              |                              |
| Rated AC grid frequency                               | 60 Hz                         |                              |                              |                              |
| AC grid frequency / range                             | 50 Hz, 60 Hz / -6 Hz...+5 Hz  |                              |                              |                              |
| Max. output current                                   | 14.4 A                        | 18 A                         | 24 A                         | 29 A                         |
| Power factor at rated power / adjustable displacement | 1 / 0.8 leading...0.8 lagging |                              |                              |                              |
| Harmonics   | < 3 %                         |                              |                              |                              |
| <b>Efficiency</b>                                     |                               |                              |                              |                              |
| Max. efficiency                                       | 98.2 %                        | 98.2 %                       | 98.5 %                       | 98.5 %                       |
| CEC efficiency  | 97.5%                         | 97.5%                        | 97.5%                        | 98.0%                        |
| <b>Protection devices</b>                             |                               |                              |                              |                              |

\*All protection and services described in detail on technical data sheet for current information, see [www.sma.de/en](http://www.sma.de/en)

\*

|   |   |                   |                   |                   |
|---|---|-------------------|-------------------|-------------------|
| DC reverse polarity protection                            | ●   | ●                 | ●                 | ●                 |
| Ground fault monitoring / Grid monitoring                 | ●   | ●                 | ●                 | ●                 |
| All-pole sensitive residual current monitoring unit       | ●   | ●                 | ●                 | ●                 |
| DC AFCI compliant to UL 1699B                             | ●   | ●                 | ●                 | ●                 |
| AC short circuit protection                               | ●   | ●                 | ●                 | ●                 |
| Protection class / overvoltage category                   | I / IV  | I / IV            | I / IV            | I / IV            |
| <b>General data</b>                                       |   |                   |                   |                   |
| Dimensions (W / H / D) in mm (in)                         | 665 / 690 / 265 (26.1 / 27.1 / 10.4)  |                   |                   |                   |
| Packing dimensions (W / H / D) in mm (in)                 | 780 / 790 / 380 (30.7 / 31.1 / 15.0)  |                   |                   |                   |
| Weight  | 55 kg (121 lbs)   |                   |                   |                   |
| Packing weight  | 61 kg (134.5 lbs)   |                   |                   |                   |
| Operating temperature range                               | -25°C...+60°C   |                   |                   |                   |
| Noise emission (typical)                                  | 51 dB(A)  |                   |                   |                   |
| Internal consumption at night                             | 1 W   |                   |                   |                   |
| Topology  | Transformerless   |                   |                   |                   |
| Cooling concept   | OptiCool  |                   |                   |                   |
| Electronics protection rating                             | NEMA 3R   |                   |                   |                   |
| <b>Features</b>   |   |                   |                   |                   |
| Display / LED indicators (Status / Fault / Communication) | - / ●   | - / ●             | - / ●             | - / ●             |
| Interfaces: Speedwire / RS485                             | ● / ○   | ● / ○             | ● / ○             | ● / ○             |
| Mounting angle range                                      | 15°...90°   | 15°...90°         | 15°...90°         | 15°...90°         |
| Warranty: 10 / 15 / 20 years                              | ● / ○ / ○   | ● / ○ / ○         | ● / ○ / ○         | ● / ○ / ○         |
| Certifications and approvals                              | UL 1741, UL 1998, UL 1699B, IEEE 1547, FCC Part 15 (Class A & B), CAN/CSA C22.2 107.1-1 |                   |                   |                   |
| NOTE: US inverters ship with gray lids                    |   |                   |                   |                   |
| *Suitable for 600 V DC max. systems                       |   |                   |                   |                   |
| Type designation  | STP 12000TL-US-10   | STP 15000TL-US-10 | STP 20000TL-US-10 | STP 24000TL-US-10 |

STP11012-24DL3110 SMA and Sunny Tripower are registered trademarks of SMA Solar Technology AG. Rrived on IEC certified pot are subject to change, even for reasons of country-specific deviations, at any time without notice. SMA assumes no liability for errors or omissions.

Toll Free +1 888 4 SMA USA  
www.SMA-America.com

SMA America, LLC



### 3. Diesel Generator Reactances and Time Constants

| Unsaturated (ref. EN60034-4) |  |   | NPE32-A/4 | NPE32-B/4 | NPE32-C/4 | NPE32-D/4 | NPE32-E/4 | NPE32-F/4 |
|------------------------------|--|---|-----------|-----------|-----------|-----------|-----------|-----------|
| <b>Xd</b>                    | Direct-axis synchronous reactance      | % | 402,8     | 378,6     | 380,2     | 388,8     | 435,5     | 379,9     |
| <b>Xd'</b>                   | Direct-axis transient reactance        | % | 19,8      | 18,5      | 17,7      | 18        | 21,4      | 18,7      |
| <b>Xd''</b>                  | Direct-axis subtransient reactance     | % | 14,1      | 13,2      | 12,6      | 12,9      | 15,3      | 13,3      |
| <b>Xq</b>                    | Quadrature-axis synchronous reactance  | % | 129,3     | 120,9     | 115,8     | 117,7     | 139,7     | 121,9     |
| <b>Xq'</b>                   | Quadrature-axis transient reactance    | % | 129,3     | 120,9     | 115,8     | 117,7     | 139,7     | 121,9     |
| <b>Xq''</b>                  | Quadrature-axis subtransient reactance | % | 43,2      | 40,4      | 38,6      | 39,3      | 46,7      | 40,7      |
| <b>X<sub>2</sub></b>         | Negative-sequence reactance            | % | 29,4      | 27,5      | 26,3      | 26,8      | 31,8      | 27,7      |
| <b>X<sub>0</sub></b>         | Zero sequence reactance                | % | 3,68      | 3,44      | 3,29      | 3,35      | 3,98      | 3,47      |
| Saturated                    |  |   |           |           |           |           |           |           |
| <b>Xd</b>                    | Direct-axis synchronous reactance      | % | 342,3     | 320,1     | 308,2     | 311,8     | 370,1     | 322,9     |
| <b>Xd'</b>                   | Direct-axis transient reactance        | % | 16,8      | 15,7      | 15        | 15,3      | 18,2      | 15,9      |
| <b>Xd''</b>                  | Direct-axis subtransient reactance     | % | 12        | 11,2      | 10,7      | 10,9      | 13        | 11,3      |
| <b>Xq</b>                    | Quadrature-axis synchronous reactance  | % | 109,9     | 102,8     | 98,3      | 100       | 118,8     | 103,6     |
| <b>Xq'</b>                   | Quadrature-axis transient reactance    | % | 109,9     | 102,8     | 98,3      | 100       | 118,8     | 103,6     |
| <b>Xq''</b>                  | Quadrature-axis subtransient reactance | % | 36,7      | 34,3      | 32,8      | 33,4      | 39,7      | 34,6      |
| <b>X<sub>2</sub></b>         | Direct-axis synchronous reactance      | % | 25        | 23,4      | 22,3      | 22,7      | 27        | 23,6      |
| <b>X<sub>0</sub></b>         | Zero sequence reactance                | % | 3,68      | 3,44      | 3,29      | 3,35      | 3,98      | 3,47      |

|                        |                            |     |       |       |       |       |       |       |
|------------------------|----------------------------|-----|-------|-------|-------|-------|-------|-------|
| <b>K<sub>cc</sub></b>  | Short circuit ratio        |     | 0,41  | 0,42  | 0,44  | 0,43  | 0,46  | 0,45  |
| <b>T<sub>d'</sub></b>  | Transient time constant    | sec | 0,051 | 0,051 | 0,052 | 0,051 | 0,065 | 0,061 |
| <b>T<sub>d''</sub></b> | Subtransient time constant | sec | 0,08  | 0,082 | 0,081 | 0,08  | 0,082 | 0,082 |
| <b>T<sub>do</sub></b>  | Open circuit time constant | sec | 1,1   | 1,05  | 1,13  | 1,08  | 1,1   | 1,08  |
| <b>T<sub>a</sub></b>   | Armature time constant     | sec | 0,02  | 0,025 | 0,026 | 0,022 | 0,025 | 0,021 |

#### 3.1 Additional Diesel Generator Data

|  |                                 |   |  |           |         |           |           |           |
|--|---------------------------------|---|--|-----------|---------|-----------|-----------|-----------|
| <b>I<sub>o</sub></b>                   | Excitation current at no load   | A | 0,4  | 0,41      | 0,5     | 0,5       | 0,7       | 0,75      |
| <b>I<sub>c</sub></b>                   | Excitation current at full load | A | 2,2  | 2,4       | 2,3     | 1,8       | 2,0       | 2,2       |
| <b>Overload</b>                        |                                 |   | 1 hour in a 6 hours period 110% rated load |           |         |           |           |           |
| Overload per 20 sec.                   |                                 | % | 300  |           |         |           |           |           |
| Heat dissipation                       |                                 | W | 1407                                       | 2118      | 2329    | 2845      | 4067      | 4442      |
| Telephone Harmonic Factor - THF        |                                 | % | <2   | <2        | <2      | <2        | <2        | <2        |
| Waveform Distors.(THD) full load LL/LN |                                 | % | 4,5 / 4,5                                  | 4,5 / 4,5 | 4 / 4   | 3,8 / 3,8 | 3,5 / 3,5 | 3,5 / 3,5 |
| Waveform Distors.(THD) no load LL/LN   |                                 | % | 6,5 / 6                                    | 6,5 / 6   | 5 / 4,5 | 4,5 / 4,5 | 3,8 / 3,8 | 3,8 / 3,8 |

## Additional Characteristics

| Data                             | NPE32-A/4           |       | NPE32-B/4 |       | NPE32-C/4 |       | NPE32-D/4 |       | NPE32-E/4 |       | NPE32-F/4 |       |       |
|----------------------------------|---------------------|-------|-----------|-------|-----------|-------|-----------|-------|-----------|-------|-----------|-------|-------|
|                                  | 50Hz                | 60Hz  | 50Hz      | 60Hz  | 50Hz      | 60Hz  | 50Hz      | 60Hz  | 50Hz      | 60Hz  | 50Hz      | 60Hz  |       |
| Damper cage                      | Copper              |       |           |       |           |       |           |       |           |       |           |       |       |
| Stator Winding Resistance (20°C) | Ω                   | 1,17  |           | 0,73  |           | 0,44  |           | 0,72  |           | 0,15  |           | 0,11  |       |
| Rotor Winding Resistance (20°C)  | Ω                   | 1,216 |           | 1,293 |           | 1,376 |           | 1,491 |           | 1,697 |           | 1,853 |       |
| Stator Exciter Resistance (20°C) | Ω                   | 11,05 |           | 11,05 |           | 11,05 |           | 11,05 |           | 11,05 |           | 11,05 |       |
| Rotor Exciter Resistance (20°C)  | Ω                   | 0,32  |           | 0,32  |           | 0,32  |           | 0,32  |           | 0,32  |           | 0,32  |       |
| Weight of complete generator     | kg                  | 77,0  |           | 83,0  |           | 90,0  |           | 102,0 |           | 120,0 |           | 132,0 |       |
| Unbalanced magnetic pull         | kN/mm               | 3,8   |           | 3,8   |           | 3,9   |           | 3,9   |           | 4,2   |           | 4,5   |       |
| Air flow                         | m <sup>3</sup> /min | 6,9   | 8,9       | 6,9   | 8,9       | 6,9   | 8,9       | 6,9   | 8,9       | 6,9   | 8,9       | 6,9   | 8,9   |
| Noise level at 1m/7m             | dB(A)               | 64/54 | 67/58     | 64/54 | 67/58     | 64/54 | 67/58     | 64/54 | 67/58     | 64/54 | 67/58     | 64/54 | 67/58 |

## Efficiencies @ 60Hz

| Models    | 415V 60Hz |      |      |      |      | 440V 60Hz |      |      |      |      | 460V 60Hz |      |      |      |      | 480V 60Hz |      |      |      |      |      |
|-----------|-----------|------|------|------|------|-----------|------|------|------|------|-----------|------|------|------|------|-----------|------|------|------|------|------|
|           | 0.25      | 0.5  | 0.75 | 1    | 1.1  | 0.25      | 0.5  | 0.75 | 1    | 1.1  | 0.25      | 0.5  | 0.75 | 1    | 1.1  | 0.25      | 0.5  | 0.75 | 1    | 1.1  |      |
| NPE32-A/4 | %         | 71,9 | 78,8 | 81,1 | 80,8 | 80,5      | 72,1 | 78,9 | 81,2 | 80,9 | 80,5      | 72,4 | 79,2 | 81,4 | 81,1 | 80,8      | 72,5 | 79,3 | 81,5 | 81,2 | 80,9 |
| NPE32-B/4 | %         | 74,5 | 78,7 | 80,9 | 80,7 | 80,6      | 74,7 | 78,8 | 81,0 | 80,8 | 80,6      | 75,0 | 79,1 | 81,2 | 81,0 | 80,9      | 75,1 | 79,2 | 81,3 | 81,1 | 81,0 |
| NPE32-C/4 | %         | 74,9 | 79,2 | 81,5 | 81,1 | 80,8      | 75,1 | 79,3 | 81,6 | 81,2 | 81,0      | 75,4 | 79,6 | 81,8 | 81,4 | 81,0      | 75,5 | 79,7 | 81,9 | 81,5 | 81,2 |
| NPE32-D/4 | %         | 75,5 | 80,9 | 82,6 | 82,1 | 81,9      | 75,7 | 81,0 | 82,7 | 82,2 | 81,9      | 76,0 | 81,3 | 82,9 | 82,4 | 82,2      | 76,1 | 81,4 | 83,0 | 82,5 | 82,1 |
| NPE32-E/4 | %         | 76,5 | 81,3 | 83,2 | 82,9 | 82,6      | 76,7 | 81,4 | 83,3 | 83,0 | 82,6      | 77,0 | 81,7 | 83,5 | 83,2 | 82,9      | 77,1 | 81,8 | 83,6 | 83,3 | 83,0 |
| NPE32-F/4 | %         | 76,4 | 81,2 | 83,0 | 82,6 | 82,3      | 76,6 | 81,3 | 83,1 | 82,7 | 82,5      | 76,9 | 81,6 | 83,3 | 82,9 | 82,6      | 77,0 | 81,7 | 83,4 | 83,0 | 82,7 |

## 4. Diesel Generator Synchronizing Module Spec Sheet



# DSE8620

## SYNCHRONISING AUTO MAINS FAILURE CONTROL MODULE

### FEATURES



### KEY FEATURES

- Mains (utility) failure detection
- Comprehensive synchronising & loadsharing capabilities
- Built-in governor and AVR control
- Base load (kW export) functionality
- Positive & negative kVAr export control
- Peak lopping & shaving functionality
- Mains (utility) power (kW, kV Ar, kV A & pf) monitoring
- Mains (utility) de-coupling protection
- Generator power (kW, kV Ar, kV A & pf) monitoring
- Advanced SMS control and fault messaging (additional GSM modem required)
- Easy access diagnostic pages including modern diagnostic pages
- Data logging and trending
- CAN, MPU and Frequency speed sensing
- Tier 4 CAN engine support
- "Protections disabled" feature
- Front panel editing with PIN protection
- Fully configurable using DSE Configuration Suite PC software via USB
- 4 Line back-lit LCD text display

### KEY BENEFITS

- Compatible with DSE8003
- 132 x 64 pixel ratio display for clarity
- Real-time clock provides accurate event logging
- Ethernet communication, provides built in advanced remote monitoring.
- Can be integrated into building management systems (BMS) and programmable logic control (PLC)
- Increased input and output expansion capability via DSENet\*
- Licence-free PC software
- IP65 rating (with supplied gasket) offers increased resistance to water ingress

- Overload (kW & kV Ar) protection
- Reverse power (kW & kV Ar) protection
- Mains (utility) kW export protection
- Unbalanced load protection
- Independent earth fault protection
- Advanced integral PLC editor
- 11 Configurable inputs
- 8 Configurable outputs
- Configurable flexible sensor inputs
- DSENet\* expansion compatibility
- User configurable RS232, RS485 and Ethernet communications
- Remote SCADA monitoring via various DSE software applications
- MODBUS RTU & TCP support
- User configurable MODBUS pages
- LED and LCD alarm indication
- Configurable display languages
- USB connectivity
- Customisable status screens
- Five key menu navigation
- 3 Configurable maintenance alarms
- Multiple date and time run scheduler
- Manual fuel pump control
- Fuel usage monitor and low fuel level protection
- Charge alternator failure protection
- Load switching (load shedding and dummy load control)
- Configurable event log (250)
- Backed up real time clock

- Ingress
- Advanced Internal PLC editor allows user configurable functions to meet specific application requirements.

### EXPANSION DEVICES

- DSE124 CAN/MSR Extender
- DSE2130 Input Expansion Module
- DSE2131 Ratio-metric Input Expansion Module
- DSE2133 RTD & Thermo-couple Expansion Module
- DSE2152 Ratio-metric Output Expansion Module
- DSE2157 Output Expansion Module
- DSE2548 LED Expansion Module

### RELATED MATERIALS

#### TITLE

DSE8620 Installation Instructions  
DSE8620 Operator Manual  
DSE8600 PC Configuration Suite Manual

#### PART NO'S

053-129  
057-142  
057-119

### DEEP SEA ELECTRONICS INC USA

3230 Williams Avenue, Rockford, IL 61101-2668 USA  
TELEPHONE +1 (815) 316 8706 FACSIMILE +1 (815) 316 8708  
EMAIL sales@deepseausa.com WEBSITE www.deepseausa.com

Deep Sea Electronics Plc maintains a policy of continuous development and reserves the right to change the details shown on this data sheet without prior notice. The contents are intended for guidance only.

Registered in England & Wales No.01319649  
VAT No.316923457

### SPECIFICATION

#### DC SUPPLY

**CONTINUOUS VOLTAGE RATING**  
8 V to 35 V continuous

#### CRANKING DROPOUTS

Able to survive 0 V for 50 ms, providing supply was at least 10 V before dropout and supply recovers to 5 V. This is achieved without the need for internal batteries

#### MAXIMUM OPERATING CURRENT

460 mA at 12 V, 245 mA at 24 V

#### MAXIMUM STANDBY CURRENT

375 mA at 12 V, 200 mA at 24 V

#### CHARGE FAIL/EXCITATION RANGE

0 V to 35 V

#### OUTPUTS

##### OUTPUT A (FUEL)

15 A DC at supply voltage

##### OUTPUT B (START)

15 A DC at supply voltage

##### OUTPUTS C & D

8 A AC at 250 V AC (Volt free)

**AUXILIARY OUTPUTS E, F, G, H, I & J**  
2 A DC at supply voltage

#### GENERATOR & MAINS

**VOLTAGE RANGE**

15 V to 333 V AC (L-N)

**FREQUENCY RANGE**

3.5 Hz to 75 Hz

**MAGNETIC PICK-UP**

**VOLTAGE RANGE**

+/- 0.5 V to 70 V

**FREQUENCY RANGE**

10,000 Hz (max)

**BUILT-IN GOVERNOR CONTROL**

**MINIMUM LOAD IMPEDANCE**

10000  
Fully isolated

**GAIN VOLTAGE**

0 V to 10 V DC

Fully isolated

**OFFSET VOLTAGE**

+/- 10 V DC

Fully isolated

**BUILT-IN AVR CONTROL**

**MINIMUM LOAD IMPEDANCE**

10000  
Fully isolated

**GAIN VOLTAGE**

0 V to 10 V DC

Fully isolated

**OFFSET VOLTAGE**

+/- 10 V DC

Fully isolated

#### DIMENSIONS

##### OVERALL

240 mm x 181 mm x 42 mm

9.4" x 6.8" x 1.6"

##### PANEL CUTOUT

220 mm x 160 mm

8.7" x 6.3"

##### MAXIMUM PANEL THICKNESS

8 mm

0.3"

##### OPERATING TEMPERATURE RANGE

-30 °C to +70 °C

##### STORAGE TEMPERATURE RANGE

-40 °C to +85 °C

055-099/05/11 (P) US

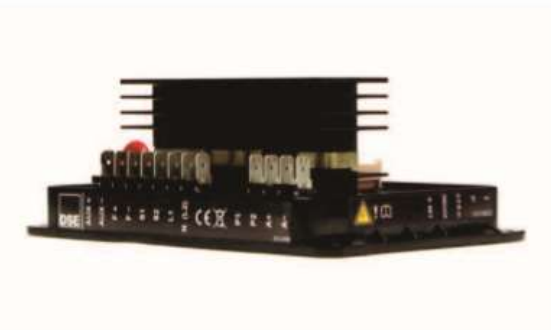
## 5. Automatic Voltage Regulator (AVR) Spec Sheet



# DSEA106

## AUXILIARY/SHUNT POWERED DIGITAL AVR

### FEATURES



### KEY FEATURES

- Soft start ramping
- Under Frequency Roll Off (UFRO) protection
- Loss of voltage sensing protection

### KEY BENEFITS

- Digital electronics ensures a smooth, stable, regulated AC output voltage from the alternator.
- Configurable to suit a wide

### SPECIFICATION

|   |
|---|
| <b>POWER SUPPLY</b>                                       |
| <b>VOLTAGE RANGE</b><br>100 V AC to 300 V AC (Ph to N/Ph) |
| <b>FREQUENCY RANGE</b><br>40 Hz to 100 Hz                 |
| <b>ALTERNATOR OUTPUT SENSING</b>                          |
| <b>VOLTAGE RANGE</b><br>15 V AC to 600 V AC (Ph to N/Ph)  |
| <b>FREQUENCY RANGE</b><br>40 Hz to 65 Hz                  |
| <b>EXCITATOR OUTPUT</b>                                   |
| <b>EXCITATOR FIELD WINDING</b>                            |
| <b>IMPEDANCE</b><br>5 $\Omega$ to 50 $\Omega$             |
| <b>CONTINUOUS VOLTAGE RATING</b><br>0 V DC to 100 V DC    |
| <b>CONTINUOUS CURRENT RATING</b><br>0 A DC to 7 A DC      |
| <b>MAXIMUM CURRENT RATING</b><br>15 A DC for 10 seconds   |
| <b>QUADRATURE DROOP CT</b>                                |
| <b>MAXIMUM SECONDARY CURRENT</b><br>5 A AC                |
| <b>BURDEN</b><br>0.25 VA                                  |
| <b>ACCURACY</b><br>1%                                     |
| <b>REMOTE VOLTAGE ADJUSTMENT</b>                          |
| <b>POTENTIOMETER</b><br>5 k $\Omega$                      |
| <b>VOLTAGE INPUT</b><br>0 V DC to 10 V DC                 |

- Over excitation protection
  - Remote voltage adjustment using 0 V to 10 V signal and 5 kΩ potentiometer.
  - DIP switch selection for voltage, frequency and stability ranges.
  - Potentiometer adjustment for voltage set points, droop, UFRO, proportional and integral gain.
  - LED indication for fault and operating status
  - Configurable via DSE Configuration Suite PC Software connected via the DSE814 Configuration Interface.
  - Chassis mountable potted enclosure
  - Spade terminals for easy connection
- range of alternators with auxiliary winding or shunt power supplies.
- Suitable for generator synchronising and load sharing applications with connections for a quadrature droop CT and remote voltage adjustment.
  - Compatible with all DSE synchronising and load sharing controllers.
  - Licence-free PC software
  - Comprehensive PC configuration using the DSE Configuration Suite PC Software and the DSE814 Configuration Interface.
  - Simple to use with onboard set up using a combination of DIP switches and potentiometers.

#### DIMENSIONS

**OVERALL**  
167 mm x 100 mm x 61 mm  
6.6" x 4.3" x 2.4"

**STORAGE TEMPERATURE RANGE**  
-40 °C to +85 °C  
-40 °F to +185 °F

**OPERATING TEMPERATURE RANGE**  
-40 °C to +70 °C  
-40 °F to +158 °F

#### RELATED MATERIALS

| TITLE  | PART NO'S |
|--|-----------|
| DSEA106 Installation Instructions              | 053-177   |
| DSEA106 Operator Manual                        | 057-241   |
| DSEA106 Configuration Suite PC Software Manual | 057-242   |
| DSE814 Datasheet                               | 055-197   |

#### DEEP SEA ELECTRONICS PLC UK

Highfield House, Hunmanby Industrial Estate, Hunmanby YO14 0PH  
**TELEPHONE** +44 (0) 1723 890099 **FACSIMILE** +44 (0) 1723 893303  
**EMAIL** sales@deepseapl.com **WEBSITE** www.deepseapl.com

Deep Sea Electronics Plc maintains a policy of continuous development and reserves the right to change the details shown on this data sheet without prior notice. The contents are intended for guidance only.

#### DEEP SEA ELECTRONICS INC USA

3230 Williams Avenue, Rockford, IL 61101-2668 USA  
**TELEPHONE** +1 (815) 316 8706 **FACSIMILE** +1 (815) 316 8708  
**EMAIL** sales@deepseausa.com **WEBSITE** www.deepseausa.com

Registered in England & Wales No.01319649  
 VAT No.316823457

095-106/07/15 (1)

## 6. Diesel Generator Governor Spec Sheet

### APECS DPG-2201-00X

Digital Controllers for  
Isochronous Generators  
with Load Sharing Capability



|  |                                     |
|--|-------------------------------------|
| Operating Voltage Range:               | 9–30 Vdc *                          |
| Rated Output Current:                  | 7 A Maximum (continuous)            |
| Maximum Surge Current:                 | 14 A (not to exceed ten seconds)    |
| Connections:                           | Terminal strip with 13 terminals    |
| Input Signal from the Magnetic Pickup: | 2.0 Vac RMS minimum during cranking |

| PARAMETER NAME   | DEFAULT | MINIMUM            | MAXIMUM             |
|--|---------|--------------------|---------------------|
| 1. No. Of Flywheel Teeth   | -001    | 0                  | 0                   |
|  | -002    | 0                  | 572                 |
| 2. Set Speed A *   | 1000    | Set Speed A Min    | Set Speed A Max     |
| 3. Set Speed B *   | 1000    | Set Speed B Min    | Set Speed B Max     |
| 4. Idle Speed *  | 500     | Idle Speed Min     | Idle Speed Max      |
| 5. Proportional  | 25      | 1                  | 99                  |
| 6. Integral  | 50      | 0                  | 99                  |
| 7. Derivative  | 25      | 0                  | 99                  |
| 8. OVG @ Set Speed A   | 20      | 1                  | 99                  |
| 9. OVG @ Set Speed B   | 20      | 1                  | 99                  |
| 10. OVG @ Idle Speed   | 20      | 1                  | 99                  |
| 11. Gain Factor  | 20      | 1                  | 99                  |
| 12. Speed Filter   | 16      | 1                  | 24                  |
| 13. Idle Hold Time   | 0       | 0                  | 9999                |
| 14. Accel Rate *   | 1000    | 1                  | 11000               |
| 15. Decel Rate *   | 1000    | 1                  | 11000               |
| 16. Startup Rate*  | 1000    | 1                  | 11000               |
| 17. Startup Limit  | 1000    | 0                  | 1000                |
| 18. Torque Limit   | 1000    | 0                  | 1000                |
| 19. Integral Low Limit   | 0       | 0                  | Integral High Limit |
| 20. Integral High Limit  | 99      | Integral Low Limit | 99                  |
| 21. % Droop  | 0       | 0                  | 100                 |
| 22. No Load Cal  | 0       | 0                  | 1000                |
| 23. Full Load Cal  | 1000    | 0                  | 1000                |
| 24. Password   | 0       | 0                  | 99                  |
| 25. Over Speed Limit   | -001    | 100                | 0                   |
|  | -002 *  | 15000              | 0                   |
| 26. Set Speed A Min *  | 10      | 10                 | Set Speed A         |
| 27. Set Speed A Max *  | 11000   | Set Speed A        | 11000               |
| 28. Set Speed B Min *  | 10      | 10                 | Set Speed A         |
| 29. Set Speed B Max *  | 11000   | Set Speed B        | 11000               |
| 30. Idle Speed Min *   | 10      | 10                 | Idle Speed          |
| 31. Idle Speed Max *   | 11000   | Idle Speed         | 11000               |
| 32. Duty Cycle Limit   | 95      | 10                 | 95                  |
| 33. Startup Speed *  | 1000    | 10                 | 11000               |
| 34. Startup Duty Cycle   | 30      | 5                  | 95                  |
| Parameters 2, 5, 6, 7, 8, 11, 12, and 33 require adjustment, while adjustments to the other parameters are optional. |         |                    |                     |

## 7. Inductor Technical Specs



Quality Products. Service Excellence.

### Heavy Current Chassis Mount 195-196 Series

**NEW SIZES**

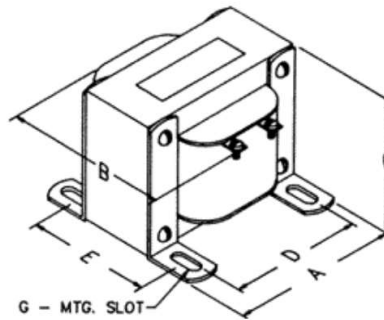


#### Features

- Open core & coil, 4-slot bracket mounting chokes.
- Tolerance of 15% on both inductance & resistance.
- Inductances measured at rated D.C. current.
- The "195" series is single coil
- The "196" series is dual coil - allowing more versatility
- Recommended maximum operating voltage 600 VAC (winding to core).
- Hipot tested at 2,500 VAC
- Connections are made to a screw terminal or heavy copper tabs with holes
- Perfect for high current power supply filtering.
- For use at 60 Hz. For higher frequency applications, try our **197 Series**



Ask About  
Custom  
Transformers  
& Chokes



| Part No. | Inductance mH<br>(Millihenries) | D.C. Current<br>(Amps) | Resistance<br>(Ohms) | Insulation<br>Class | Dimensions |      |      |      |      | Mounting Slot<br>G | Weight<br>(lbs.) |
|----------|---------------------------------|------------------------|----------------------|---------------------|------------|------|------|------|------|--------------------|------------------|
|          |                                 |                        |                      |                     | A          | B    | C    | D    | E    |                    |                  |
| 195T10   | 100                             | 10                     | 0.42                 | B                   | 7.50       | 6.00 | 6.25 | 6.00 | 4.25 | 0.38 x 0.63        | 35               |

## References

- [1] N. Hatziargyriou, H. Asano, R. Iravani, and C. Marnay, "Microgrids," *IEEE power & energy magazine*, vol. 5, no. august, pp. 78–94, 2007.
- [2] H. Nikkhajoei and R. H. Lasseter, "Distributed Generation Interface to the CERTS Microgrid," *IEEE Trans. POWER Deliv.*, vol. 24, no. 3, pp. 1598–1608, 2009.
- [3] K. P. Schneider, F. K. Tuffner, M. A. Elizondo, C. C. Liu, Y. Xu, and D. Ton, "Evaluating the Feasibility to Use Microgrids as a Resiliency Resource," *IEEE Trans. Smart Grid*, vol. 8, no. 2, pp. 687–696, 2017, doi: 10.1109/TSG.2015.2494867.
- [4] D. E. Olivares *et al.*, "Trends in microgrid control," *IEEE Trans. Smart Grid*, vol. 5, no. 4, pp. 1905–1919, 2014, doi: 10.1109/TSG.2013.2295514.
- [5] J. A. P. Lopes, C. L. Moreira, and A. G. Madureira, "Defining control strategies for microgrids islanded operation," *IEEE Trans. Power Syst.*, vol. 21, no. 2, pp. 916–924, 2006, doi: 10.1109/TPWRS.2006.873018.
- [6] R. H. Lasseter *et al.*, "CERTS microgrid laboratory test bed," *IEEE Trans. Power Deliv.*, vol. 26, no. 1, pp. 325–332, 2011, doi: 10.1109/TPWRD.2010.2051819.
- [7] N. S. Coleman *et al.*, "Hardware setup of a solar microgrid laboratory," in *IEEE Power and Energy Society General Meeting*, 2017, pp. 1–5, doi: 10.1109/PESGM.2017.8274100.
- [8] B. Zhao, X. Zhang, and J. Chen, "Integrated microgrid laboratory system," *IEEE Trans. Power Syst.*, vol. 27, no. 4, pp. 2175–2185, 2012, doi: 10.1109/TPWRS.2012.2192140.
- [9] D. Cornforth, A. Berry, and T. Moore, "Building a microgrid laboratory," in *8th International Conference on Power Electronics - ECCE Asia*, May 2011, pp. 2035–2042, doi: 10.1109/ICPE.2011.5944501.
- [10] I. Szeidert, I. Filip, O. Prostean, and C. Vasar, "Laboratory setup for microgrid study," in *INES 2016 - 20th Jubilee IEEE International Conference on Intelligent Engineering Systems, Proceedings*, 2016, pp. 289–292, doi: 10.1109/INES.2016.7555138.
- [11] D. A. Sbordone, K. M. M. Huq, and M. Baran, "An experimental microgrid for laboratory activities," in *2015 IEEE 15th International Conference on Environment and Electrical Engineering, IEEEIC*, 2015, pp. 363–367, doi: 10.1109/IEEEIC.2015.7165188.
- [12] C. Patrascu, N. Muntean, O. Cornea, and A. Hedes, "Microgrid laboratory for educational and research purposes," in *2016 IEEE 16th International Conference on Environment and Electrical Engineering (IEEEIC)*, 2016, pp. 1–6, doi: 10.1109/IEEEIC.2016.7555682.
- [13] Y. Liu, C. Farnell, K. George, H. A. Mantooth, and J. C. Balda, "A scaled-down microgrid laboratory testbed," in *2015 IEEE Energy Conversion Congress and Exposition, ECCE*, 2015, pp. 1184–1189, doi: 10.1109/ECCE.2015.7309825.
- [14] A. D. Paquette and D. M. Divan, "Providing improved power quality in microgrids: Difficulties in competing with existing power-quality solutions," *IEEE Industry Applications Magazine*, vol. 20, no. 5, pp. 34–43, 2014.
- [15] C. M. Colson and M. H. Nehrir, "A review of challenges to real-time power management of microgrids," in *2009 IEEE Power and Energy Society General Meeting*, 2009, pp. 1–8,



doi: 10.1109/PES.2009.5275343.

- [16] S. Nepal, A. Shakya, R. Fourney, J. Sternhagen, and R. Tonkoski, "Development of real-time control of Commercial Off-The-Shelf inverter/charger for Energy Management of microgrids," in *2016 IEEE Power and Energy Society General Meeting (PESGM)*, 2016, pp. 1–5, doi: 10.1109/PESGM.2016.7742025.
- [17] Q. Li, D. L. Lubkeman, N. Lu, and X. Zhu, "Control strategies for residential microgrids during islanded situation," in *2016 IEEE Power and Energy Society General Meeting (PESGM)*, 2016, pp. 1–5, doi: 10.1109/PESGM.2016.7741387.
- [18] J. Sachs and O. Sawodny, "A Two-Stage Model Predictive Control Strategy for Economic Diesel-PV-Battery Island Microgrid Operation in Rural Areas," *IEEE Trans. Sustain. Energy*, vol. 7, no. 3, pp. 903–913, 2016, doi: 10.1109/TSTE.2015.2509031.
- [19] X. Wang and G. G. Karady, "Hybrid battery charging strategy for maximizing PV customers' economic benefits," in *2016 IEEE Power and Energy Society General Meeting (PESGM)*, 2016, pp. 1–5, doi: 10.1109/PESGM.2016.7741127.
- [20] IEEE Std 1547-2018 (Revision of IEEE Std 1547-2003), *IEEE Std. 1547-2018. Standard for Interconnection and Interoperability of Distributed Energy Resources with Associated Electric Power Systems Interfaces*. New York, NY, 2018.
- [21] C. Schauder, "Advanced Inverter Technology for High Penetration Levels of PV Generation in Distribution Systems," Report NREL/SR-5D00-60737, 2014.
- [22] California Public Utilities Commission (CPUC), "Advanced Inverter Technologies Report - Grid Planning and Reliability Energy Division," Jan. 2013.
- [23] "Common Functions for Smart Inverters: Version 2," EPRI Report 1026809, 2016.
- [24] S. Gonzalez, F. Hoffmann, M. Mills-Price, M. Ralph, and A. Ellis, "Implementation of advanced inverter interoperability and functionality," in *2012 38th IEEE Photovoltaic Specialists Conference*, 2012, pp. 1362–1367, doi: 10.1109/PVSC.2012.6317853.
- [25] J. Johnson, S. Gonzalez, M. E. Ralph, R. Broderick, and A. Ellis, "Test Protocols for Advanced Inverter Interoperability Functions," SANDIA REPORT SAND2013-9880 Unlimited, Nov. 2013. [Online]. Available: <https://energy.sandia.gov/wp-content/gallery/uploads/SAND2013-9880.pdf>.
- [26] R. J. Bravo, R. Yinger, S. Robles, and W. Tamae, "Solar PV inverter testing for model validation," in *2011 IEEE Power and Energy Society General Meeting*, 2011, pp. 1–7, doi: 10.1109/PES.2011.6039850.
- [27] R. J. Bravo, S. Robles, and R. Salas, "Evaluation of German 3-phase solar PV inverter," in *2014 IEEE PES General Meeting | Conference & Exposition*, 2014, pp. 1–5, doi: 10.1109/PESGM.2014.6939536.
- [28] R. J. Bravo, "DER volt-VAr and voltage ride-through needs to contain the spread of FIDVR events," in *2015 IEEE Power & Energy Society General Meeting*, 2015, pp. 1–3, doi: 10.1109/PESGM.2015.7286246.
- [29] W. Peng, C. Hicks, O. Gonzalez, B. Blackstone, and Y. Baghzouz, "Experimental test on some autonomous functions of advanced PV inverters," in *2016 IEEE Power and Energy*

- Society General Meeting (PESGM)*, 2016, pp. 1–5, doi: 10.1109/PESGM.2016.7741780.
- [30] R. J. Bravo, S. A. Robles, and E. Muljadi, “Assessing solar PV inverters’ anti-islanding protection,” in *2014 IEEE 40th Photovoltaic Specialist Conference (PVSC)*, 2014, pp. 2668–2671, doi: 10.1109/PVSC.2014.6925478.
- [31] J. Neely, S. Gonzalez, M. Ropp, and D. Schutz, “Accelerating Development of Advanced Inverters: Evaluation of Anti-Islanding Schemes with Grid Support Functions and Preliminary Laboratory Demonstration,” SANDIA REPORT SAND2013-10231, 2013. [Online]. Available: <http://energy.sandia.gov/wp/wp-content/gallery/uploads/SAND2013-10231.pdf>.
- [32] W. Peng, C. Hicks, Y. Baghzouz, and S. Haddad, “Experimental Test on the Islanding of an Advanced PV Inverter,” in *2016 International Symposium on Power Electronics, Electrical Drives, Automation and Motion (SPEEDAM)*, 2016, pp. 1342–1347, doi: 10.1109/SPEEDAM.2016.7525994.
- [33] C. Hicks, B. Blackstone, O. Gonzalez, and Y. Baghzouz, “Experimental test on intentional islanding of diesel generator - PV microgrid,” in *2017 IEEE Power & Energy Society General Meeting*, 2017, pp. 1–5, doi: 10.1109/PESGM.2017.8274187.
- [34] B. Blackstone and Y. Baghzouz, “Value Added Sequential Services for BTM Storage when Paired with PV Systems,” in *2020 19th International Conference on Harmonics and Quality of Power (ICHQP)*, Jul. 2020, pp. 1–6, doi: 10.1109/ICHQP46026.2020.9177904.
- [35] Tesla, “Powerwall Tesla.” <https://www.tesla.com/powerwall> (accessed Mar. 10, 2017).
- [36] G. Laliberte, “A Comparison of Generator Excitation Systems,” 2016.
- [37] T. A. Theubou Tameghe, I. Kamwa, and R. Wamkeue, “Diesel Generator Modelling for Microgrid Power Plant Parameters Assessment,” in *EIC Climate Change Technology Conference*, 2015, pp. 1–12.
- [38] C. D. Rakopoulos and E. G. Giakoumis, *Diesel Engine Transient Operation - Principles of Operation and Simulation Analysis*, 1st ed. Springer-Verlag London, 2009.
- [39] IEEE Standard 421.5-2016 (Revision of IEEE Std 421.5-2005), “IEEE Recommended Practice for Excitation System Models for Power System Stability Studies,” New York, NY, 2016. doi: 10.1109/IEEESTD.2016.7553421.
- [40] G. M. Masters, *Renewable and Efficient Electric Power Systems*, 2nd ed. Wiley Press, 2013.
- [41] A. M. Trzynadlowski, *Introduction to Modern Power Electronics*, 2nd ed. John Wiley, 2010.
- [42] T. Esumi and P. L. Chapman, “Comparison of photovoltaic array maximum power point tracking techniques,” *IEEE Trans. Energy Convers.*, vol. 22, no. 2, pp. 439–449, 2007, doi: 10.1109/TEC.2006.874230.
- [43] S. R. Abate, T. E. McDermott, M. Rylander, and J. Smith, “Smart inverter settings for improving distribution feeder performance,” in *2015 IEEE Power & Energy Society General Meeting*, 2015, pp. 1–5, doi: 10.1109/PESGM.2015.7286560.
- [44] T. Stetz, W. Yan, and M. Braun, “Voltage Control in Distribution Systems with High

- Level PV-Penetration,” in *25th European Photovoltaic Solar Energy Conference and Exhibition*, 2010, pp. 1–7.
- [45] W. Zhang, M. Baran, A. De, and S. Bhattacharya, “Fast Volt-VAR control on PV dominated distribution systems,” in *2014 IEEE PES T&D Conference and Exposition*, 2014, pp. 1–5, doi: 10.1109/tdc.2014.6863236.
- [46] J. W. Smith, W. Sunderman, R. Dugan, and B. Seal, “Smart inverter volt/var control functions for high penetration of PV on distribution systems,” in *2011 IEEE/PES Power Systems Conference and Exposition*, 2011, pp. 1–6, doi: 10.1109/PSCE.2011.5772598.
- [47] B. Guha, R. J. Haddad, and Y. Kalaani, “Anti-islanding techniques for Inverter-based Distributed Generation systems - A survey,” in *SoutheastCon 2015*, 2015, pp. 1–9, doi: 10.1109/SECON.2015.7133045.
- [48] A. Khamis, H. Shareef, E. Bizkevelci, and T. Khatib, “A review of islanding detection techniques for renewable distributed generation systems,” *Renew. Sustain. Energy Rev.*, vol. 28, pp. 483–493, 2013, doi: 10.1016/j.rser.2013.08.025.
- [49] H. Laaksonen, “Advanced islanding detection functionality for future electricity distribution networks,” *IEEE Trans. Power Deliv.*, vol. 28, no. 4, pp. 2056–2064, 2013, doi: 10.1109/TPWRD.2013.2271317.
- [50] L. E. Miller, J. Schoene, R. Kunte, and G. Y. Morris, “Smart grid opportunities in islanding detection,” in *2013 IEEE Power & Energy Society General Meeting*, 2013, pp. 1–4, doi: 10.1109/PESMG.2013.6672727.
- [51] R. T. Mahadeva and Y. Baghzouz, “Islanding Test Results of Some Local Grid-Tied Photovoltaic Systems,” 2006.
- [52] P. Gupta, R. S. Bhatia, and D. K. Jain, “Average absolute frequency deviation value based active islanding detection technique,” *IEEE Trans. Smart Grid*, vol. 6, no. 1, pp. 26–35, 2015, doi: 10.1109/TSG.2014.2337751.
- [53] E. J. Estebanez, V. M. Moreno, A. Pigazo, M. Liserre, and A. Dell’Aquila, “Performance evaluation of active islanding-detection algorithms in distributed-generation photovoltaic systems: Two inverters case,” *IEEE Trans. Ind. Electron.*, vol. 58, no. 4, pp. 1185–1193, 2011, doi: 10.1109/TIE.2010.2044132.
- [54] F. De Mango, M. Liserre, A. Dell’Aquila, and A. Pigazo, “Overview of anti-islanding algorithms for PV systems. Part I: Passive methods,” *EPE-PEMC 2006 12th Int. Power Electron. Motion Control Conf. Proc.*, pp. 1878–1883, 2007, doi: 10.1109/EPEPEMC.2006.283133.
- [55] H. H. Zeineldin and S. Kennedy, “Sandia frequency-shift parameter selection to eliminate nondetection zones,” *IEEE Trans. Power Deliv.*, vol. 24, no. 1, pp. 486–487, 2009, doi: 10.1109/TPWRD.2008.2005362.
- [56] A. Elmitwally and M. Rashed, “Flexible operation strategy for an isolated PV-diesel microgrid without energy storage,” *IEEE Trans. Energy Convers.*, vol. 26, no. 1, pp. 235–244, 2011, doi: 10.1109/TEC.2010.2082090.
- [57] T. Taylor, O. Gonzalez, and Y. Baghzouz, “Analysis of current distortion in a 12 kW photovoltaic system installation,” in *2016 17th International Conference on Harmonics*

- and Quality of Power (ICHQP)*, 2016, pp. 243–248, doi: 10.1109/ICHQP.2016.7783432.
- [58] G. Fitzgerald, J. Mandel, J. Morris, and H. Touati, “The Economics of Battery Energy Storage - How Multi-use, Customer-sited Batteries Deliver the Most Services and Value to Customers and the Grid,” Rocky Mt. Inst., 2015.
- [59] K. Ardani, E. O’Shaughnessy, R. Fu, C. Mc Clurg, J. Huneycutt, and R. Margolis, “Installed Cost Benchmarks and Deployment Barriers for Residential Solar Photovoltaics with Energy Storage: Q1 2016,” NREL/TP-7A40-67474, 2017.
- [60] C. Prapanukool and S. Chaitusaney, “An appropriate battery capacity and operation schedule of battery energy storage system for PV Rooftop with net-metering scheme,” in *2017 14th International Conference on Electrical Engineering/Electronics, Computer, Telecommunications and Information Technology (ECTI-CON)*, 2017, pp. 222–225, doi: 10.1109/ECTICon.2017.8096213.
- [61] R. Suzuki, Y. Hayashi, and Y. Fujimoto, “Determination method of optimal planning and operation for residential PV system and storage battery based on weather forecast,” in *2012 IEEE International Conference on Power and Energy (PECon)*, 2012, pp. 343–347, doi: 10.1109/PECon.2012.6450235.
- [62] S. Barcellona, L. Piegari, V. Musolino, and C. Ballif, “Economic viability for residential battery storage systems in grid-connected PV plants,” in *IET Renewable Power Generation*, 2018, pp. 135–142, doi: 10.1049/iet-rpg.2017.0243.
- [63] A. Nottrott, J. Kleissl, and B. Washom, “Storage dispatch optimization for grid-connected combined photovoltaic-battery storage systems,” in *2012 IEEE Power and Energy Society General Meeting*, 2012, pp. 1–7, doi: 10.1109/PESGM.2012.6344979.
- [64] P. Etha, A. K. Janjua, A. Chelladurai, and G. G. Karady, “Customer benefit optimization for residential PV with energy storage systems,” in *2017 IEEE Power & Energy Society General Meeting*, Jul. 2017, pp. 1–5, doi: 10.1109/PESGM.2017.8274153.
- [65] K. Vatanparvar and R. Sharma, “Battery Optimal Approach to Demand Charge Reduction in Behind-The-Meter Energy Management Systems,” in *2018 IEEE Power & Energy Society General Meeting (PESGM)*, Aug. 2018, pp. 1–5, doi: 10.1109/PESGM.2018.8586597.
- [66] R. K. Lam, D. H. Tran, and H.-G. Yeh, “Economics of residential energy arbitrage in california using a PV system with directly connected energy storage,” in *2015 IEEE Green Energy and Systems Conference (IGESC)*, Nov. 2015, pp. 67–79, doi: 10.1109/IGESC.2015.7359453.
- [67] J. Hoppmann, J. Volland, T. S. Schmidt, and V. H. Hoffmann, “The economic viability of battery storage for residential solar photovoltaic systems - A review and a simulation model,” in *Renewable and Sustainable Energy Reviews*, 2014, pp. 1101–1118, doi: 10.1016/j.rser.2014.07.068068.
- [68] A. I. Nousedilis, G. C. Kryonidis, E. O. Kontis, G. K. Papagiannis, G. C. Christoforidis, and I. P. Panapakidis, “Economic Viability of Residential PV Systems with Battery Energy Storage Under Different Incentive Schemes,” in *2018 IEEE International Conference on Environment and Electrical Engineering and 2018 IEEE Industrial and*

*Commercial Power Systems Europe (EEEIC / I&CPS Europe)*, Jun. 2018, pp. 1–6, doi: 10.1109/EEEIC.2018.8494492.

- [69] N. Energy, “Residential Electric Rates,” 2021.  
[https://www.nvenergy.com/publish/content/dam/nvenergy/brochures\\_arch/about-nvenergy/rates-regulatory/np\\_res\\_rate.pdf](https://www.nvenergy.com/publish/content/dam/nvenergy/brochures_arch/about-nvenergy/rates-regulatory/np_res_rate.pdf) (accessed Feb. 11, 2021).
- [70] NVEnergy, “Energy Storage Incentives,” 2021.  
[https://www.nvenergy.com/publish/content/dam/nvenergy/brochures\\_arch/cleanenergy/handbooks/EnergyStorage-Handbook.pdf](https://www.nvenergy.com/publish/content/dam/nvenergy/brochures_arch/cleanenergy/handbooks/EnergyStorage-Handbook.pdf).

## Curriculum Vitae

### BRANDON BLACKSTONE

blkstone@hotmail.com

---

#### EDUCATION:

|   |               |
|---|---------------|
| University of Nevada, Las Vegas                           | Las Vegas, NV |
| ■ Ph.D., Electrical Engineering                           | Spring 2021   |
| ■ M.S., Electrical Engineering, emphasis Electromagnetics | August 2006   |
| ■ B.S., Electrical Engineering, Cum Laude                 | December 2003 |

#### EXPERIENCE:

JT4 2019–Present  
Las Vegas NV  
*Radar Engineer*

Department of Navy 2017–2019  
China Lake, CA  
*Task Team Lead (TTL)*

University of Nevada, Las Vegas 2011–2017  
Las Vegas, NV  
*Laboratory Director for the Electrical and Computer Engineering Department*

University of Nevada, Las Vegas 2005–2011  
Las Vegas, NV  
*Laboratory Manager for the Electrical and Computer Engineering Department*

#### PUBLICATIONS

- C. Hicks, B. Blackstone, O. Gonzalez, and Y. Baghzouz, "Experimental test on intentional islanding of diesel generator — PV microgrid (# 1894)," 2017 IEEE Power & Energy Society General Meeting, Chicago, IL, USA, 2017, pp. 1-5, doi: 10.1109/PESGM.2017.8274187.

- B. Blackstone, C. Hicks, O. Gonzalez, and Y. Baghzouz, "Improved islanded operation of a diesel generator — PV microgrid with advanced inverter," 2017 IEEE 26th International

Symposium on Industrial Electronics (ISIE), Edinburgh, UK, 2017, pp. 123-127, doi:  
10.1109/ISIE.2017.8001234.

- W. Peng, B. Blackstone, Z. Mohammad, P. Ginobbi and Y. Baghzouz, "On determining the control techniques embedded in a commercial single-phase grid-tied PV inverter," 2015 IEEE Eindhoven Powertech, Eindhoven, Netherlands, 2015, pp. 1-6, doi:  
10.1109/PTC.2015.7232711.

- W. Peng, C. Hicks, O. Gonzalez, B. Blackstone, and Y. Baghzouz, "Experimental test on some autonomous functions of advanced PV inverters," 2016 IEEE Power and Energy Society General Meeting (PESGM), Boston, MA, USA, 2016, pp. 1-5, doi:  
10.1109/PESGM.2016.7741780.

- B. Blackstone, C. Hicks, O. Gonzalez, and Y. Baghzouz, "Development of an Outdoor Diesel Generator – PV Microgrid for Education and Research," 2018 IEEE Power & Energy Society General Meeting (PESGM), Portland, OR, USA, 2018, pp. 1-5, doi:  
10.1109/PESGM.2018.8586424.

- B. Blackstone, Y. Baghzouz and S. Premrudeepreechacharn, "Determining MPPT and anti-islanding techniques in a grid-tie PV inverter," 2012 IEEE 15th International Conference on Harmonics and Quality of Power, Hong Kong, China, 2012, pp. 409-413, doi:  
10.1109/ICHQP.2012.6381263.

- B. Blackstone and Y. Baghzouz, "Value Added Sequential Services for BTM Storage when Paired with PV Systems," 2020 19th International Conference on Harmonics and Quality of Power (ICHQP), Dubai, United Arab Emirates, 2020, pp. 1-6, doi:  
10.1109/ICHQP46026.2020.9177904.